Syracuse University

SURFACE

5-2015

STRESS-STRAIN BEHAVIOR BY IMAGE ANALYSIS, MIX DENSITY AND PRE-STRAIN EFFECTS OF EPS GEOFOAM

Chen Liu
Syracuse University

Follow this and additional works at: https://surface.syr.edu/thesis

Part of the Civil and Environmental Engineering Commons

ABSTRACT

In order to have a deeper understanding of the engineering performances of EPS geofoam, it is necessary to study the stress-strain response and internal strain distribution when loaded. In this investigation, the key objective is to study the stress-strain behavior of EPS geofoam under different conditions and develop construction practical suggestions when using geofoam. The scope of this research is divided into three main sections: (1) study the effect of induced anisotropy on the stress-strain behavior of EPS geofoam; (2) evaluate stress distribution within EPS blocks by using image analysis system; (3) analyze the effect of combining different EPS densities and also the different stress-strain reactions for the conditions of with and without continuous joints.

The pre-strain behavior of EPS blocks was analyzed by doing pre-loading tests on fresh samples and exhumed samples. Characteristics of inherent and induced anisotropy of EPS geofoam was investigated by testing pre-stressed geofoam. Induced anisotropy was observed to reduce the modulus significantly.

The non-contact image analysis system, ARAMIS, was used to search the different forms of stress-strain behavior and how the strain is distributed within the solid EPS blocks as well as the combined EPS with soft blocks, stiff blocks and those in-between. A GeoJac automatic load testing system with conventional displacement transducer was used together with ARAMIS. The strain distribution within the whole EPS geofoam and the average property of strain is illustrated and compared.

The effect of combining different EPS densities and the condition of with or without continuous joints when installed are demonstrated by doing laboratory tests and Finite Element Analysis at the same time.

STRESS-STRAIN BEHAVIOR BY IMAGE ANALYSIS, MIX DENSITY AND PRE-STRAIN EFFECTS OF EPS GEOFOAM

By

Chen Liu

B.S., China University of Geosciences, Beijing, China, 2012

Dissertation submitted in partial fulfillment of the

requirements for the degree of

Master of Science in Civil Engineering

Syracuse University, Syracuse, New York

May 2015

Acknowledgements

I would like to express my sincere appreciation to my thesis advisor, Professor Dawit Negussey for the continuous encouragement and guidance of my master study and research, for his patience, motivation, enthusiasm, and immense knowledge. His support helped me in all the time of research and writing of this thesis.

In addition, special thanks to Dr. S.K. Bhatia, Dr. Lui and Dr. H. Ataei for their valuable suggestions, insightful comments, and hard questions. I am grateful to all the people who contributed their efforts and time toward the completion of this research.

My graduate assistantship provided by the Department of Civil and Environmental Engineering throughout my course of study at Syracuse University is also appreciated. Thanks to all my friends and fellow graduate students for making my more than two years of graduate school more pleasant and meaningful.

Last but not the least, I would like to thank my family: my parents Dewei Liu and Guobi Chen, for giving birth to me at the first place and supporting me financially and spiritually throughout my life.

Table of Contents

Figures and Tables

List of Figures:

List of Tables:

CHAPTER 1

INTRODUCTION

1.1 The History and Development of EPS Geofoam

Geofoam (Expanded Polystyrene, EPS) refers to block or planar rigid cellular foam polymeric material used in geotechnical engineering applications (ASTM D 6817). Ever since it was put into use in Norway in 1972 (Coleman, 1974), EPS has been widely applied in geotechnical engineering as lightweight fill. Nowadays, geofoam is a kind of material that is universally used in many parts of the world. Compared with XPS (Extruded Polystyrene), EPS is more commonly used for geotechnical construction (Aabøe, 1981). EPS geofoam is much lighter, approximately 1% the weight of soil and less than 10% the weight of other lightweight fill alternatives, and suitable to reduce vertical and lateral stresses. Since the 1970s, EPS has been used in construction of highways in Europe. EPS use began in Japan in 1985 (Elragi, 2000) and interest grew rapidly. Geofoam application in Japan used almost half of the geofoam used worldwide in the mid-1990s.

1.2 Geofoam - EPS in Geotechnical Applications

EPS geofoam can be easily cut and shaped onsite, which further reduces jobsite challenges. EPS geofoam is available in up to 7 types that can be selected by the designer for specific applications (BASF, 1993). Its service life is

comparable to other construction materials (Frydenlund and Aabøe, 1996). It retains its physical properties in service, unaffected by weather conditions. Geotechnical engineering applications of EPS include road embankments, bridge, retaining walls, slope stabilization, thermal insulation and innovative foundation on soft soils. Overall, the usage of EPS for insulation makes up to 70% of the total production, while packing accounts for 20%, other usages take up 10% (Negussey, 1998; Elragi, 2000; Anasthas, 2001). By using EPS geofoam, the overall cost of project and time of construction can be reduced (Elragi, 2000).

In Colorado in 1989, a 61m section of US highway 160 failed and resulted in the closure of the east-bound lane of a heavily traveled highway. In order to increase the safety, 648m^3 EPS geofoam was used to fill in the crest of the slope. The $160,000 total cost of the project was much less than the estimated cost of $1,000,000 for an alternative retaining wall solution (Yeh and Gilmore, 1989). In 1994, EPS material played an important role in Hawaii (Mimura and Kimura, 1995) for construction of a 21m embankment for an emergency truck escape ramp. In New York, EPS blocks were used to treat an unstable clay soil embankment slope (Jutkofsky, et al., 2000). When facing the problem of low bearing capabilities above the ground, EPS geofoam provides a good way for decreasing the settlement usually associated with heavier fills (Thompsett, 1995). In Issaquah, Washington, Cole (2000) predicted a settlement of 0.3~0.5m by using conventional bridge fill

material. When about1800m³ EPS geofoam was utilized, only 1.25cm settlement developed after six months. Frydenlund (1996) reported on another application of EPS as a support foundation for bridge abutments in Norway. Lakkeberg Bridge is a temporary single lane steel bridge with 36.8m span across road E6 close to the Swedish border. It was constructed in 1989 directly on top of EPS blocks instead of pile foundations. Average settlements were slightly higher than 1% of the overall height of the EPS fill.

1.3 Area of Study and Purpose of Research

In order to expand the usage of EPS geofoam, it is of great importance to study the engineering stress-strain behavior. In this investigation, engineering behavior of geofoam as a potential lightweight fill material in geotechnical engineering is further explored.

Essential engineering properties of geofoam while under cyclic loading within and outside of the elastic range were studied. Displacement and stress-strain results derived from conventional global measurements were compared with data recorded by the ARAMIS system, which is a 3D optical noncontact detection system. The local strain distributions were obtained using this innovative system. To investigate the importance of quality assurance and proper installation of EPS geofoam blocks, lab tests with and without different densities and also with and

without vertical continuous joints were performed. Lab tests were also simulated in FLAC (Finite Difference Model).

This study will enable engineers to understand geofoam better, and assist them to design and conduct more innovative applications in the future.

CHAPTER 2

GEOFOAM UNCONFINED COMPRESSION TESTS AND PROPERTIES

2.1 Unconfined/Uniaxial Compression Test

There are two qualities of EPS fill material, which are quite important for geotechnical application, namely the compression loading capacity and interface shearing strength. The most significant form of loading capacity during construction of embankments is due to dead load or gravity. Loads coming from the pavement structure as well as the cover soil and the traffic can demand a high compressive strength from the EPS. Both short term and long term compressive strengths of EPS are the main aspects of design. Short term strength of EPS is essential for live loads and extreme event loads. Long term strength and deformation performance is important for support of dead load.

ASTM D 1621 standard specifies the test method for rigid cellular polystyrene geofoam. In this investigation, the compressive properties of EPS geofoam are obtained by using unconfined/uniaxial compression tests. Unconfined/Uniaxial compression means there is no confining pressure applied to the specimen during testing. The dimensions of the sample, the mode of loading as either load or deformation controlled, the rate of loading and temperature conditions are additional test considerations.

2.1.1 Test Specifications

In Figure 2.1, by using the GeoJac load frame system, the EPS samples are perpendicularly loaded without confining stress. GeoJac automatic load testing system is purposely made for geotechnical testing. The test system has several benefits. Real time plots enable users to make decisions and improvements in the process of testing. The stress cell mounted on the crossbar of the loading frame tracks the vertical load applied to the sample. The vertical deformation of the sample is measured by the LVDT (linear voltage displacement transducer). The data collection systems is a centrally located data logger and controller to which all the transducers, power suppliers, A/D and D/A convertors are linked. Values of load and displacement are recorded at pre-set time intervals. The system setup in which GeoJac load frame is used is shown in Figure 2.2. In this investigation, most of the tests were performed at 22^0C room temperature and a controlled displacement rate of 10% axial strain per minute.
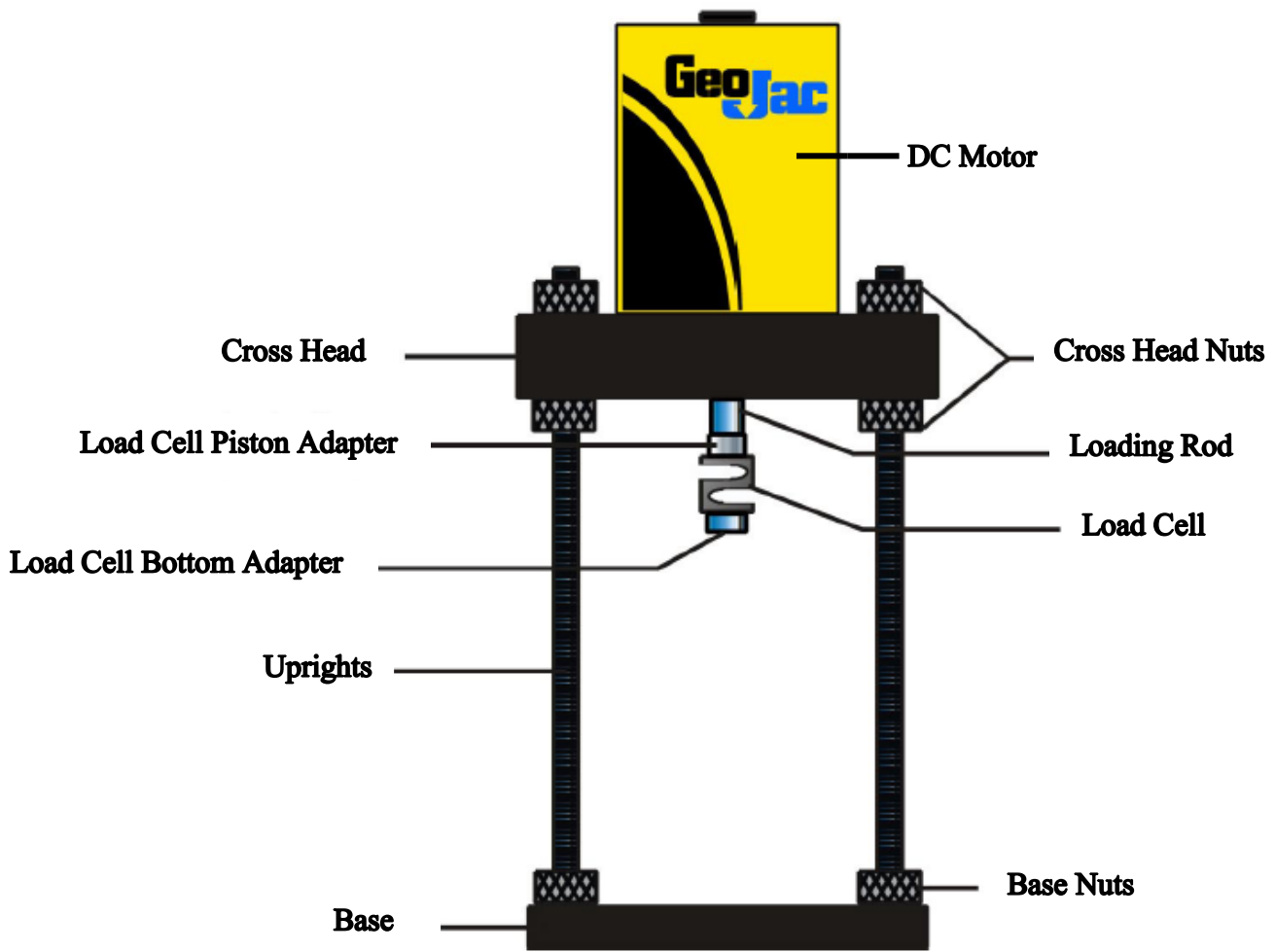
Figure 2.1. GeoJac Load Frame Setup
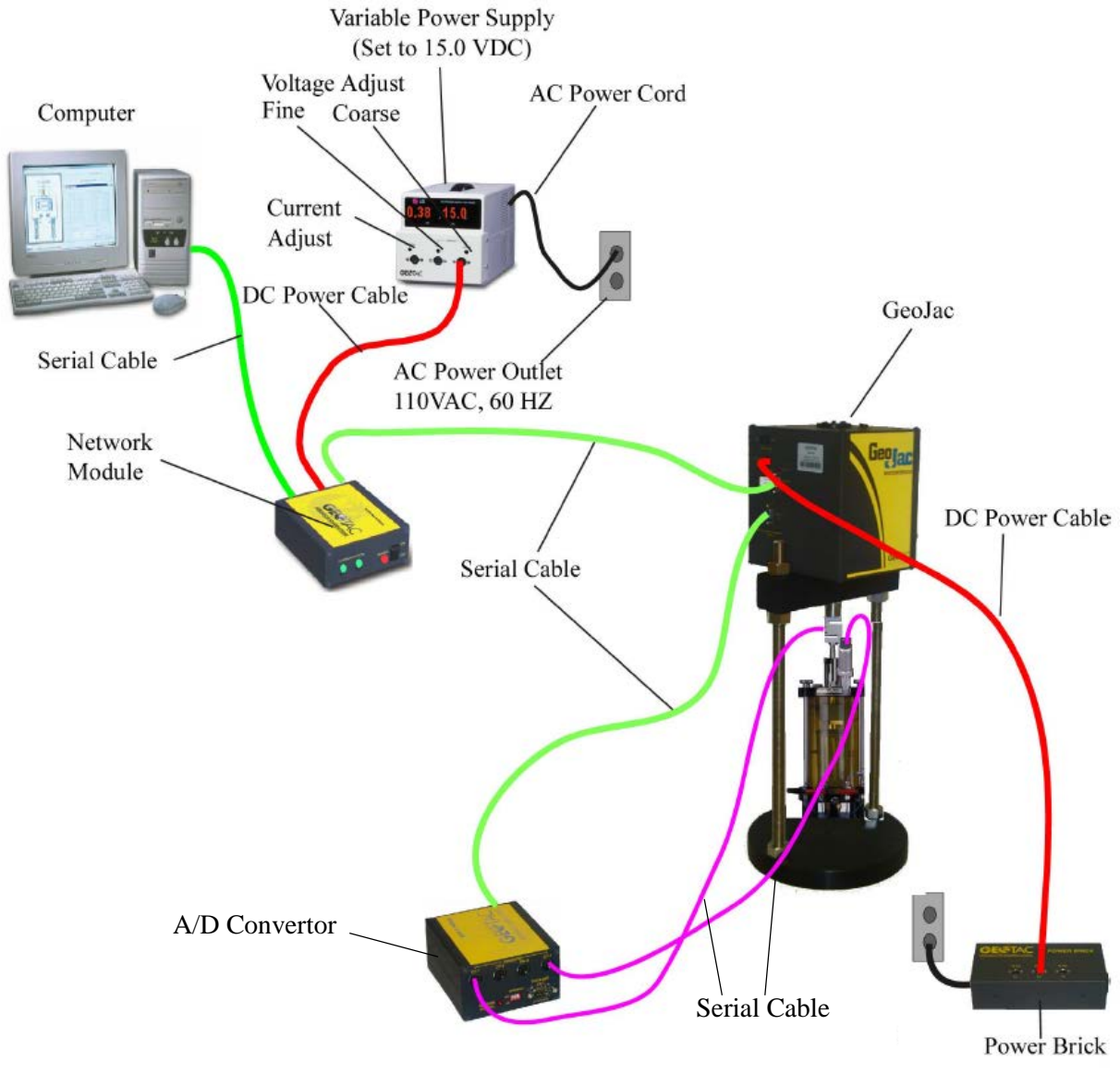
Figure 2.2. GeoJac System Hardware Setup

2.1.2 Test Results

Figure 2.3 shows a typical stress-strain performance of a standard 2in cube EPS sample. The green is a corrected curve of the blue for which seating errors have been removed. The stress-strain curve shows linear elastic behavior within a relatively small strain, usually up to 2% corrected strain. The slope of the initial

steep segment of the stress-strain curve is the elastic or Young's modulus.
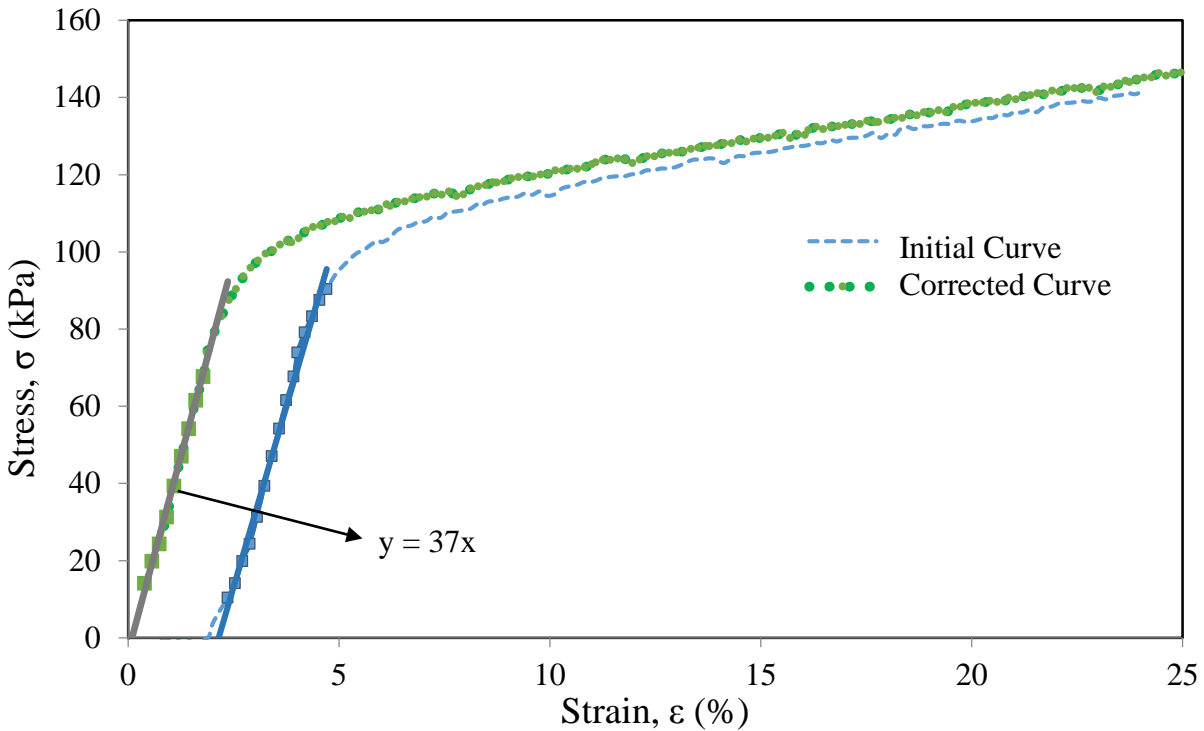
Figure 2.3. Typical Stress-Strain Behavior for EPS Specimen

By applying Equation 2.1, the initial EPS's tangent Young's modulus would be obtained.

$$E_{ti} = \Delta\sigma/\Delta\varepsilon \text{.. Equation 2.1}$$

In which the E_{ti} refers to the initial tangent Young's modulus; $\Delta\sigma$ is the compressive pressure increment, and $\Delta\varepsilon$ is the corresponding change in strain within the elastic range.

In compression tests, EPS samples show no sign of rupture or fracture. EPS can be recycled to produce solid polystyrene.

2.2 EPS Properties

Table 2.1 presents EPS geofoam material properties as provided in ASTM D 6817. The properties of Young's modulus, density and compressive resistance will be further discussed.

Table 2.1. Physical Properties of EPS Geofoam

TYPE - ASTM D 6817	EPS12	EPS15	EPS19	EPS22	EPS29	EPS39
Minimum Density, kg/m^3, (lb/ft^3)	11.2 (0.70)	14.4 (0.90)	18.4 (1.15)	21.6 (1.35)	28.8 (1.80)	38.4 (2.40)
Minimum Compressive Resistance @ 1% deformation, kPa (psi)	15 (2.2)	25 (3.6)	40 (5.8)	50 (7.3)	75 (10.9)	103 (15.0)
Minimum Compressive Resistance @ 5% deformation, kPa (psi)	35 (5.1)	55 (8.0)	90 (13.1)	115 (16.7)	170 (24.7)	241 (35.0)
Minimum Compressive Resistance @ 10% deformation, kPa (psi)	40 (5.8)	70 (10.2)	110 (16.0)	135 (19.6)	200 (29.0)	276 (40.0)
Flexural Strength min., kPa (psi)	69 (10.0)	172 (25.0)	207 (30.0)	276 (40.0)	345 (50.0)	414 (60.0)
Maximum Water Absorption by total immersion, volume %	4.0	4.0	3.0	3.0	2.0	2.0
Minimum Oxygen Index, volume %	24.0	24.0	24.0	24.0	24.0	24.0

2.2.1 Young's Modulus

Young's modulus of EPS is important for design with geofoam. The Young's modulus of EPS samples is usually obtained from the unconfined compression testing of cubic or cylindrical specimens. More often, Young's modulus values are obtained from unconfined compression tests on 50mm cube specimens in accordance with ASTM D 1621, C 165, EN 826 or ISO 844.

Duškov (1990) reported back-calculated elastic modulus of EPS geofoam from impulsive force, was between 13MPa and 34MPa, much higher than 5MPa achieved from unconfined compression tests. Investigations of 20kg/m³ density EPS at low temperatures, freezing/thawing cycles and potential moisture absorption have not shown significant effects on EPS behavior. Srirajan (2001) reported that both initial Young's modulus and post-yield modulus of EPS blocks increase with density for traditional 50mm cube specimens. With increasing ambient stress, the initial Young's modulus and the post-yield modulus can decrease. Changes in initial modulus with increasing density reported in previous investigations are shown in Figure 2.4 (Eriksson and Trank, 1991; Horvath, 1995; Van Dorp, 1996; BASF, 1997; Sun, 1997; Duskov, 1997; Elragi, 2000; Anasthas, 2001). For design of roads on EPS subgrades, a modulus of 5MPa is commonly used (Negussey, 2007).
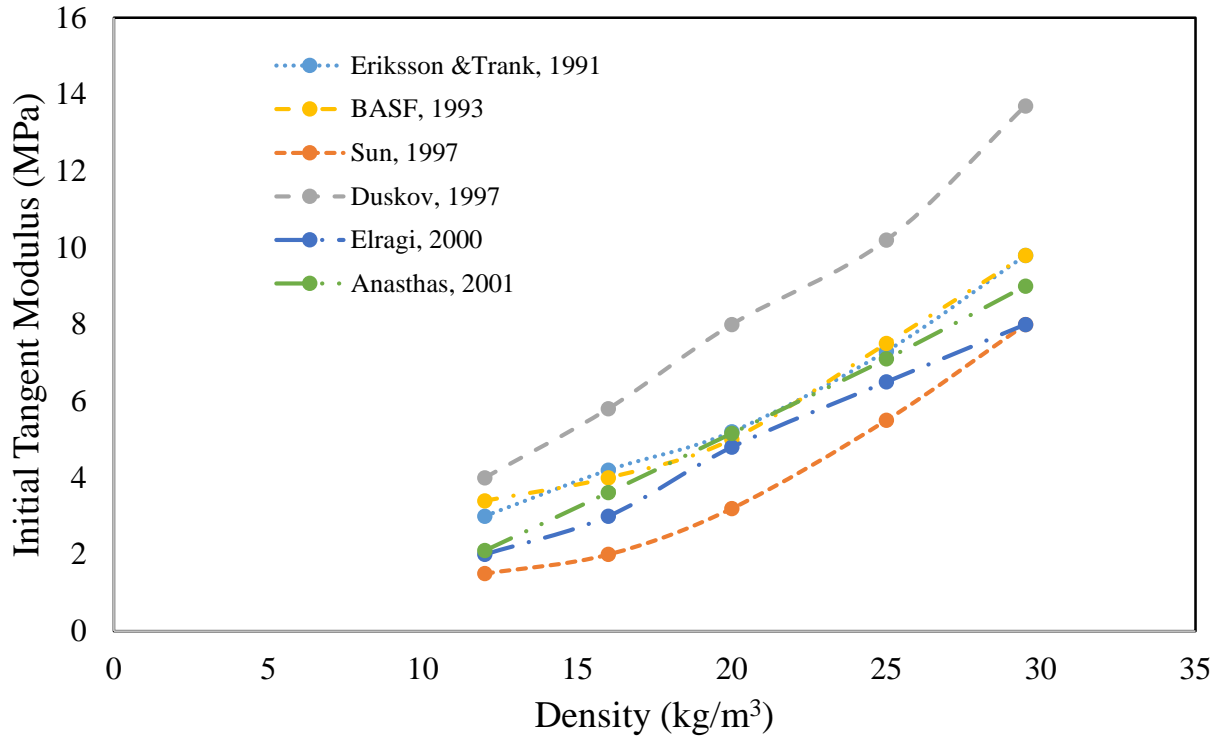
Figure 2.4. Initial Tangent Moduli of EPS Geofoam from Previous Investigations

2.2.2 Sample Size and Density

2.2.2.1 Sample Size

Available information suggested that it was not unusual to observe significant differences in the measured initial modulus between samples obtained from the same product or block (Elragi, 2000; Anasthas, 2001). These differences could be up to ± 0.5MPa for low density samples and up to ± 1.5MPa for high density samples. If these maximum variations were considered and applied to the average measured values of the initial modulus of elasticity for all nominal densities, it was computed that the percent deviation from reference values was

12

between $\pm 25\%$ and $\pm 40\%$. Accordingly, the significant increase in measured initial modulus values could be attributed to the effect of sample size.

Elragi et al. (2000) evaluated the performance of EPS geofoam under unconfined compression using traditional 50mm cubes, 600mm cubes and cylindrical samples of 76mm diameter with density of 15 and 29kg/m^3, respectively. The traditional 50mm cube samples significantly over-estimated initial deformations and thus underestimated Young's modulus values for geofoam, which may have partly resulted from the crushing and damage near the EPS block and rigid plate loading interfaces. In the large cubic EPS as well as cylindrical samples, vertical deformation was also observed for gauge length in the middle third of the height. The results indicated that the distribution of vertical strains over the height of geofoam block was not uniform. The segment on top of the EPS block had the lowest modulus of 1.2MPa. The end parts of the specimen were more severely deformed than the mid-segment of the EPS block. The major reason of the relatively high deformation of the small scale samples should be attributed to the seating and the end effects near the geofoam and rigid plate-loading interface. The values of Poisson's Ratio of small samples were relatively low compared with the results from large size blocks. Atmatzidis (2001) tested the EPS blocks with the transverse section of 100mm×100mm and the various aspect ratio of 0.5, 1.0 and 2.0. According to Atmatzidis (2001), the shape, size and the aspect ratio of EPS

13

geofoam specimens that were checked in the unconfined compression test showed comparatively little effects on the yield pressure and compression resistance. However, shape, size and the aspect ratio of EPS geofoam seemed to have some impacts on the initial elastic modulus. It would achieve comparatively higher initial modulus when the size of the specimen was larger than the traditional 50mm cubes. If the test results of 50mm cubes were taken into designing, the developed strains or deformation would likely be overestimated by a factor of 2. Eriksson and Trank (1991) suggested a suitable dimension of EPS blocks would be $200\times200\times t/3$ mm, where t/3 is the thickness of the specimen and t is the thickness of the whole large block.

The size of the specimens also will greatly influence the creep performance of the EPS blocks. As the specimen size increases, the stiffness of EPS also increases leading to a decrease in creep. Apart from the size of the samples, previous results also indicated that the modulus and strength of EPS depend on the loading rate. The standard loading rate used in ASTM D 6817 is 10% strain per minute. Awol (2012) indicted that decreasing loading rate has a tendency of increasing initial tangent modulus.

2.2.2.2 Density

The density of EPS geofoam material is regarded as the major indicator of behavior. EPS material is mostly made up of air-filled space. The air space of the

geofoam material is approximately 98% of the block volume, the density of the material is low. The densities of EPS geofoam vary between 12 and 30 kg/m^3, among which the 20kg/m^3 (1.25pcf) is the most widely used for civil engineering applications (Lingwall, 2011). According to Negussey (2007), the initial modulus of EPS samples with 20kg/m^3 density is 5MPa, which is in the range normally associated with very soft to soft clays (Das, 1998) when compared to typical design values with different types of soil. The performance of EPS geofoam with a density of 24kg/m^3 showed that over 8MPa modulus implied by field data and were better with stiffer clays (Negussey, 2007). While the modulus of about 8 to 10MPa for bigger samples of 32kg/m^3 density geofoam was in better agreement with the modulus estimates from field observations of 32kg/m^3 density EPS. When used for other purposes, insulation for example, the denser EPS is slightly better although XPS may be preferred (van Dorp, 1988). EPS geofoam is much lighter and easier to handle than soil, rock and other fill materials that are widely used in conventional geotechnical constructions.

According to the survey of Eriksson and Trank (1991), the bulk density may vary within the EPS blocks. Therefore, the samples tested should be selected from the EPS blocks by taking the variation in bulk density into consideration. The same amount of samples should be selected for testing from the upper layer, center layer

and lower layer together. There is no evidence that indicates the density of EPS is affected by the age of EPS material.

The price of resin and then EPS blocks increase with the price of oil and the EPS density. For large volume use of EPS, more savings can be realized with low density EPS. Figure 2.4 indicates the initial modulus increase with the increase of EPS densities from previous investigations. The stress-strain relationships are reflected in Figure 2.5 according to Negussey and Elragi (2000). Denser EPS geofoam tends to have higher initial modulus compared to EPS geofoam with lower density. Figure 2.6 indicates the various stresses at 1, 5 and 10% strain levels increase with geofoam densities (after BASF, Corp., 1997). As is indicated in Figure 2.6, when the density goes up, the strengths and the modulus go up as well. There is comparatively little difference between stress levels at 5 and 10% strain that are used as design strengths. Srirajan (2001) reported that density also had influence on the creep performance of the EPS. EPS of higher density developed less creep at the same relative pressure.
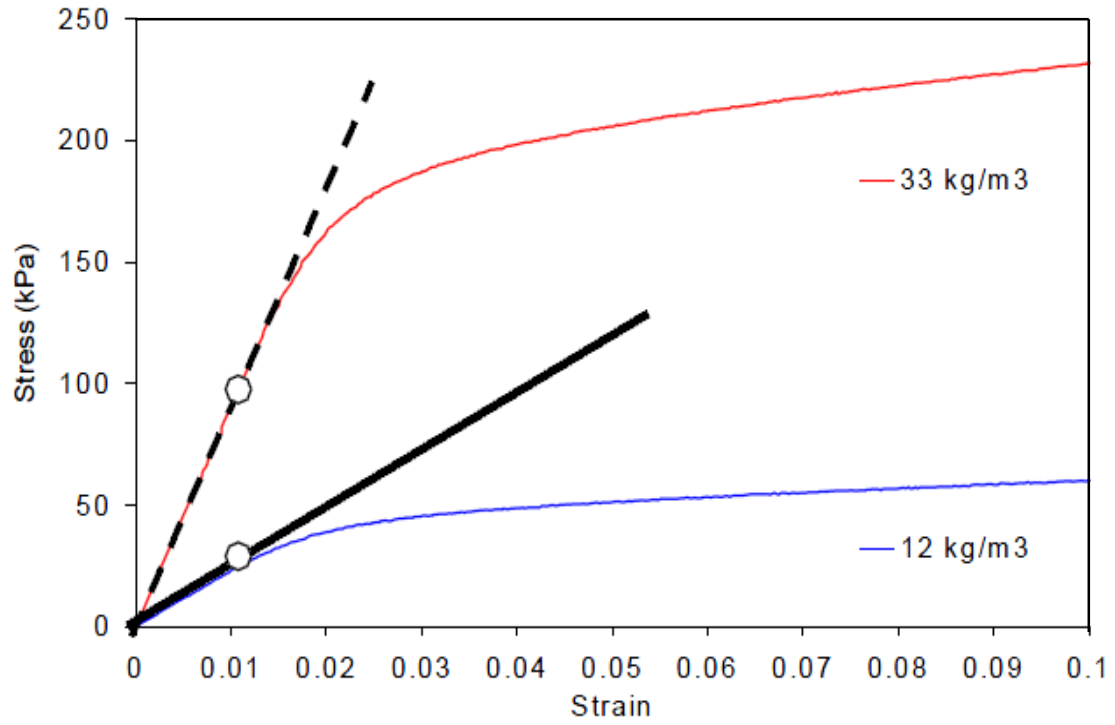
Figure 2.5. EPS Uniaxial Compression Stress-Strain Curves (after Negussey and
Elragi, 2000)
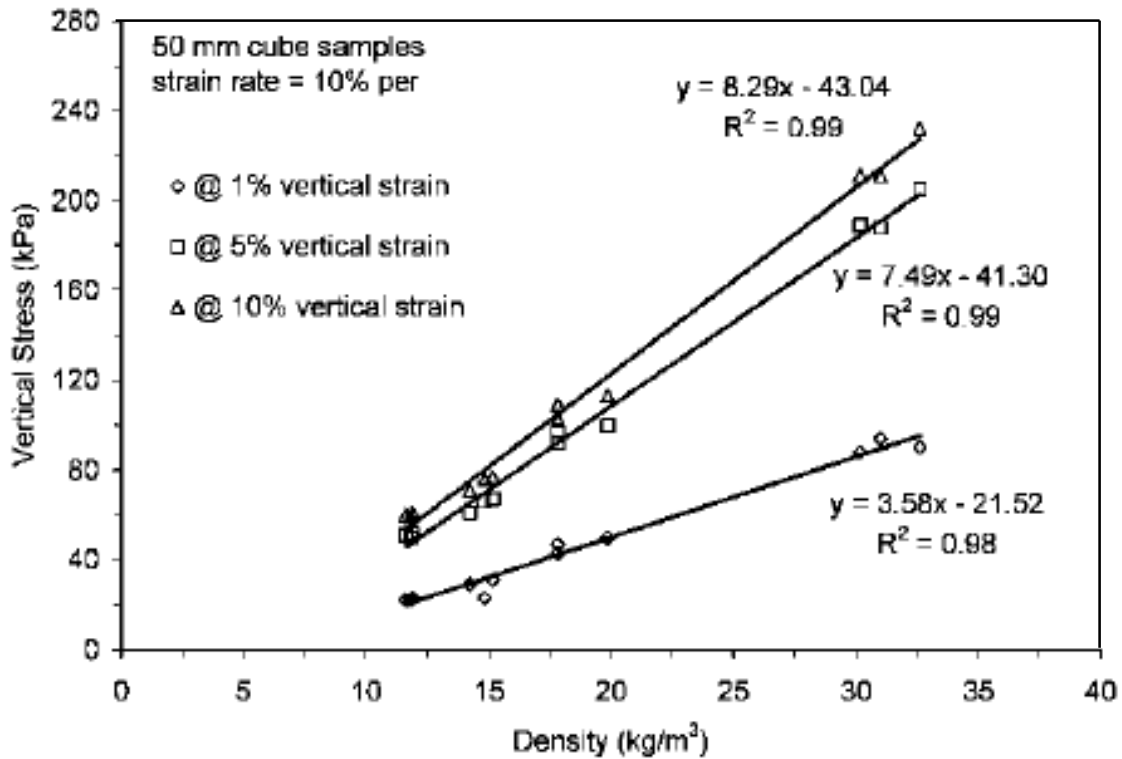
Figure 2.6. Strength at 1, 5 and 10% Strain Levels with Increasing Geofoam Density (after BASF, Corp., 1997)

2.2.2.3 Experimental Setup and Procedure

Effects of specimen dimensions and density on compression behavior of EPS blocks were investigated.

EPS blocks of 1pcf, 1.25pcf, 1.5pcf and 2pcf densities and the sample size with the following series were prepared and tested: (a) 2in and 4in cubes, (b) blocks with 4in × 4in cross-section and aspect ratio of 0.5 and 1.0, namely the 2in cubes, 2in by 4in by 4in cuboid, and 4 in cubes as shown in Figure 2.7. The EPS producers provided the test samples in 24in cubes. The hot wire cutter in the lab

18

was used to cut the specimen to the required size. Before test, the sample

dimension were measured with digital caliper of 0.01mm precision. The samples

were weighed on an electronic balance of 0.01g sensitivity. All specimens were

maintained at regulated room temperature of 20 to 22 ^{0}C for at least 7 days before

testing.
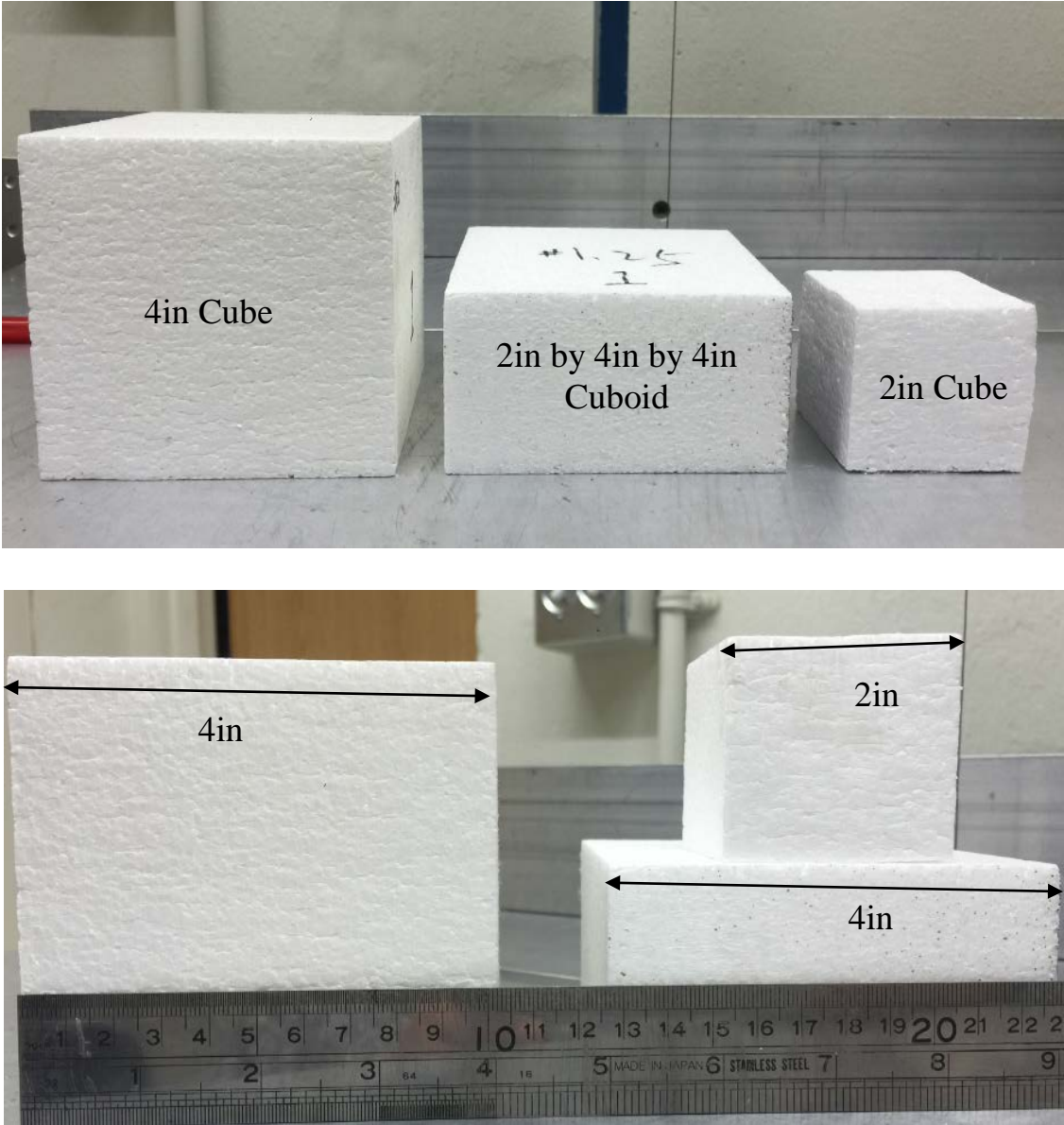
Figure 2.7. EPS Samples Used in Tests
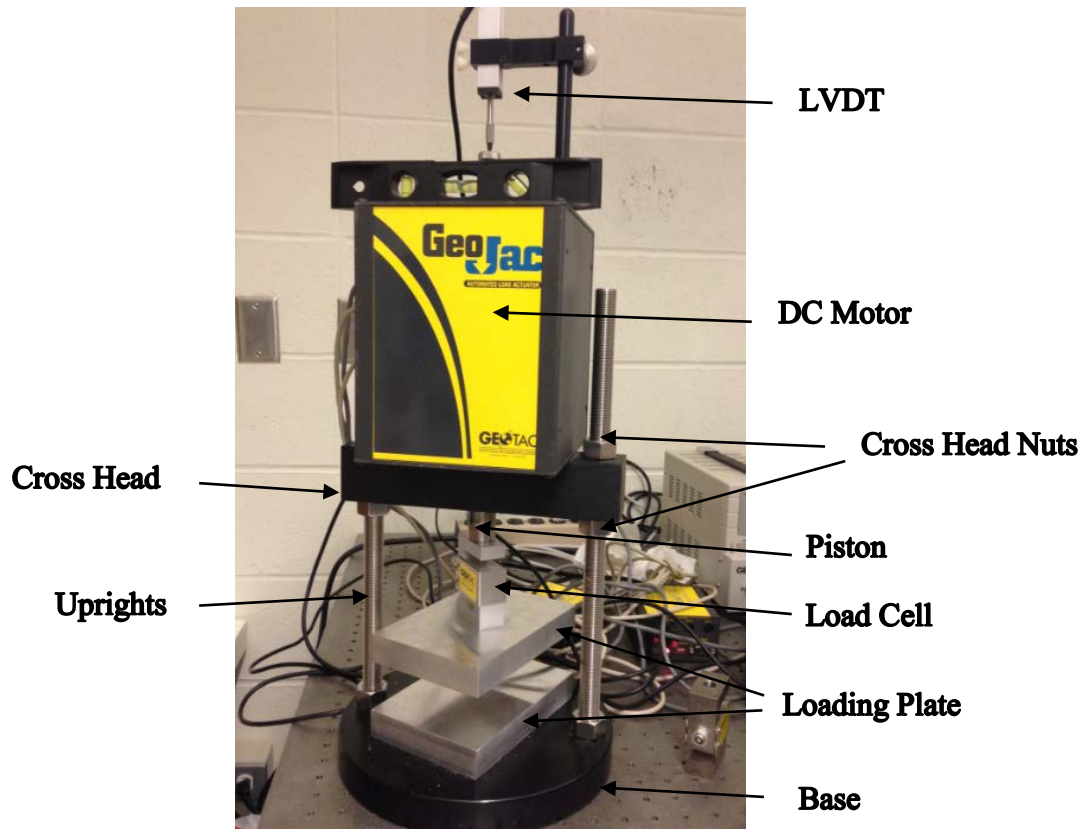
Figure 2.8. GeoJac Loading System

The EPS geofoam specimens were tested by a tabletop DC motor loading

system, as shown in Figure 2.8. The load cell was installed and the displacement

transducer travelled with the actuator maintaining the supporting cross head. The

large-area top loading plate was attached to the load cell. The bottom loading plate

was fixed to the base plate of the loading frame. The testing data was retrieved by

two channels, for the load cell and the other for vertical displacement transducer.

All tests made with the GeoJac loading system were displacement controlled at the

same strain rate of 10% per minute.

2.2.2.4 Test Results

Unconfined compression tests were conducted in order to evaluate the effect of sample geometry and densities on the observed behavior of the EPS geofoam. A minimum of two samples were tested for each test combination and all the stress-strain curves and strength values were obtained for each block. The stress-strain curves were corrected at very low strain levels in order to exclude seating errors.

2.2.2.4.1 Test Results of Sample Size
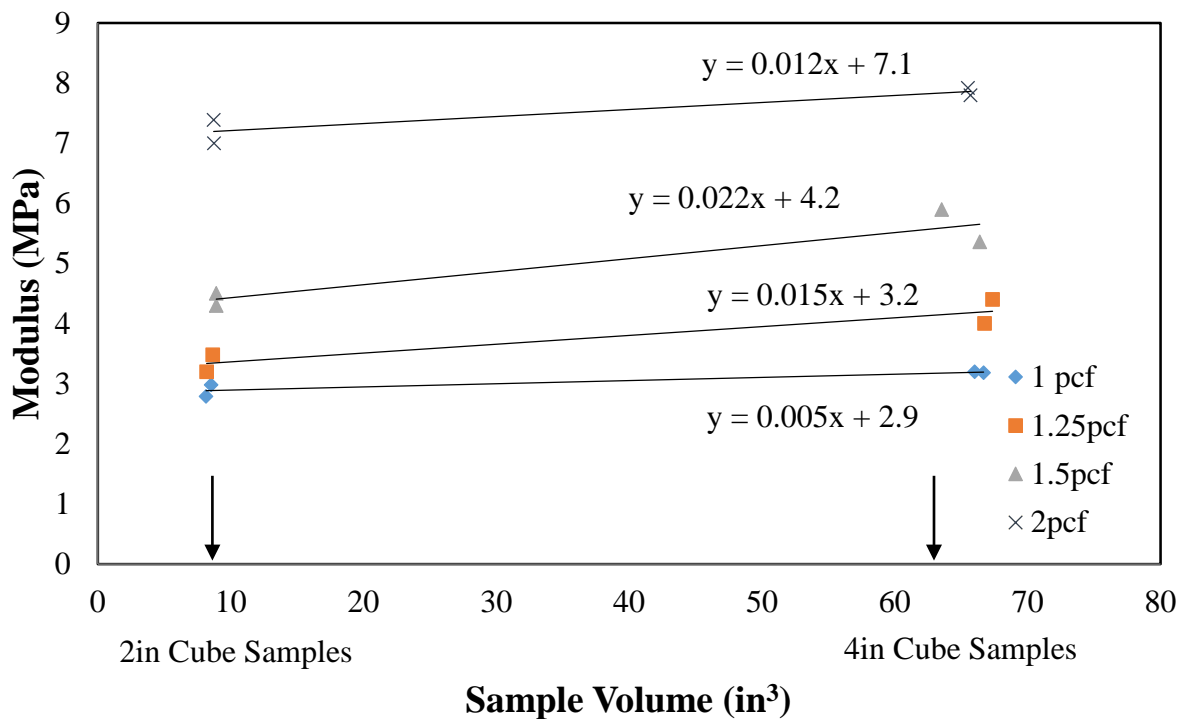
Figure 2.9. Sample Size Effect on Moduli for 2 and 4in Cubes

According to the lab tests, the strengths of 2in cube EPS geofoam were all relatively smaller than bigger cubic samples, which means that the size of the samples affect the strength of EPS regardless of the density. As for the samples

21

with an aspect ratio of 1, namely the 2in cube and 4in cube samples, the initial

modulus of EPS blocks increased with the increase of sample size, as shown in

Figure 2.9. For all nominal densities tested, the 4in cube samples had a 10% higher

initial modulus than the 2in cube samples.

The previous investigations (Eriksson and Trank, 1991; van Dorp, 1996;

Elragi, 2000) showed the large sample based modulus could be almost double that

of the small sample of the same density due to end effects of surface between the

loading plate and the sample. But for the tests that were presented in this

investigation, the variations in the sizes of the samples were not significant, and

this might be one reason that the differences of the modulus of the different size

samples were not obvious. The tests done by Negussey (2007) with a height of

24in cube samples showed that, due to the 24in cube samples were closer to the

thickness of common full size EPS blocks, the modulus of about 10MPa for the

24in cube samples agreed better with the modulus estimated with field observation.

The modulus values derived from laboratory tests on small size samples were too

small or too unrealistic to be used directly in the field design. A possible

explanation is that the end effects would be proportionally more significant for

small-sized samples and could cause large differences in modulus obtained from

small and big EPS samples. The rigid loading plate (Figure 2.10) on top of the EPS

block in laboratory tests can impose uniform deformation across the section area of

test samples. According to Taylor (1948), rigid loading plate would produce higher stresses toward the edges of samples. The average deformation near the rigid loading plate was shown to be higher than the deformations across the geofoam to geofoam interfaces according to Elragi (2000). With development of image analysis processes, an alternative means for measuring and investigating the interface pressure distributions becomes possible. This will be discussed in a later chapter.
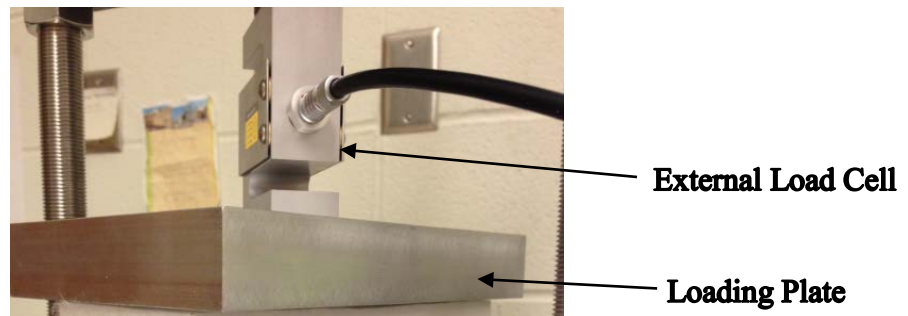
Figure 2.10. Load Cell and Top Loading Plate
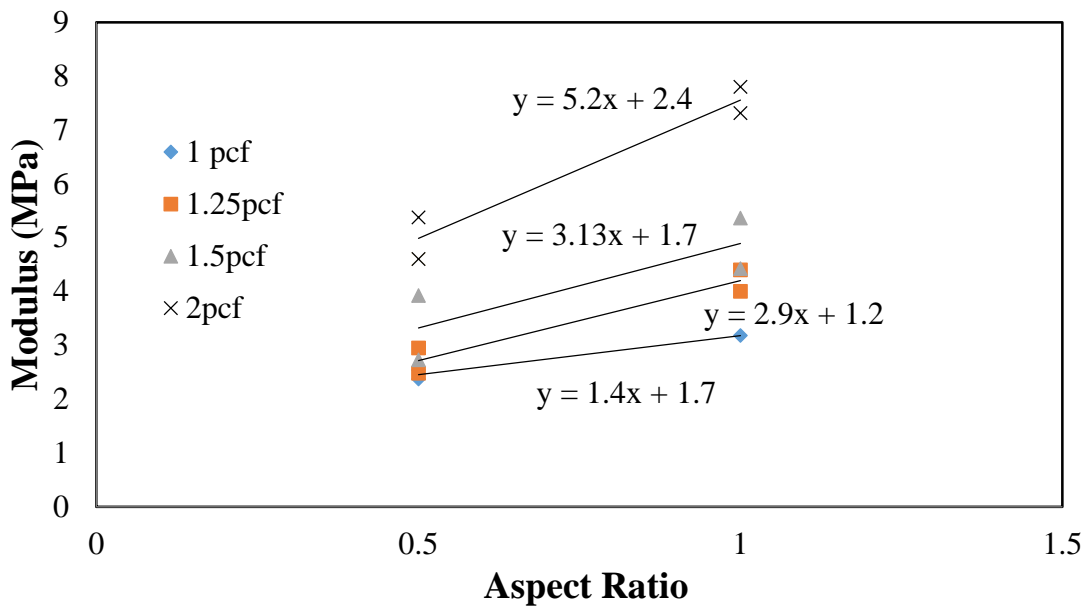
Figure 2.11. Comparison of Moduli for Different Aspect Ratio

The results obtained from tests on 4in cubes (aspect ratio is 1) and results obtained from the prisms with 4in×4in cross-section and 2in height for aspect ratio equal to 0.5 are shown in Figure 2.11. A reduction of the aspect ratio from 1.0 to 0.5 resulted in decrease of elastic modulus by 15% for 1pcf to 60% for 2pcf density.

2.2.2.4.2 Test Results of Density

The stress-strain curves for different densities of 2in cube samples are shown in Figure 2.12. The stress-strain behaviors of all the density types are very similar. It clearly shows that the initial modulus of EPS blocks increases with density, so does yield. The samples with densities of 2pcf are stiffer than the 1pcf and 1.5pcf EPS and the 1pcf ones are the softest. All the EPS blocks yield at about the same strain level, which is around 2.2%.
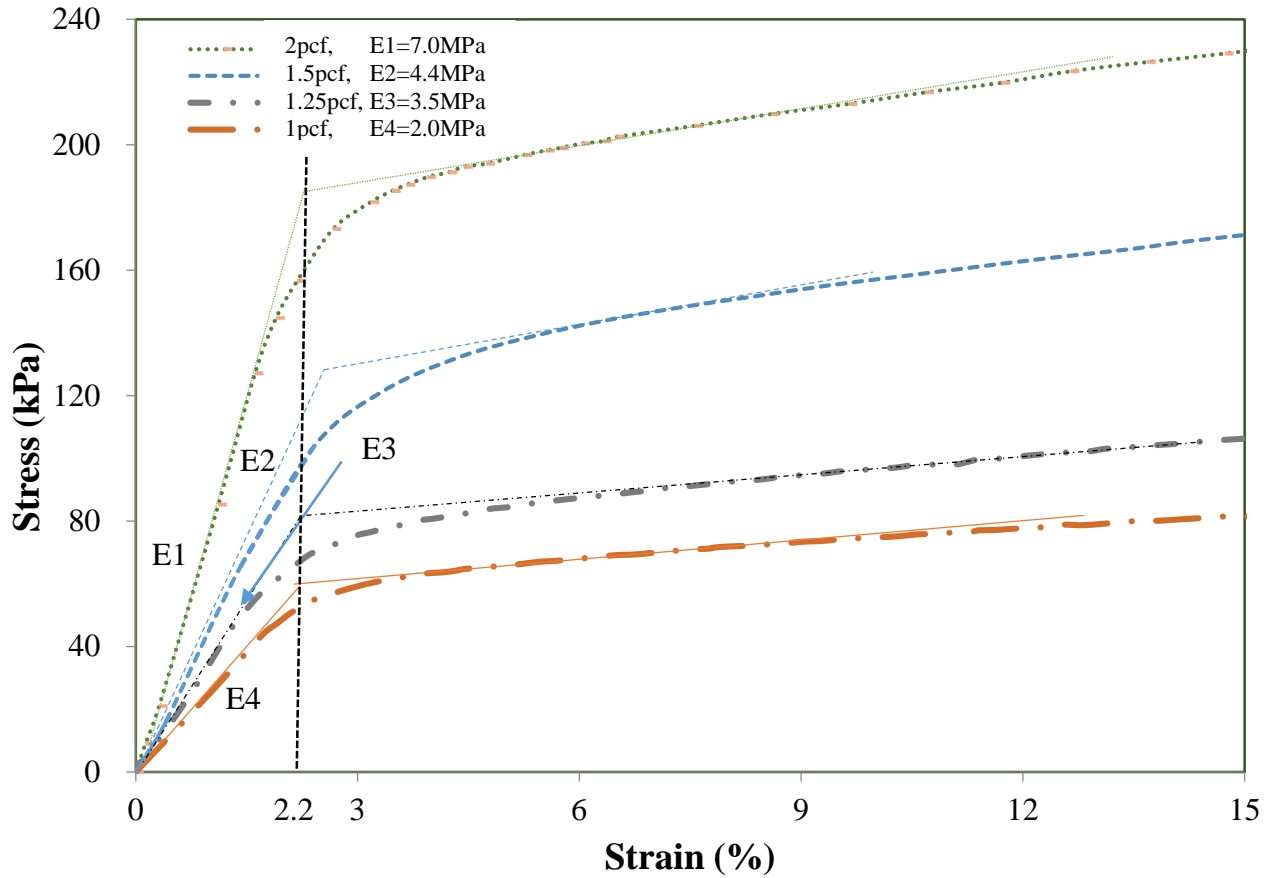
Figure 2.12. Stress-Strain Distribution Curves from Traditional Testing of 2in Cube Samples

All results obtained from unconfined compression tests on 2in and 4in cubes and 4in×2in×4in prisms are presented in Figure 2.13. According to Figure 2.13, the initial modulus of the EPS geofoam increases with the increase of EPS densities for all the sample sizes. The moduli of 1pcf (16kg/m^3), 1.25pcf (20kg/m^3), 1.5pcf (24kg/m^3) and 2pcf (32kg/m^3) density EPS are all relatively lower than the values obtained from ASTM D 8617.
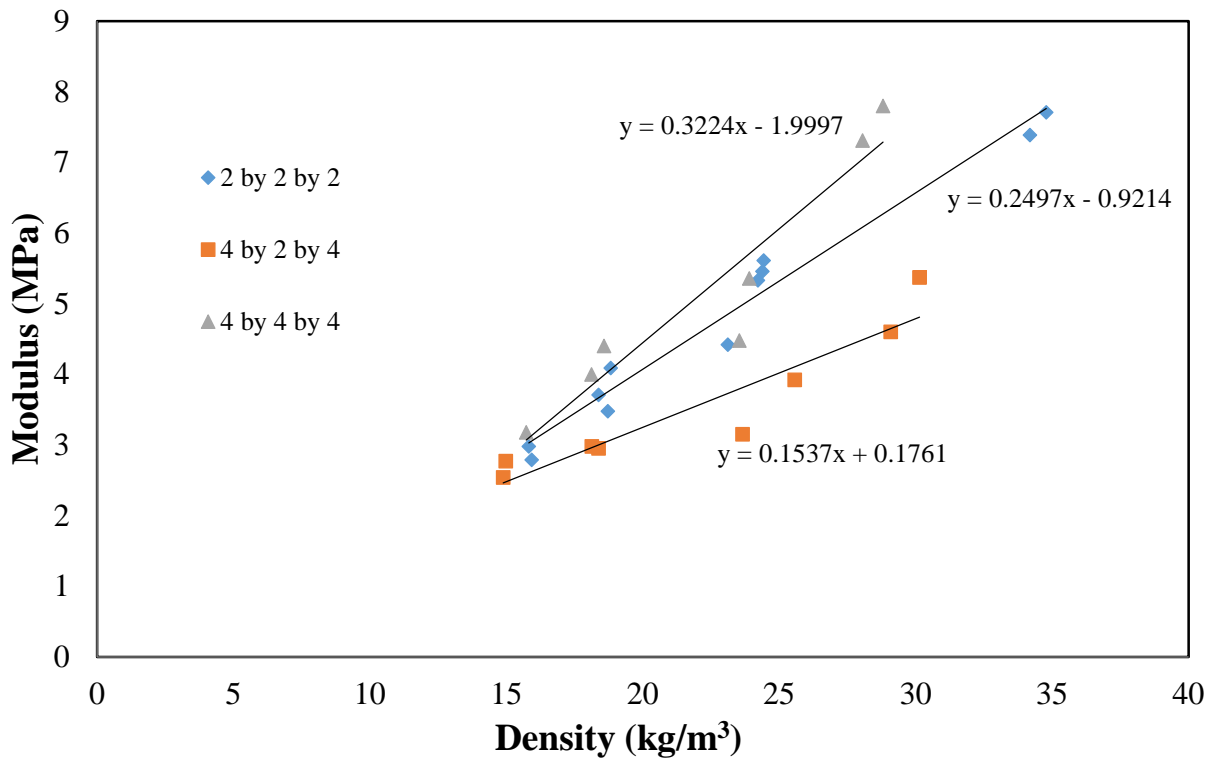
Figure 2.13. Moduli of EPS with Different Densities

2.2.2.5 Conclusions

1. The sample size and density affect the strength of EPS samples as was also suggested by (Eriksson and Trank, 1991; Horvath, 1995; van Dorp, 1996; Elragi, 2000; Atmatzidis, 2001; Awol, 2012). The foregoing information and observations indicate that, in addition to the anticipated scatter of data due to density deviation from nominal values, the results of unconfined compression test are affected by the size as well as by the aspect ratio of the samples tested. The bigger samples have larger modulus than smaller ones and the EPS with higher density have higher strength than the EPS with lower density.

26

2. Shape, size and aspect ratio of EPS geofoam samples have relatively insignificant effects on measured yield stress and compressive strength. However, size and aspect ratio have a significant effect on the initial modulus of elasticity which attains higher values (up to 100%) when the sample volume is one order of magnitude larger than the conventional 2in cubes. When results from testing 2in cubes are used for design purposes, expected strains or deformations may be overestimated by a factor of 2.

3. Beyond adjustments for seating error, the reason for the noted significant difference in modulus obtained from small and large size samples was assumed to be due to end effects at the loading plate boundaries.

2.2.3 Compressive Strength and Insulation Property

Table 2.2. Heat Insulation Properties of Different EPS Types

Type – ASTM C 578	Type XI	Type I	Type VIII	Type II	Type IX
Minimum Density, kg/m^3, (lb/ft^3)	12 (0.75)	16 (1.00)	20 (1.25)	24 (1.5)	32 (2)
Minimum compressive resistance at yield or 10% deformation, whichever occurs first (with skins intact), psi (kPa)	5.0 (35)	10.0 (69)	13.0 (90)	15.0 (104)	25.0 (173)
Thermal resistance of 1.00-in.(25.4mm) thickness, min, $F.ft^2.h.Btu$ ($K.m^2/W$) Mean Temperature: 75 ± 2 ºF (24 ± 1 ºC)	3.1 (0.55)	3.6 (0.63)	3.8 (0.67)	4.0 (0.70)	4.2 (0.74)

In the US and Canada, ASTM C 578 (Table 2.2) presents EPS heat insulation, thermal resistance, and the compressive strength for different densities of EPS geofoam. The classification of EPS types for ASTM C 578 is slightly different from ASTM D 6187 (Table 2.1).

In order to meet the requirements of the compressive strength that are required in ASTM C 578, polystyrene heat insulation board offer compressive resistance with 10% distortion when tested in conformity with the requirements of ASTM D 1621. ASTM C 578 Type I material whose density is usually 0.9pcf is the most appropriate material to be used in foundation or the construction of the wall where the pressure requirements of the insulation values are the least. According to the creep testing of geofoam specimens at various pressure levels, 50% of the overall compression resistance was identified as the upper limit of consideration working stress for designing with geofoam (Srirajan, 2001).

2.2.4 Creep Behavior

Creep is an important consideration for designing with EPS geofoam.

Sun (1997) performed creep tests on 50mm cube of average 18kg/m^3 density EPS geofoam using cantilever static loading system. For sustained pressure of 30% of 85kPa compressive working strength at 5% strain, creep strain after 461days were 0.8%, and for 50% strain were 3%, and for 70% the creep strain were 14.4%.

Compression loads of 30% or less would have little impact on the creep deformation performance.

Duskov (1997) also did creep tests and achieved similar results from cylindrical of geofoam samples. In the first set of experiments, a specimen with a diameter of 200mm, height of 100mm and density of 20kg/m^3 was tested with a 20kPa pressure. After 400days, the strain value was only 0.20% and most of the strains happened in the very first day. In the second set, however, the specimen with diameter of 100mm, height of 300mm and density of 15 and 20kg/m^3 was loaded to10kPa and 20kPa respectively. The result of the former (10kPa pressure) was 0.25% and the later (20kPa pressure) was 0.5% after 400days. The instant strains under the 20 and 10kPa were 0.3 and 0.15%, respectively. There was little difference in the creep behavior with the two 15 and 20kg/m^3 different specimen densities.

Sheeley (2000) reported creep test results for 50mm cubes with 21kg/m^3 density, and subjected to 30%, 50%, and 70% of compression strength at 5% strain. The investigation showed that for 30% and 50% loading, the strain mostly occurred in the first two days. For the sample loaded to 30% of compressive strength, a total strain of 0.95% occurred in 500 days in which 66% was observed in the first day. For the sample loaded at 50% compressive strength, a total strain of 1.35% occurred in 500 days in which 68% was observed in the first day. For the

specimen loaded at 70% compression strength, there was much more creep deformation and about 4% of the strain occurred in the first day. A total of 22% strain occurred in the following 500days.

Working stress values are selected to limit creep deformations to acceptable levels over the EPS service life. Creep is negligible if the initial strain does not exceed 0.5% (Frydenlund and Aabøe 2001). At working stress level of less than 50% of the yield, geofoam is found to have insignificant creep deformation (Negussey and Jahanandish 1993).

Creep deformations are minimized or essentially avoided in most design procedures by limiting allowable loads or surcharge pressures to below the prescribed compressive strengths of the EPS geofoam (usually 30% of the strength at 5 or 10% strain). A commonly used design approach developed in Norway is based on limiting the allowable surcharge load over geofoam to 30% of the compressive strength at 5% strain. If geofoam is exposed to loads greater than 50% of the compressive strength at 5% strain, larger creep deformations occur.

CHAPTER 3

PRE-STRAIN INDUCED ANISOTROPY OF EPS GEOFOAM

The operation of heavy machinery or trucks during construction may result in the pre-straining of EPS fills. Pre-straining of the EPS fills may also result from seismic loading during an earthquake. In addition, improper working loads may produce strains outside of the elastic range. In most embankment construction, EPS blocks become subjected to higher level of stress during placement and compaction. However, the effect of prior pre-stressing has not been closely investigated. It is of great importance to closely understand the stress-strain behavior of EPS while under cyclic loading within and outside of the elastic range. In this investigation, EPS blocks of different densities were tested separately and in combination in loading and reloading experiments. Comparison between densities and modulus changes due to pre-strain history are examined.

3.1 Background

Use of EPS as a lightweight alternative material is widespread not only in the US but also in other parts of the world. EPS geofoam is commonly installed under pavement structures and over soft and compressible soils to minimize settlements. However, unanticipated strains may exist either due to machine operation during construction or confining stress effects. Stresses beyond the elastic limit of EPS material would induce plastic strains and hence induce

31

anisotropy. Thus, the effect of such stress or strain anisotropy on EPS geofoam performance should be investigated to appropriately design geofoam fills.

The design of EPS geofoam fill is based on the premise that strain induced in the fill remains between 1 and 2 %. In addition, EPS geofoam is assumed to be isotropic inherently. The property of EPS blocks was also found to show anisotropy (Amsalu, 2014). Anisotropy is the property of being directionally dependent, as opposed to isotropy which implies identical properties in all directions. Anisotropy can be defined as a difference when measured along different axes in the EPS material's physical or mechanical properties. Two different forms of anisotropy in EPS geofoam can be distinguished, namely inherent and induced.

Inherent anisotropy is an attribute acquired in the material manufacturing process. Kutara et al. 1989 reported that specimens loaded perpendicular to the direction of fabrication showed higher deviator stresses at failure than those loaded parallel to the direction of fabrication. The compressibility of EPS geofoam is highly affected by the shape of the cells. Cells close to the mold wall are usually flattened due to the molding processes. If the compressive loads are applied perpendicular to the direction of stretching, the flattened cells will be flattened more and smaller values of compressive strength are obtained (BASF 1998). Therefore, a higher bearing capacity can be expected if the foam is loaded

32

perpendicular to the direction of fabrication. This can be explained as the effect of inherent anisotropy of EPS blocks. Isotropy is regardless of material dimension. If there is inherent anisotropy, it tends to be small. Geofoam is generally considered to be inherent isotropy.

Induced anisotropy is due to the strain associated with an applied stress. It is hard to find a relatively easy experimental technique for demonstrating the degree of anisotropy that exists at any loading level in EPS blocks. A separation of the effects of inherent and induced anisotropy can be achieved by treating the anisotropy of the original EPS material as the inherent anisotropy. The stress-strain behavior of this original EPS sample can then be compared with another EPS sample subjected to an identical stress path and then reloaded with or without change in the principal stress direction. Here the effect of an unloading stress path is not included. Defining the degree of anisotropy which exists on reloading is not a simple matter of initial stiffness and volume compressibility exhibited on reloading with different principal stress directions. The variation in modulus during reloading is complex and indicates a varying persistence in the influence of the anisotropy existing at the beginning of reloading. The purpose here is not primarily to be quantitative, but rather to illustrate the effect of pre-loading, which may result in the induced anisotropy on EPS geofoam. The effect of induced anisotropy on

EPS characteristics was investigated by compression tests conducted on pre-stressed foam. The practical significance of induced anisotropy was also discussed.

3.2 Test Procedures

3.2.1 Tests on Exhumed Samples from Field

The I88 culvert at Carrs Creek in the town of Sydney, Delaware County, NY collapsed during a flood in June 2006 and was rapidly reconstructed by using EPS geofoam fill as light weight material. EPS geofoam of 20 kg/m^3 (1.25pcf) density was selected and placed on soil bedding over the culvert in three layers for 2.7m height on the eastbound embankment and two layers for 1.8m on the westbound embankment. A total of 3.3m of compacted soil and pavement was placed over the geofoam in the east bound and 2.4m on the west bound. The settlement of the reconstructed pavement on the culvert became evident shortly after the completion of the construction and the EPS geofoam fill was eventually removed.

Laboratory tests were performed on fresh samples (Figure 3.1) with nominal density of 20 kg/m^3 (1.25pcf) provided by the geofoam supplier as well as on the exhumed blocks recovered on removal of the geofoam fill. From the exhumed big blocks, which were pre-strained, 2in cube samples were cut from the middle by noting the orientation of pre-loading. All the unconfined compression tests were done on 2in cube samples as per ASTM D 1621 maintaining a strain rate of 10% per minute. Tests were done both in the same and orthogonal direction to the pre-

loading direction in the lab and in the field. Figure 3.1 clearly shows the dimension

and loading direction of tested EPS blocks; starting from known virgin, pre-

strained, pre-strained and rotated states.
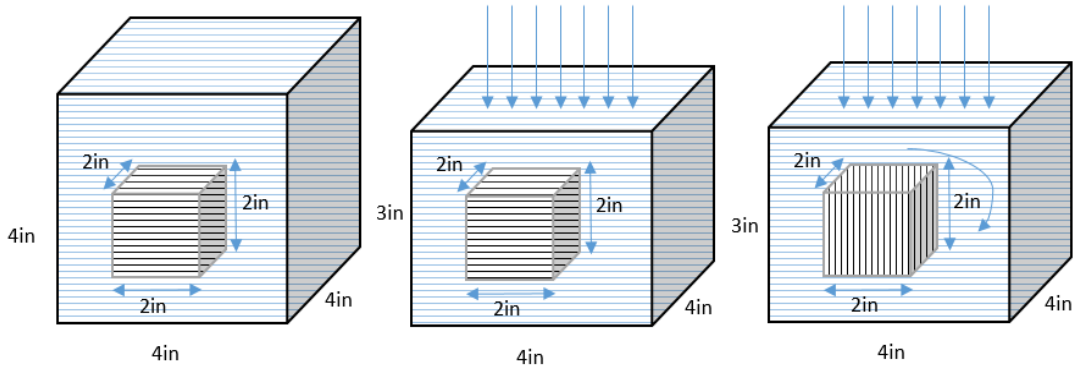
Figure 3.1 (a)   Figure 3.1 (b)   Figure 3.1 (c)

Virgin Sample (V)   Pre-strained Sample Loaded   Pre-strained Sample Loaded

(Density of 1.25pcf)   in the Same Direction   in the Orthogonal Direction

Figure 3.1. Dimension and Loading Direction of Tested EPS Blocks
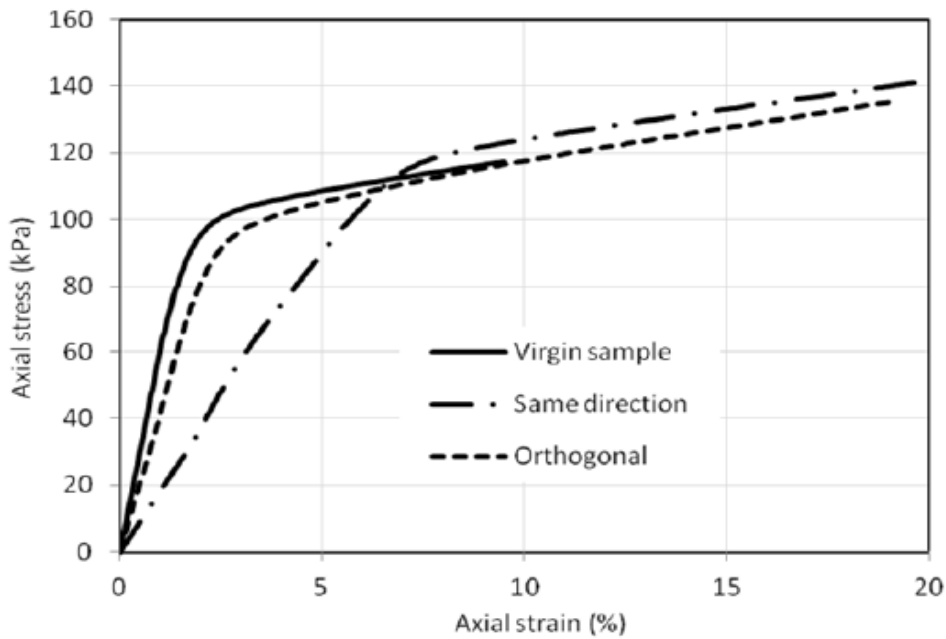
Figure 3.2. Unconfined Compression Results of Virgin Sample and Pre-loaded

Samples

The practical implications of tests on virgin samples and pre-strained to 10%

samples can be seen in Figure 3.2. The initial modulus of virgin sample and the

pre-strained sample loaded to the orthogonal direction are close. The pre-strain

EPS block has decreased initial modulus and lower work stress when loaded to the

same direction as pre-straining.
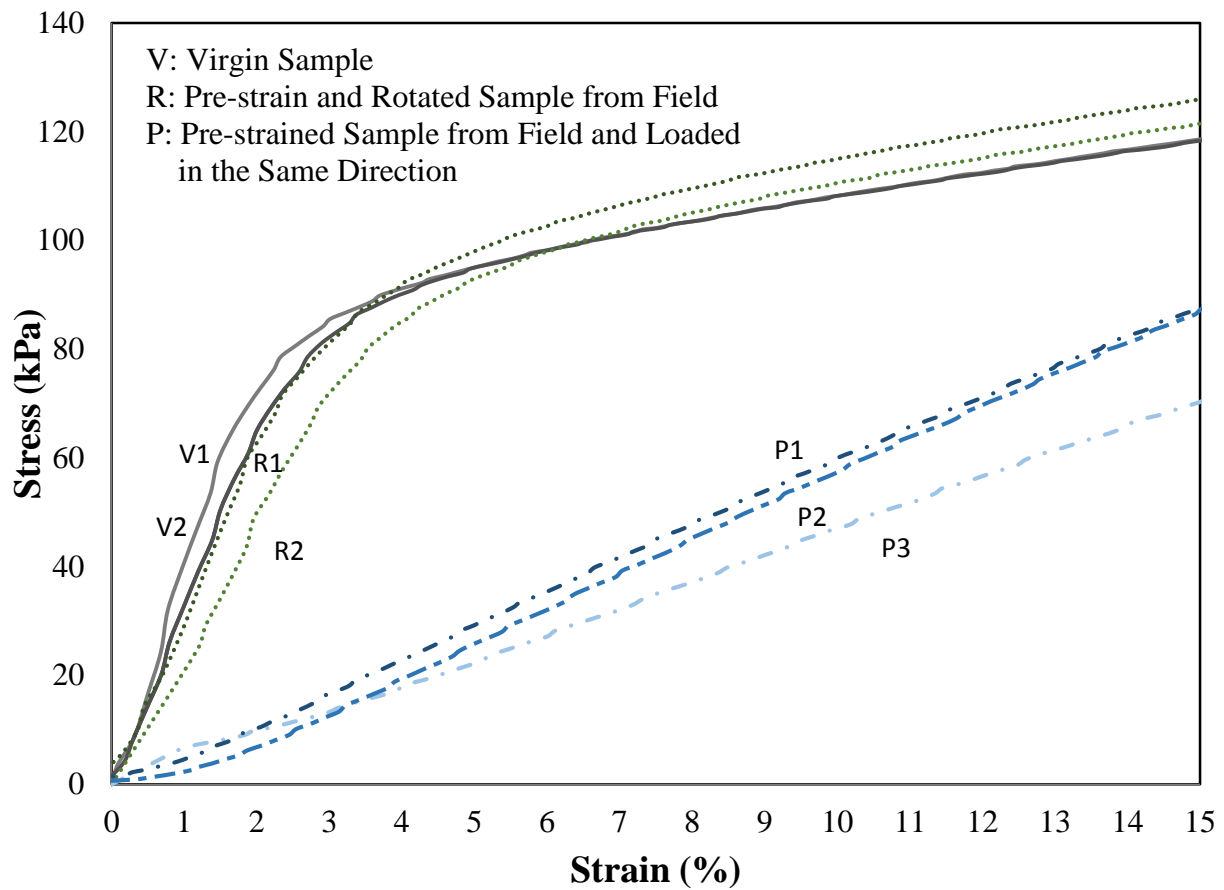
Figure 3.3. Unconfined Compression Results for Pre-strained Samples Cut from
the Exhumed Blocks and Virgin Samples

Figure 3.3 shows the effect of pre-stressing on the stress-strain relation when

the samples were reloaded in the same direction as the pre-loading and in the

orthogonal direction to the pre-straining for the field samples from Carrs Creek. The modulus ranges of the virgin samples, the pre-strained and rotated field samples, and the pre-strained field samples who loaded in the same direction are 3.2~3.8MPa, 2.3~3.0MPa and 0.47~0.59MPa respectively. The compression stress of the virgin samples, the pre-strained and rotated field samples, and the pre-strained field samples that were loaded in the same direction at 1% strain are 34~41kPa, 21~28kPa and 2~6kPa respectively. The compression stress of the virgin samples, the pre-strained and rotated field samples, and the pre-strained field samples that were loaded in the same direction at 10% strain are 108kPa, 112~115kPa and 46~60kPa respectively. The test results reveal that the initial modulus for loading in the pre-strained direction (P_1, P_2 and P_3) were much lower than for the samples loaded in the direction transverse (R_1 and R_2) to the pre-strain and for virgin loading conditions (V_1 and V_2). The observation of inferior strengths at 1% strain and strengths at 10% strain as for the pre-strained samples could be attributed to the induced anisotropy that were caused by prior loading beyond yield, and crushing of the EPS microstructure. The stress-strain curves of the tests that were conducted in the orthogonal direction (R_1 and R_2) to the pre-straining direction remained relatively unaffected, with just minor strength degradation compared to the curves of virgin loading conditions (V_1 and V_2).

37

The practical implications of such tests can be interpreted from Figure 3.2 and 3.3. The anisotropic behavior of EPS geofoam can affect the deformation characteristics of the material. The EPS geofoam fill material that has controlled pre-pressure is of great importance in decreasing the original deformation while the permissible pressure scope increases. If analysis of EPS fill is based on parameters obtained from virgin samples, the deformations computed would be small due to higher values of initial modulus. However such computed deformations would be greater if some percentage of pre-straining EPS geofoam during construction or operation had occurred.

3.2.2 Lab Tests on Different Pre-strain Conditions

In order to investigate the effect of different pre-strain states for different loading and reloading conditions, supplementary laboratory tests were conducted on fresh samples. This section presents deformation-based load to pre- and post-yield stages at test strain rate of 10% per minute and up to 30% strain limit.

3.2.2.1 Test Specimens

The test samples were cut into 2in cubes (As shown in Figure 3.1 (a)) by using the hot wire cutter in the lab. Two different nominal densities of EPS types, 1.25pcf and 2pcf, were used in the tests (As shown in Figure 3.4). The summary of the test information is shown in Table 3.1.

1.25pcf (Type VIII)   2pcf (Type IX) EPS

Figure 3.4. 1.25pcf (Type VIII) and 2pcf (Type IX) EPS Blocks Used in Tests

Table 3.1. Test Information for the EPS Samples

Test Parameters		
Sample Dimension	2in×2in×2in	
EPS Type (Density, pcf)	VIII (1.25)	IX (2)
Test Strain Rate	10%/min	
Test Strain Limit	30%	

3.2.2.2 Tests Program

Different loading and reloading methods were used to investigate the pre-strain effects on EPS strength for both 1.25 and 2pcf densities. The test programs were set as the following three types: 1) Load/Unload and reload cycles were

39

performed in the pre-yield stages; 2) Load post yield to 30% strain before full

unloading and reloading cycles; 3) Load post yield to 30% strain before applying

partial unloading and reloading cycles.

3.2.2.3 Characteristics of the Stress-Strain Behavior of EPS Geofoam

The initial moduli and moduli after 4 cycles of loading and unloading are

shown in Table 3.2, Figure 3.5, Figure 3.6 and Figure 3.7.

Table 3.2. Summary of the Reloading Test Results

Sample Number	Test Description	Initial Modulus E_0 (MPa)		Test Description	E_1 (MPa)		E_2 (MPa)		E_3 (MPa)		E_4 (MPa)	
	(pcf)	1.25	2	(pcf)	1.25	2	1.25	2	1.25	2	1.25	2
1	Load to post yield stage	3.93	6.98	Full unloading and reloading	1.49	2.43	1.12	2.86	1.20	2.76	1.22	2.82
2		2.83	8.00		1.12	2.49	0.91	2.94	1.04	3.10	0.84	3.24
3		3.85	6.97		1.24	2.76	1.49	2.95	1.50	2.96	1.58	3.04
4		3.75	7.12		1.32	2.66	1.43	2.89	1.66	2.92	1.76	3.01
5		3.83	8.25	Partial unloading and reloading	2.01	7.09	2.41	7.31	2.88	7.28	2.81	7.01
6		3.96	7.57		2.44	5.66	2.63	6.76	3.03	6.55	2.72	6.63
7		3.21	8.04		2.45	6.23	2.73	6.30	2.59	7.63	2.63	6.61
8		2.72	7.00		2.60	6.21	2.96	7.04	3.17	7.70	3.37	8.20
9	Load in pre-yield stage	3.03	9.61		4.03	9.64	4.13	10.50	4.22	9.65	4.12	11.10
10		2.40	8.28		3.35	9.99	3.50	9.90	3.02	10.15	3.78	9.27
11		3.02	8.25		3.55	10.04	3.78	9.31	3.15	9.00	3.57	9.89
12		3.05	8.50		3.87	10.54	3.84	10.41	3.51	10.31	3.87	9.93
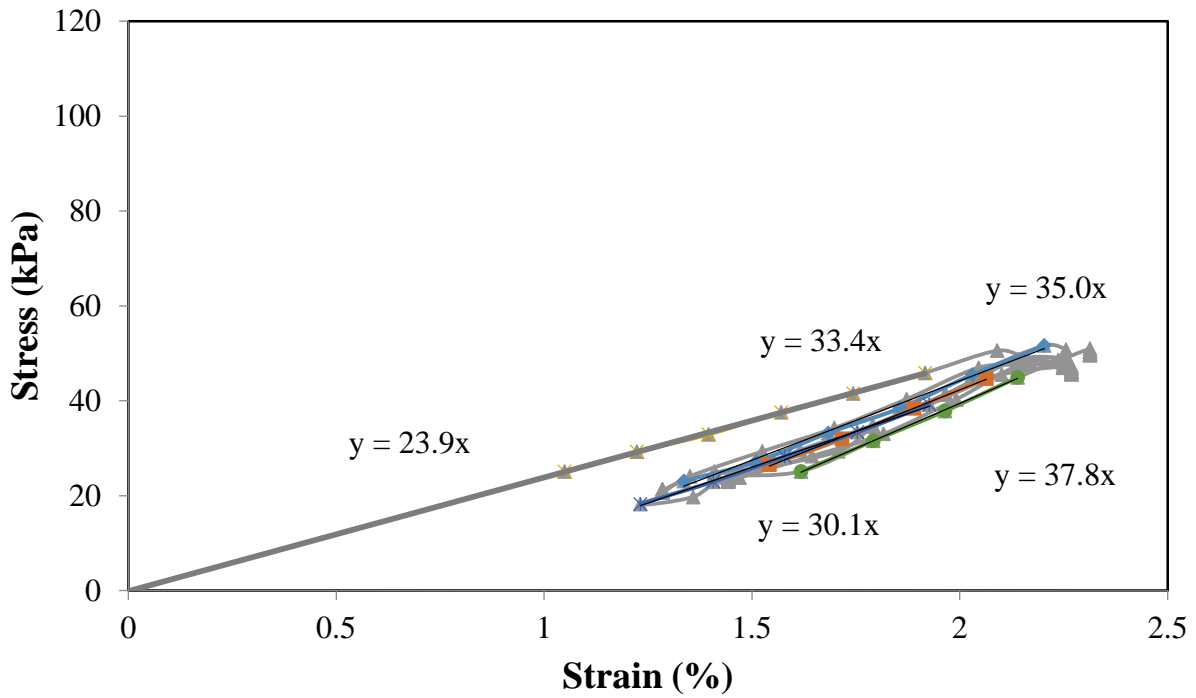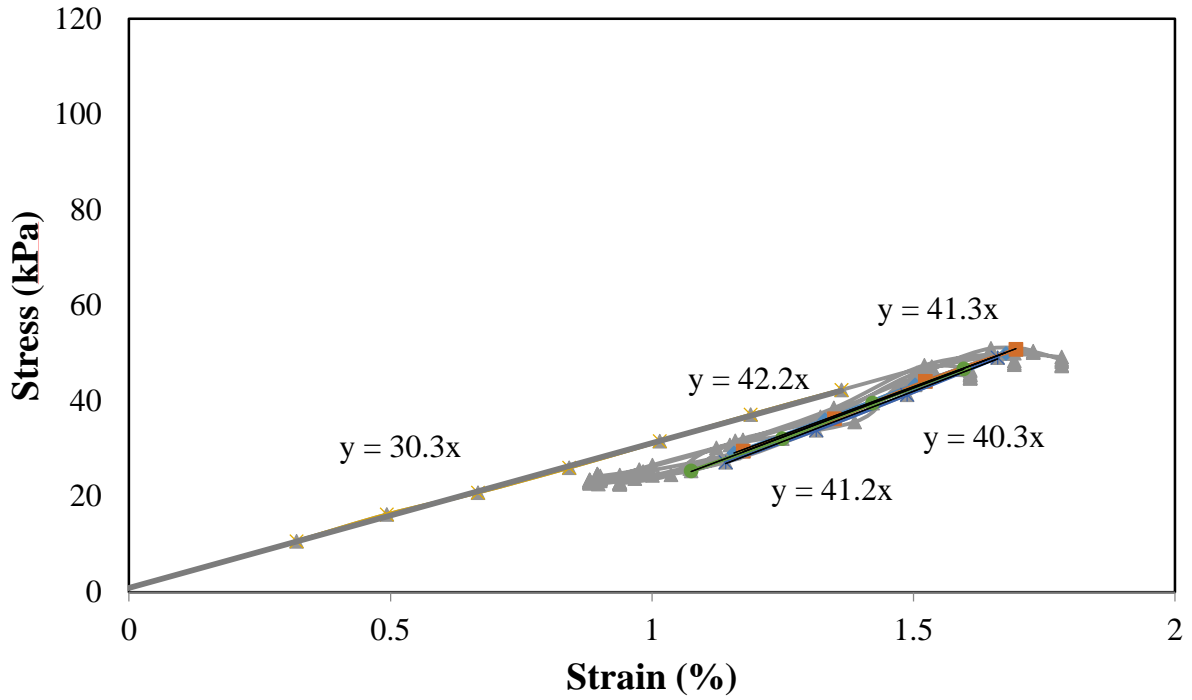
Figure 3.5 (1). Stress-Strain Curves for 1.25pcf EPS

Figure 3.5. Unconfined Compression Test for Load and Unload

In/Near Pre-yield Stages
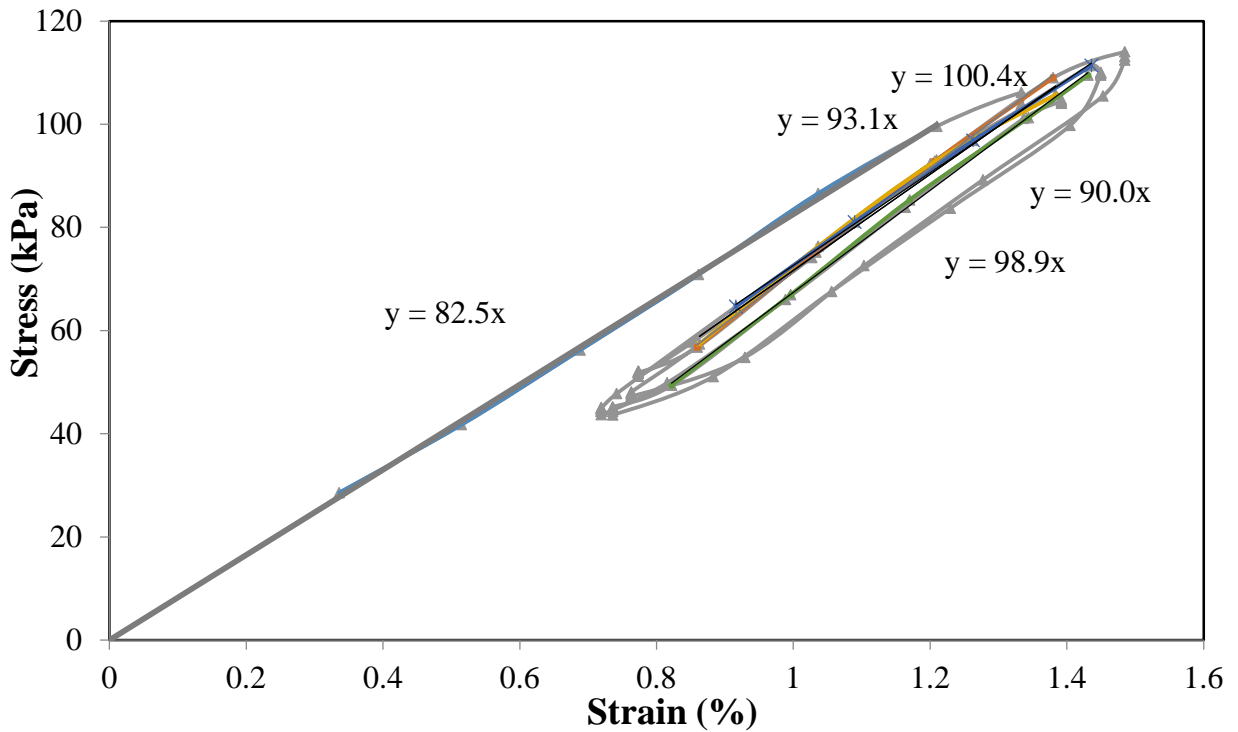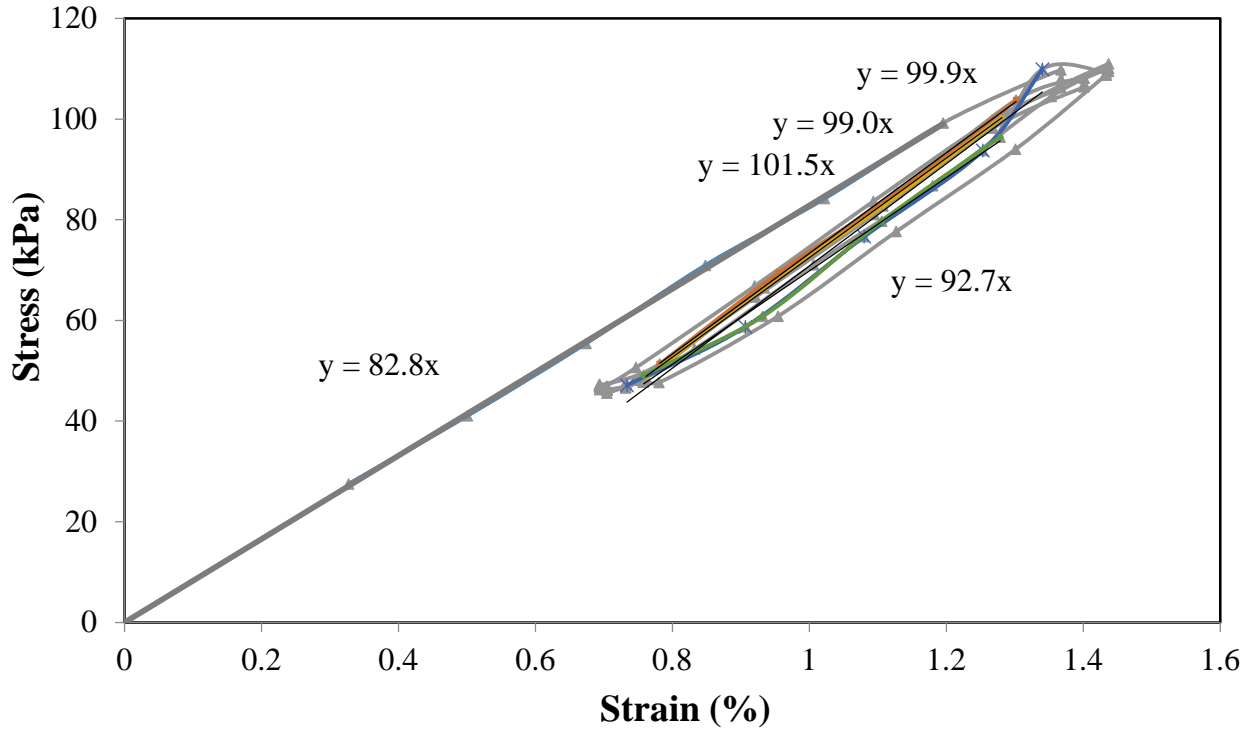
Figure 3.5 (2). Stress-Strain Curves for 2pcf EPS

Figure 3.5. Unconfined Compression Test for Load and Unload

In/ Near the Pre-yield Stages

Figure 3.5 is the stress-strain plot for four cycles of unloading and reloading to near yield (1-2%) at strain rate of 10%/minute for both 1.25 and 2pcf geofoam densities. The load and unload cycles were near yield and in pre-yield stages. The cyclic loading and unloading did not change the initial modulus of elasticity. This suggests EPS geofoam behaved elastically when the axial strain limit remained below 2%. Similar conclusions were obtained from previous researches. Flaate (1987) reported cyclic loading tests on EPS geofoam withstood an unlimited number of cyclic loads as long as the loads were below 80% of the compressive strength. Van Dorp (1988) also reported that there was no change in the initial tangent modulus when a $20kg/m^3$ EPS was subjected to 2 million cycles of straining between 0 and 1% at a cyclic strain rate of 10Hz.
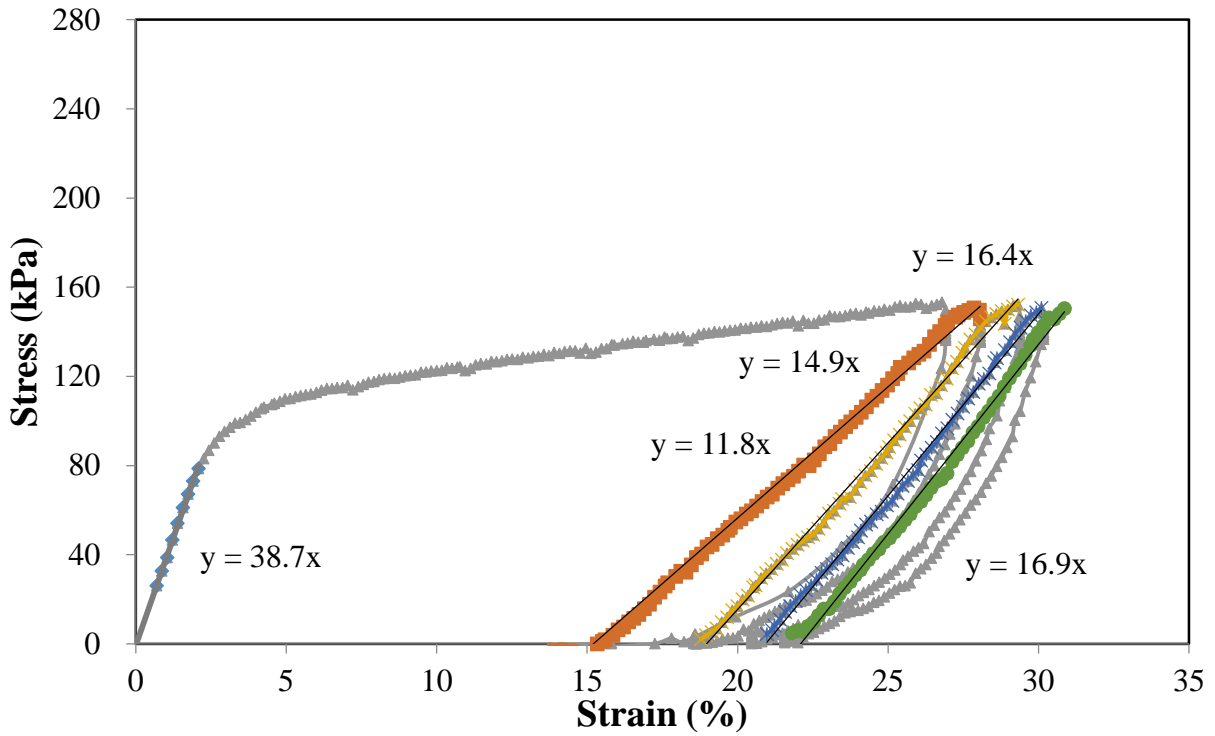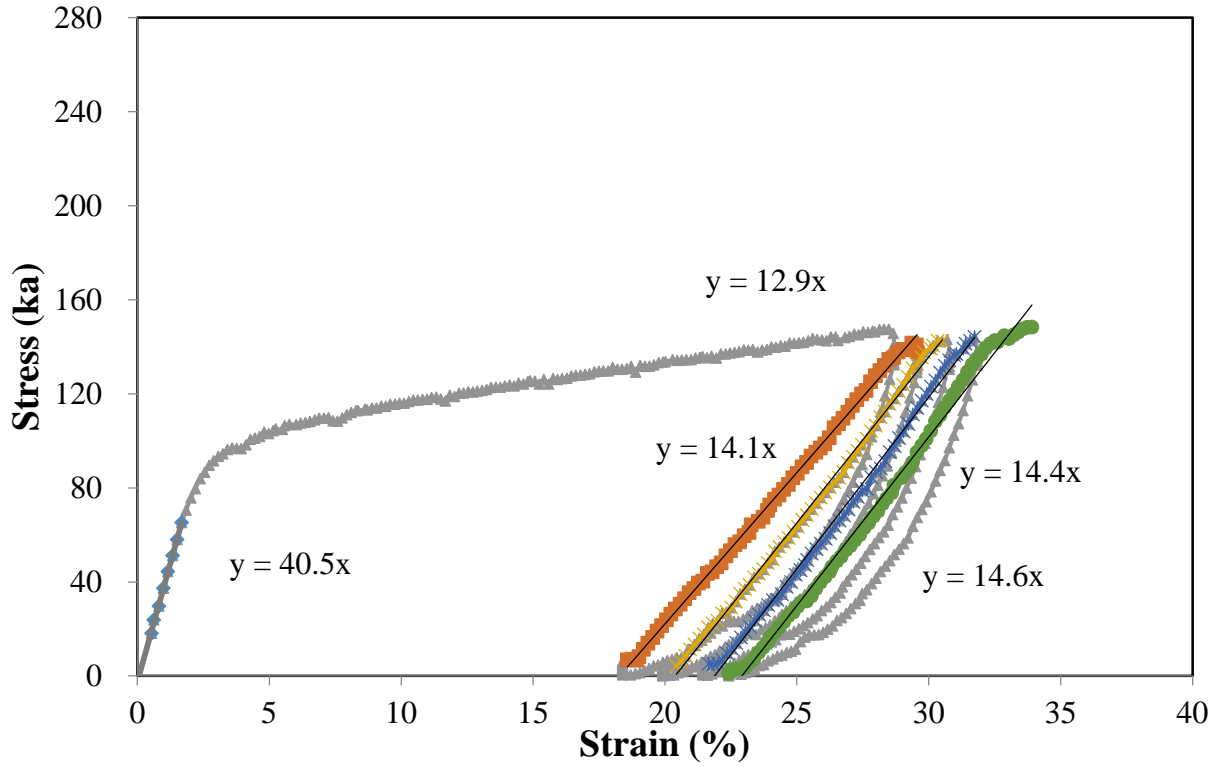
Figure 3.6 (1). Stress-Strain Curves for 1.25pcf EPS

Figure 3.6. Unconfined Compression Test for Post-yield Loading to 30% Strain

Before Full Unloading and Reloading Cycles
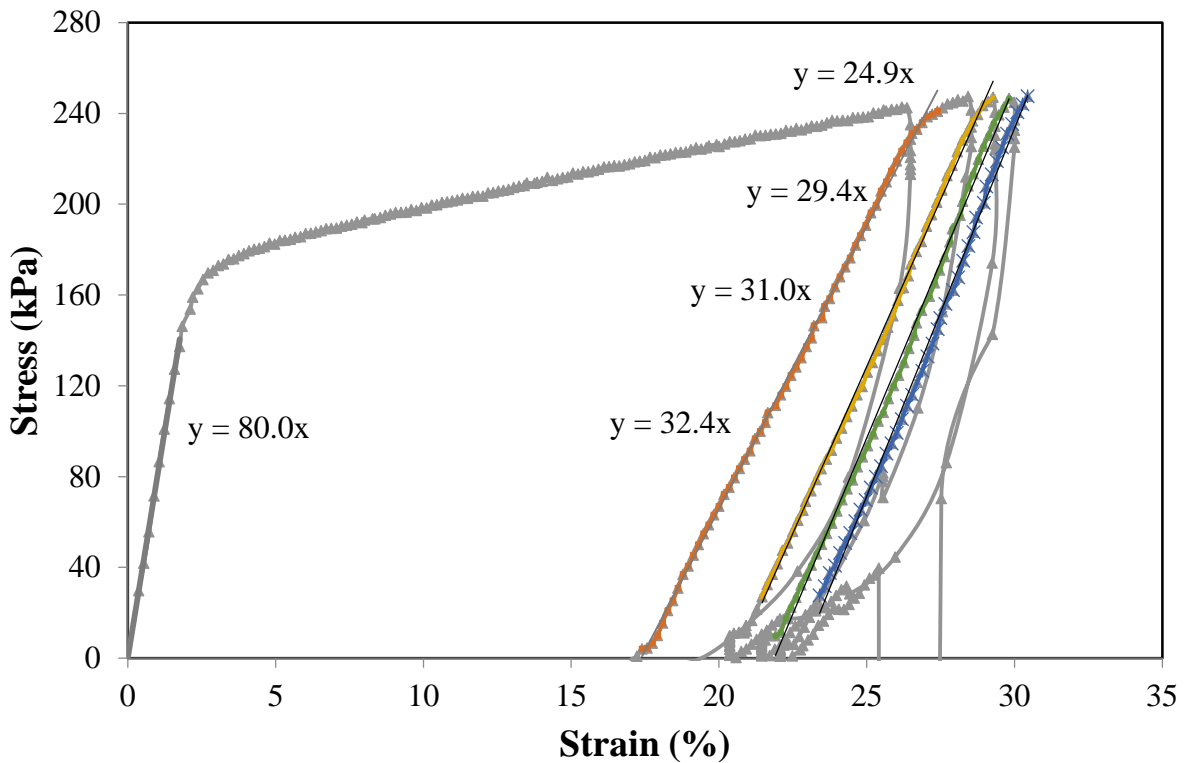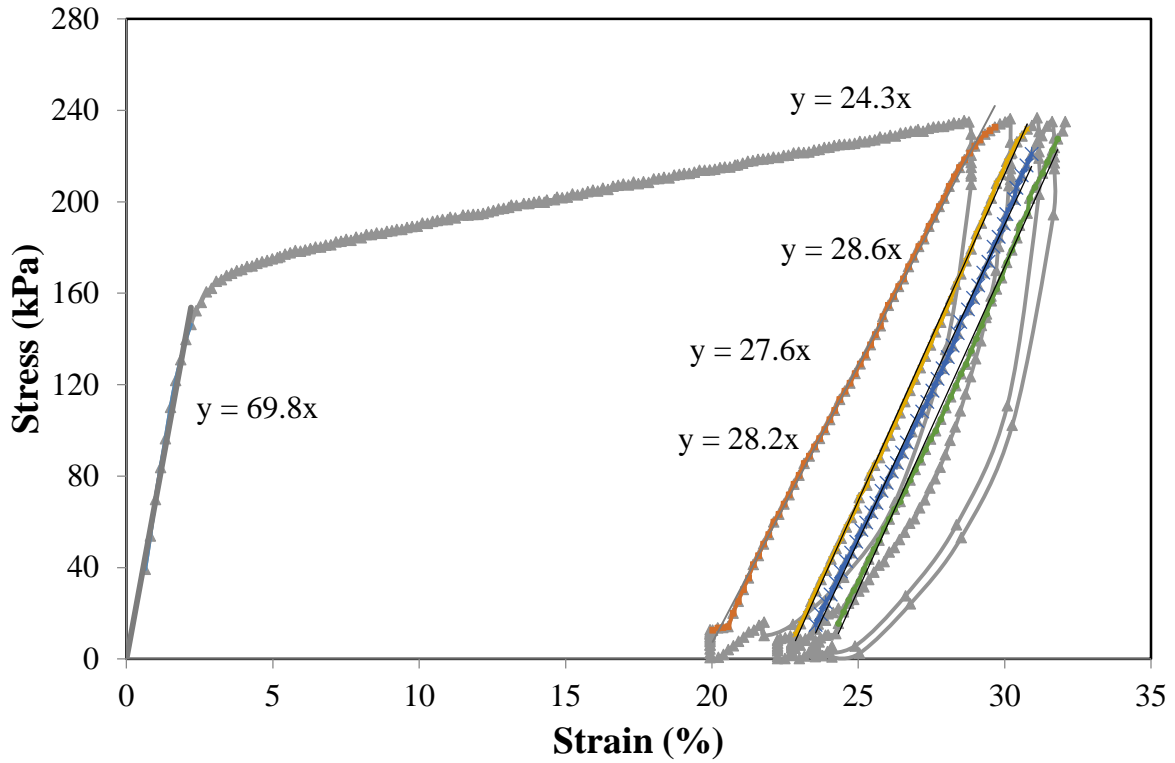
Figure 3.6 (2). Stress-Strain Curves for 2pcf EPS

Figure 3.6. Unconfined Compression Test for Post-yield Loading to 30% Strain

Before Full Unloading and Reloading Cycles

Figure 3.6 shows the stress-strain behavior of the EPS blocks for post-yield loading to 30% strain before full unloading and reloading cycles for both 1.25 and 2pcf geofoam densities. The EPS blocks were first loaded to 30% strain level. The reloading cycles shown in Figure 3.6 started from unloading to 0kPa stress, which means the EPS blocks were completely unloaded. The plastic strain accumulation and reloading modulus degraded relative to the initial elastic modulus. Loading to post-yield and full unloading and reloading cycles produced significant modulus degradation of 56~68% of initial modulus for both 1.25 and 2pcf geofoam densities. There is little difference between the modulus of repeated loadings.
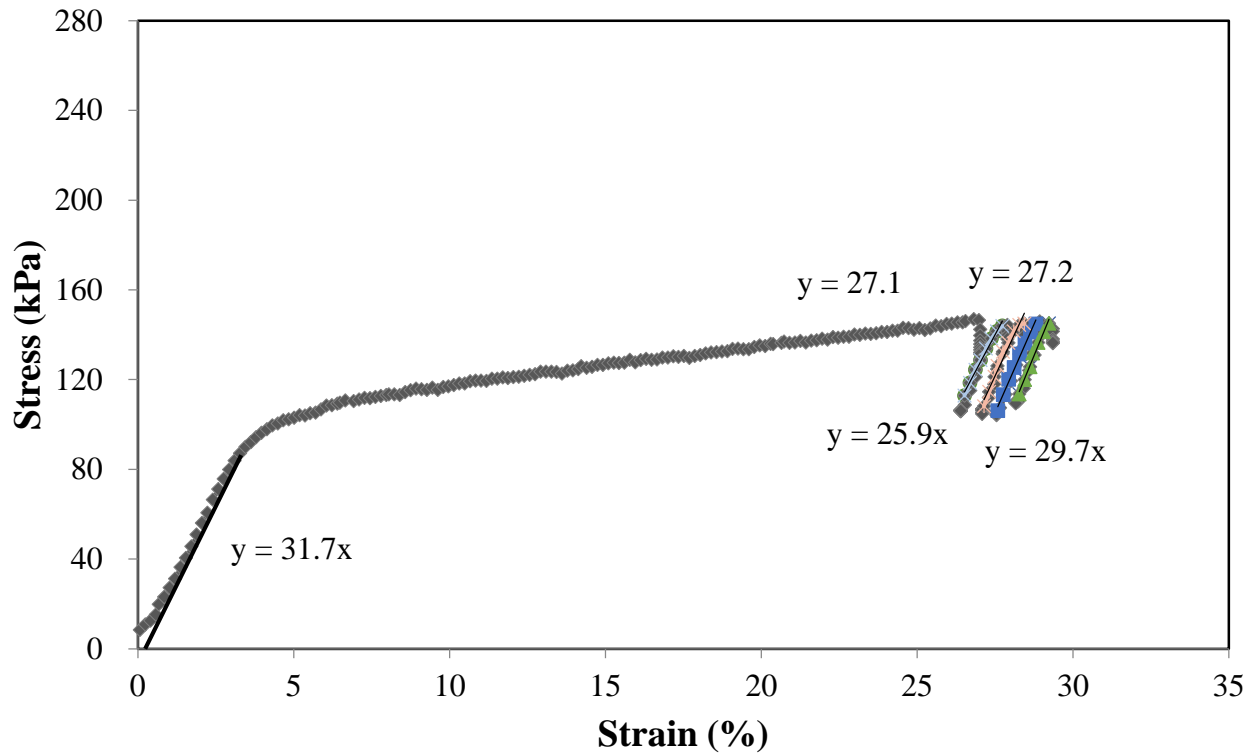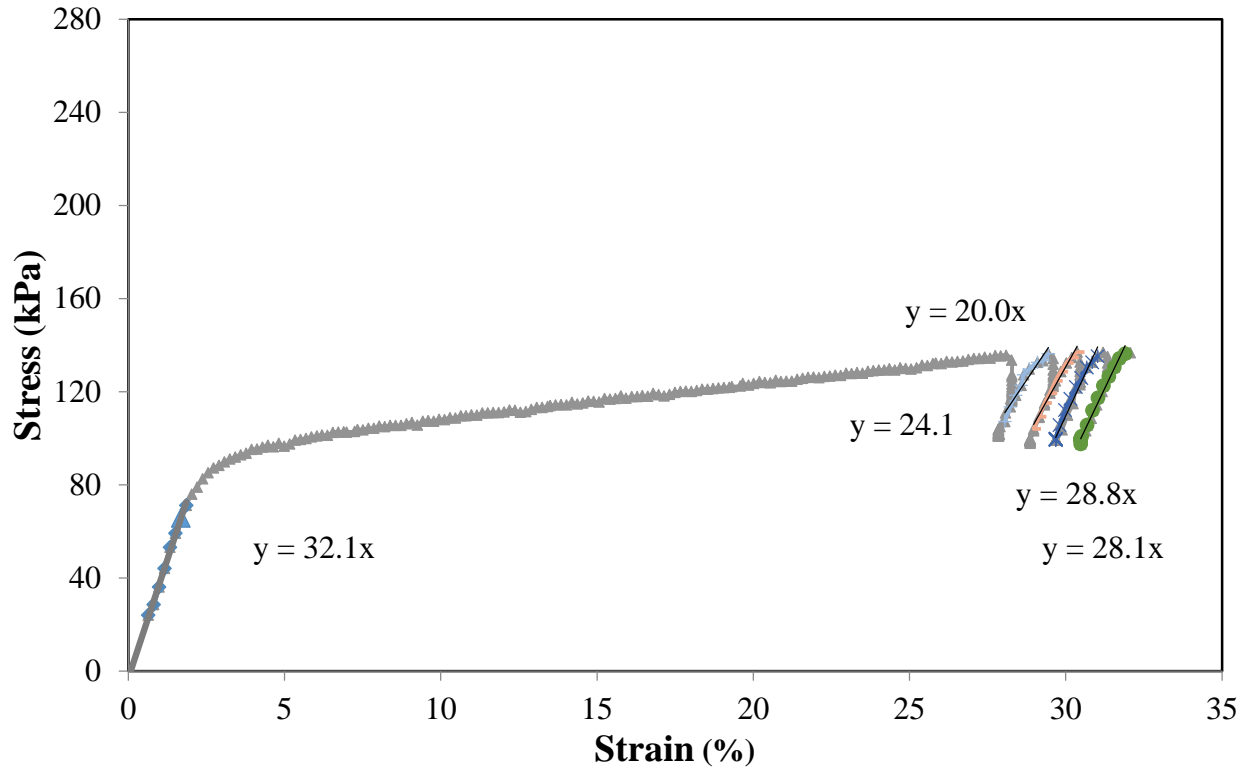
Figure 3.7 (1). Stress-Strain Curves for 1.25pcf EPS

Figure 3.7. Unconfined Compression Test for Post-yield Loading to 30% Strain

Before Partial Unloading and Reloading Cycles
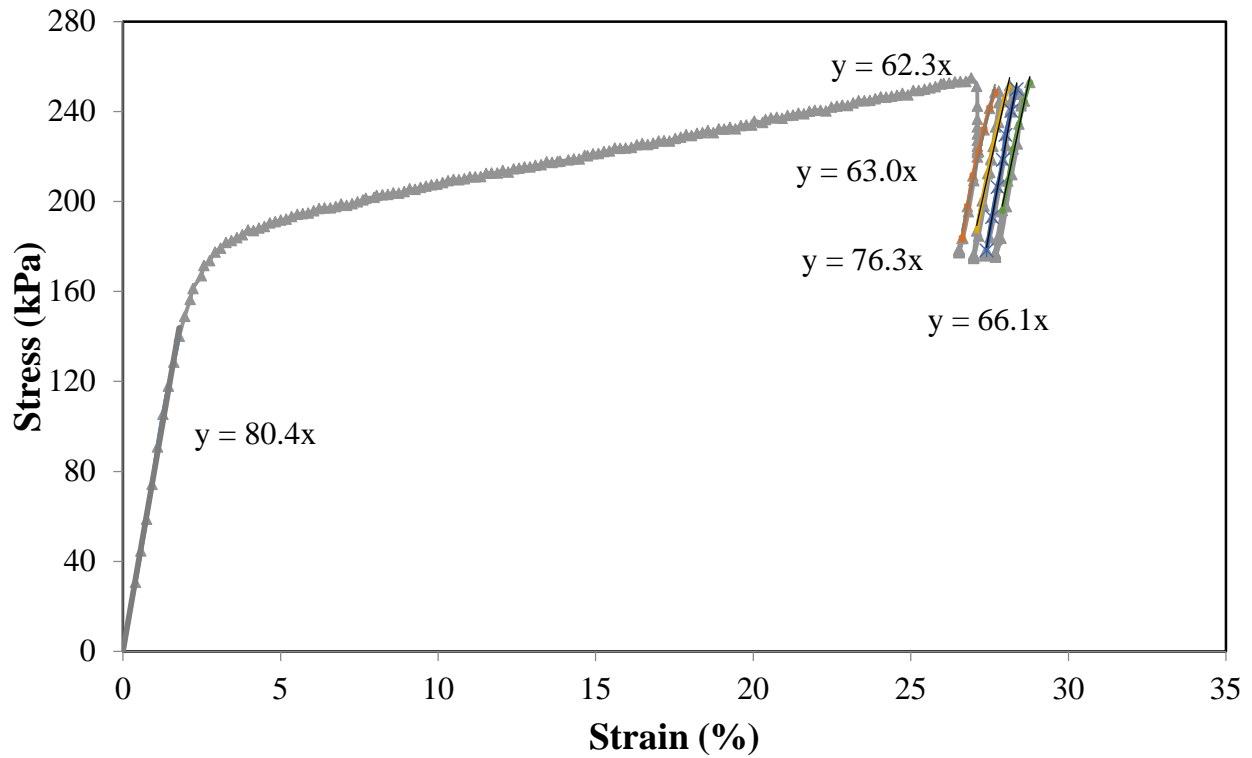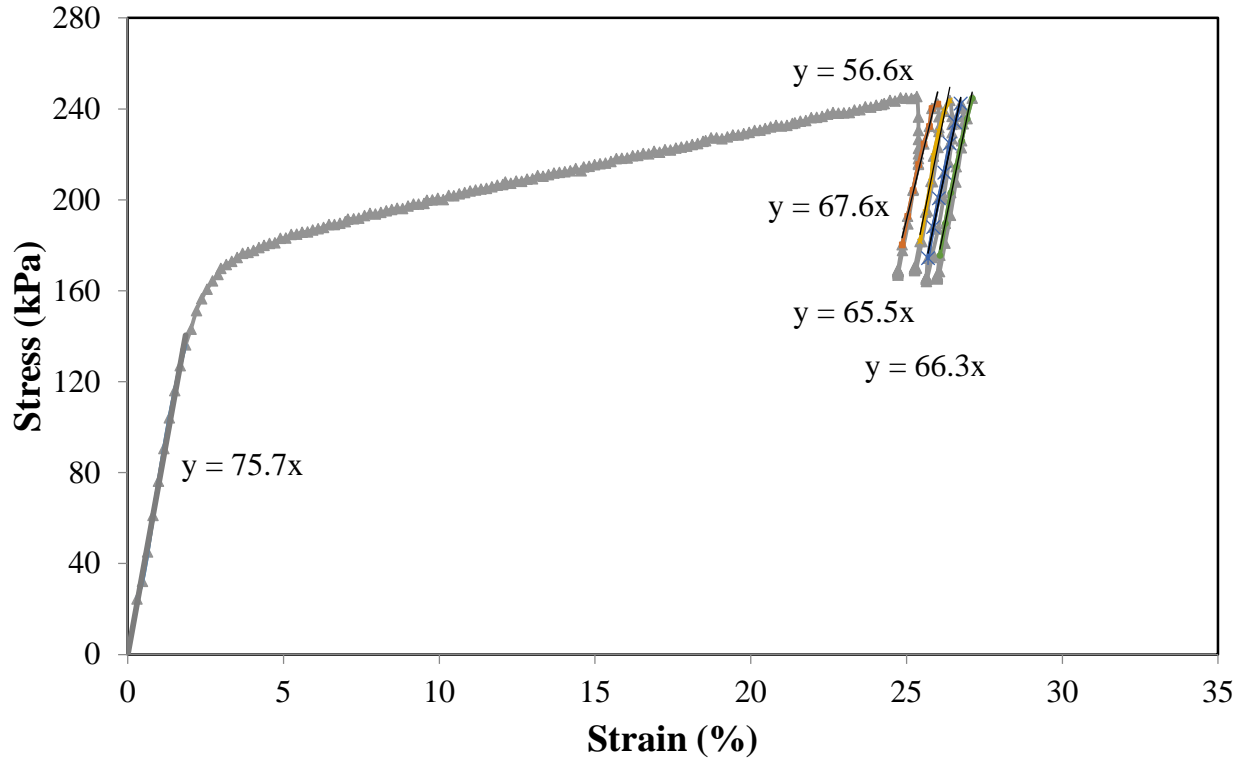
Figure 3.7 (2). Stress-Strain Curves for 2pcf EPS

Figure 3.7. Unconfined Compression Test for Post-yield Loading to 30% Strain

Before Partial Unloading and Reloading Cycles

Figure 3.7 shows the stress-strain behavior of the EPS blocks for loading post-yield to 30% strain before partial unloading and reloading cycles. The EPS blocks were firstly loaded to 30% strain level, then unloaded by 40kPa stress from the first maximum loading stress and reloaded four times afterwards. For this condition, loading and unloading occurred at a strain level outside of the elastic range. There were only 4~20% modulus degradation for the partial unloading and reloading cycles. Compared to the full unloading and reloading cycles, the reloading modulus degradation is less for partial unloading and reloading cycles.
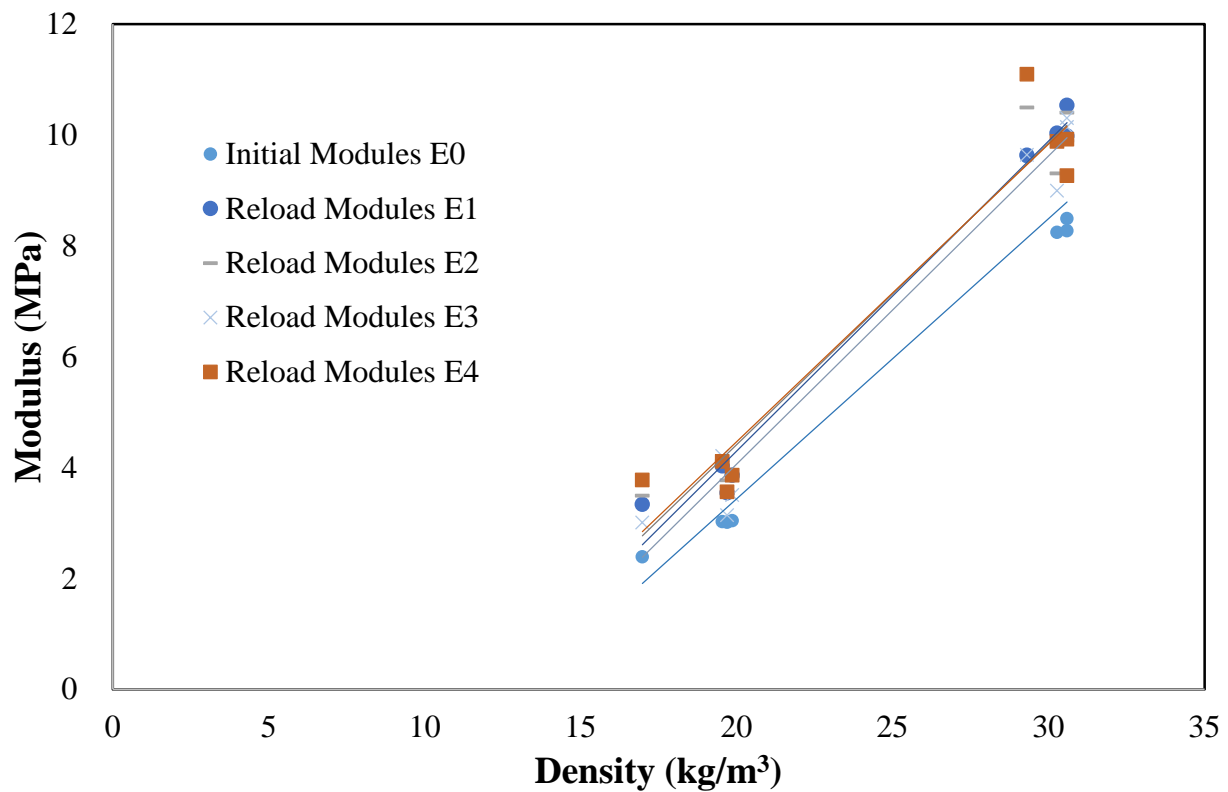
Figure 3.8. Test Results for Loading and Unloading to 40% Working Stress and Below Yield
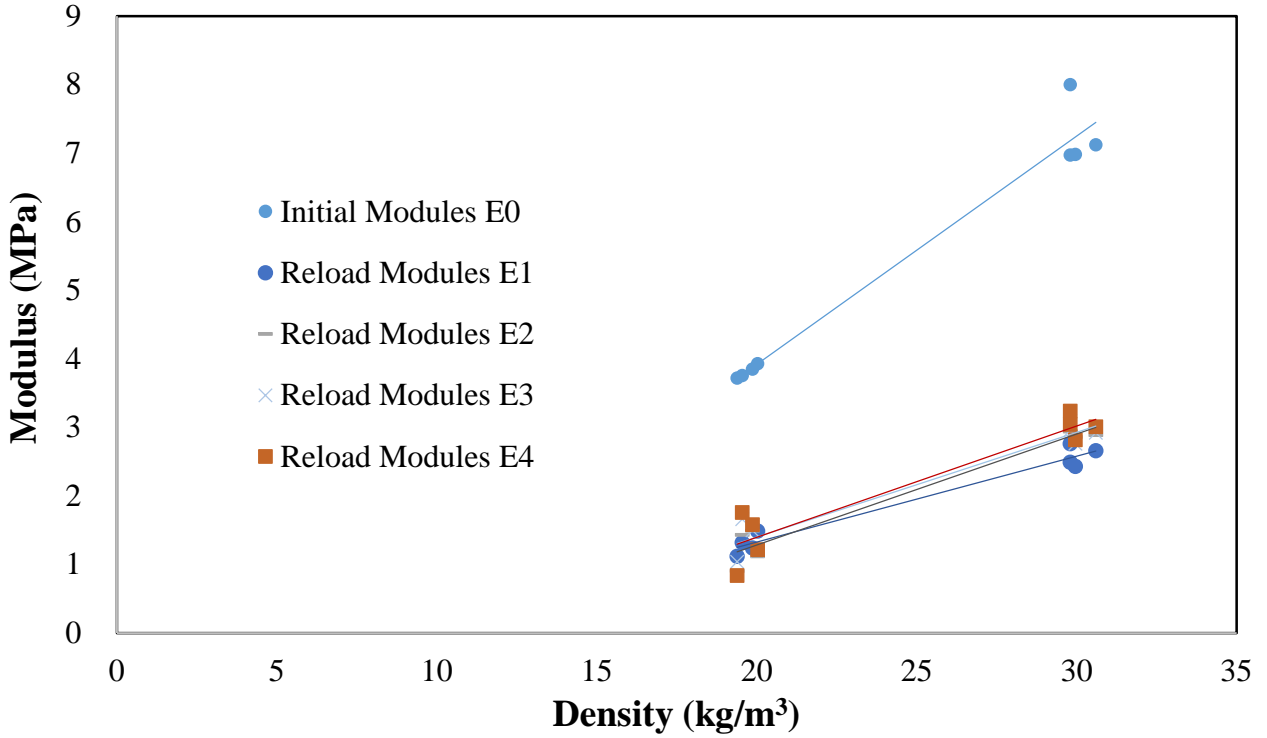
Figure 3.9. Test Results for Loading to Post-yield Stage and Full Unloading and Reloading Cycles
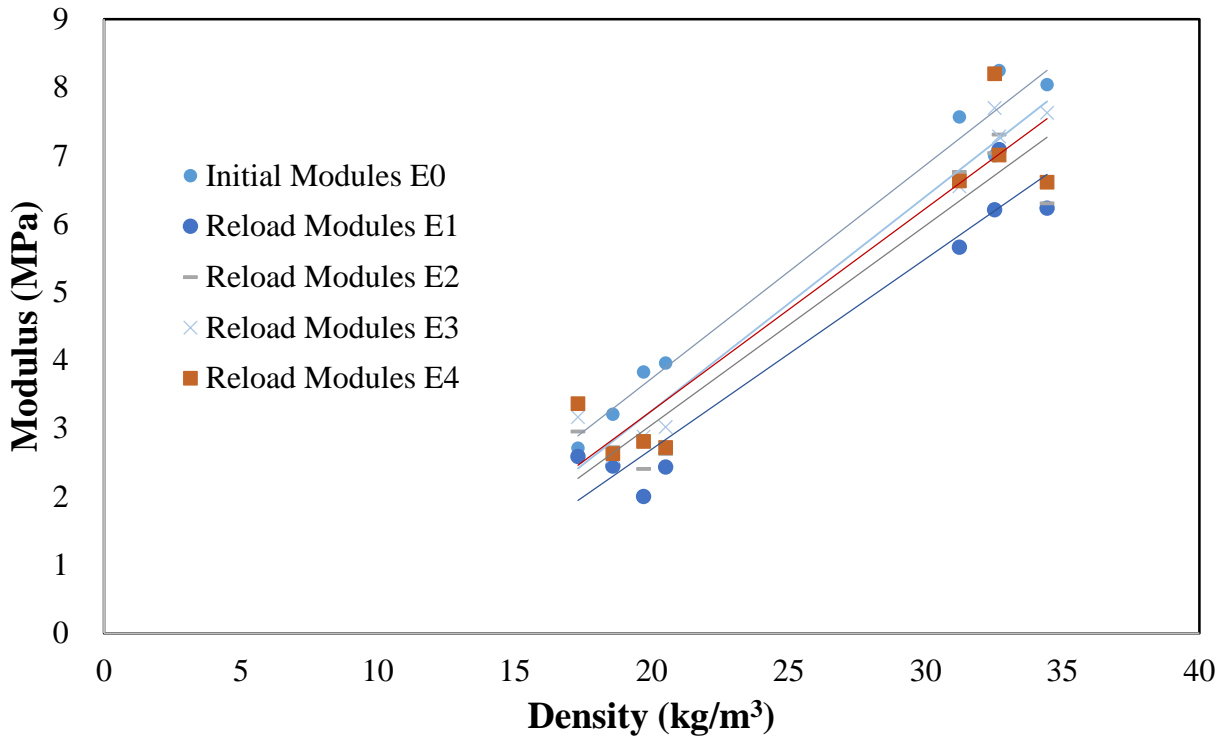
Figure 3.10. Test Results for Loading to Post-yield Stage and Partial Unloading and Reloading Cycles

EPS geofoam behaved elastically when the axial strain limit remained around 1%. The cyclic loading and unloading did not change the initial modulus of elasticity (Figure 3.8). The plastic strain accumulation and reloading modulus degraded relative to the initial elastic modulus if the loading and unloading occurred at a strain level outside of the elastic range (Figure 3.9 & 3.10). There were modulus degradation of up to 56~68% of initial modulus for both 1.25 and 2pcf geofoam densities if the EPS blocks were fully unloaded (Figure 3.9). If EPS blocks were unloaded only partially (Figure 3.10) after a first loading, the reloading modulus decreased less compared to the reloading modulus of the tests that were unloaded completely (Figure 3.9). There is not much difference in terms of densities.
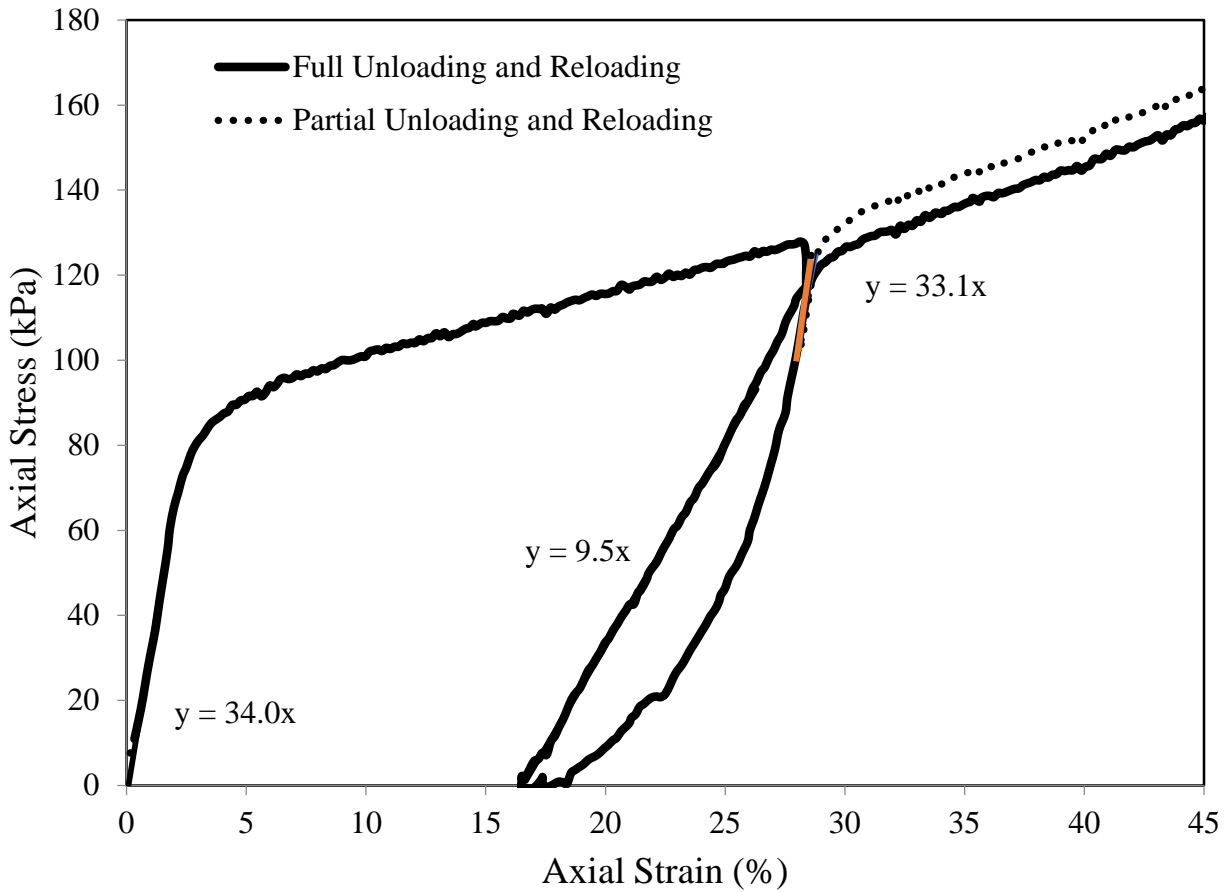
Figure 3.11. Stress-Strain Curves for Loading to Post-yield Stage and Full &
Partial Unloading and Reloading for 1.25pcf EPS

Figure 3.11 presents the stress-strain curves together for loading to post-yield stage and full & partial unloading and reloading. It clearly shows the reloading modulus degradation is less for partial unloading and reloading of EPS compare to full unloading and reloading at the post-yield stage. If pre-straining results in suppressing creep deformation, the increase in proportional limit and moderate degradation in response to partial unloading and reloading cycles may be a favorable development.

3.3 Conclusions

1. Loading and unloading cycles conducted in the pre-yield stage or near yield did not produce significant modulus degradation.

2. Loading to post-yield stage and full unloading and reloading cycles produced significant modulus degradation of up to 56~68% of initial modulus.

3. Loading to post-yield stage and partial unloading and reloading cycles produced much less modulus degradation than full unloading and reloading cycles.

4. On unloading and reloading, the proportional limit increases with accumulated strain. The results suggested controlled pre-stressing of geofoam fill can be beneficial in reducing initial deformations while improving the allowable working stress range. EPS geofoam tends to develop softer reloading modulus but continue to strain harden, and stiffen beyond the max load history level.

5. If pre-straining results in suppressing creep deformation, the increase in proportional limit and moderate degradation in response to partial unloading and reloading cycles may be a favorable development.

CHAPTER 4

STRESS DISTRIBUTION WITHIN EPS BLOCKS BY USING

IMAGE ANALYSIS

Previous laboratory testing of EPS geofoam relied on physical contact and global deformation monitoring to characterize stress-strain behaviors. Displacement monitoring in conditions involving submersion in water and confining pressure or tests in extreme temperature chambers are difficult to perform with contact detection. ARAMIS is a 3D optical displacement tracking system for full field or localized non-contact continuous monitoring. A GeoJac automatic load testing system with a conventional displacement transducer was used together with ARAMIS. The ARAMIS system consists of two CCD cameras mounted on a tripod and a track beam. The separation of the cameras and distance of the tripod can be adjusted to accommodate full field exposure of the test sample. Displacement and stress-strain results derived from conventional global measurements were compared with data recorded by the ARAMIS system.

4.1 Background

Determining the deformation response of geofoam under load is important in developing an in-depth understanding of the engineering behavior. Current strain determination methods employed as part of compression tests mostly assume that the strain is uniform throughout the specimen and, hence, are incapable of

determining local strains. There is no specified standards for the scattering of the vertical strains over the height of the EPS specimen. In order to determine the local deformation and internal strain distribution of EPS specimens, many attempts were done by previous researchers. The geofoam material was installed with strain gauges and had occasionally been instrumented with extensometers (Elragi, 2001). However, these direct contact methods had limitations in fully defining strain distributions in a test specimen. With the development of technology, a new 3D optical displacement tracking system for full field or localized continuous monitoring provide the possibility of developing a more effective way of tracking deformations without contacting the material.

4.2 ARAMIS System

ARAMIS refers to an optical 3D non-contact deformation measurement system. Using high resolution digital cameras and advanced techniques of tracking and distributing the coordinates of pixels, the surface structure of the material is observed. The observation process starts with calibration of the system with known distance. Subsequently, segmental images of the test material are determined using proprietary software. For the materials that do not have surfaces with color or grey scale contrast, prior application of spray pattern will be necessary. Under live and dead load conditions, ARAMIS is especially preferable to track dynamic deformation states as an optical system.

4.3 Test Procedure

The ARAMIS CCD cameras set up is shown in Figure 4.1. After the setup and calibration of the measuring system with the software, the changing images of the samples at different stages of loading are segmentally recorded. Comparing sample states in different images, deformation and strain states can be determined by ARAMIS over the full field of view. In order to reduce noise and data scatter, inbuilt tools are used in processing the data statistic. Using photogrammetric principles, the 3D coordinates of the entire surface of the specimen are calculated. The results provide the 3D shape of the component, the 3D displacements, and the plane strain tensor of every point on the surface of the object.

ARAMIS optical system was used together with the GeoJac automated load test system.
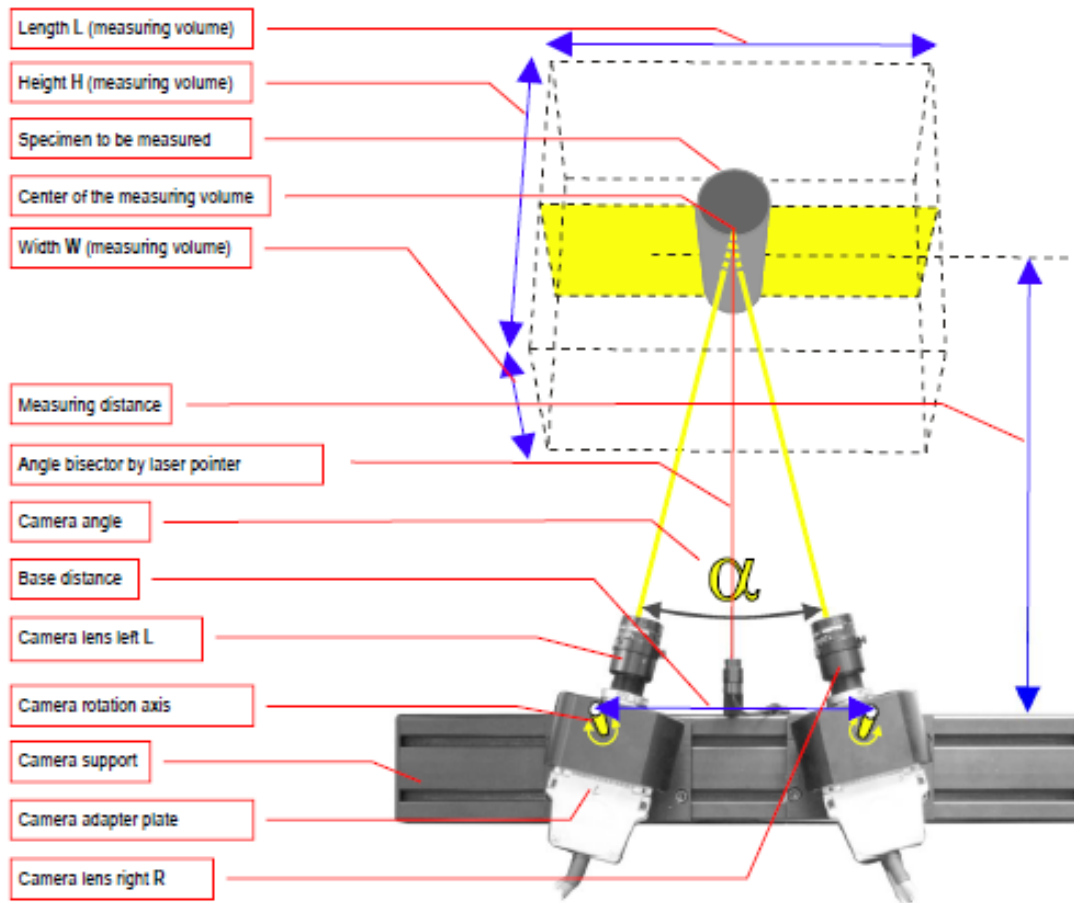
3D Sensor Unit in Top View

Figure 4.1. ARAMIS Camera Bar and Computer Setup

4.3.1 ARAMIS Setup

The ARAMIS pre-set up process includes deciding field of view and frame rate of CCD cameras, setting up camera spacing, lenses and focus, and calibrating the system.

4.3.1.1 Decide Field of View and Frame Rate

The main difference between the ARAMIS system variants is the camera type used. Table 4.1 shows an overview of the main system families. Before the measurement, the individual measuring capacity should be chosen according to the specimen size and requirement of the image accuracy. As for this investigation, ARAMIS 5M System was used according to the tested maximum EPS size of 4in by 2in by 4in (100×50×100mm) and 5M cameras are the mostly used ones. The camera resolution of ARAMIS 5M System is 2448×2050 pixel. At a convenient working distance, the different lenses are chose to get the field of view. The overall accuracy of the ARAMIS 5M System with 3D image correlation is conservatively stated as 1/60,000 (1/30 pixel and 2000 pixel across) the field of view. For example, for the 2448×2050 pixel cameras with a 6cm field of view, sensitivity is 1 micron, and for this case with a 100mm field of view (EPS length), it is 1.6 microns (100mm/60,000). The measuring volume determines the distance between sensor and specimen and the set of lenses.

Table 4.1. Overview of the Main ARAMIS System Families

System Configurations	2M	5M	4M	12M	HS
Frame Rate (Hz)	up to 15 (29)	up to 15 (29)	up to 168 (1334)	up to 58 (464)	up to 500 (4000)
Camera Resolution (pixel)	1624 x 1236	2448 x 2050	2400 x 1728	4000 x 3000	1280 x 1024
Measuring Area	mm² to > m²	mm² to > m²	mm² to > m²	mm² to > m²	mm² to > m²
Strain Measuring Range (%)	0.005 up to > 2000	0.005 up to > 2000	0.005 up to > 2000	0.005 up to > 2000	0.005 up to > 2000
Strain Measuring Accuracy (%)	up to 0.005	up to 0.005	up to 0.005	up to 0.005	up to 0.005
Ring Buffer	•	•	•	•	•
Image Memory	uses PC RAM	uses PC RAM	uses PC RAM	uses PC RAM	uses PC RAM
Tool Free Mounting	•	•	•	•	•
Integrated Cable Guide	•	•	•	•	•
Positioning Pointers	1 or 3	1 or 3	1 or 3	1 or 3	1 or 3
Illumination	integrated	integrated	integrated	integrated	external
High-End PC	•	•	•	•	•
Notebook	•	•	–	–	–
Control Device	Sensor Controller	Sensor Controller	Sensor Controller	Sensor Controller	Sensor Controller
Operating Temperature	5-40°C	5-40°C	5-40°C	5-40°C	5-40°C
Specimen Temperature		typ. -100°C up to +1500°C		typ. -100°C up to +1500°C	

As shown in Figure 4.2 and 4.3, the ARAMIS 5M System was employed in this experiment, in which the measuring volume in mm^3 was 100×80×80 (EPS size of 4in by 2in by 4in) with sensitivity of 1.6 microns (100mm/60,000), and the resolution was 2448×2050 pixels. The test information is stored in the RAM of the computer used for evaluation.

Figure 4.2. ARAMIS Cameras Used in Tests

Figure 4.3. ARAMIS Measure Tracking System

4.3.1.2 Set up Cameras and Calibrate the System

The measuring system should be adjusted according to the requirements

before the first commissioning, including setting up the angle relations of the

lenses (only for 3D setup with 2 cameras), the focus and the aperture. The

measurement of the material begins after the 3D images is corrected by taking

calibration readings. The 3D image calibration uses NIST (National Institute of Standards and Technology) -traceable calibration panels for each field of view. A sequence of pictures of the panel at different distances and orientations is captured. Then a photogrammetry process known as bundle adjustment is used to establish the precise relationship between the two cameras. This is essentially a ray-tracing process to find unique intersection points, similar to how a GPS system triangulates coordinates. Each dot on the calibration panel occupies more than 100 pixels on each camera sensor, so dot centers can be interpolated with sub-pixel accuracy.

For measurements after calibration, the edges of each facet are located based on local features of the applied pattern. An example final calibration result is shown in Figure 4.4.
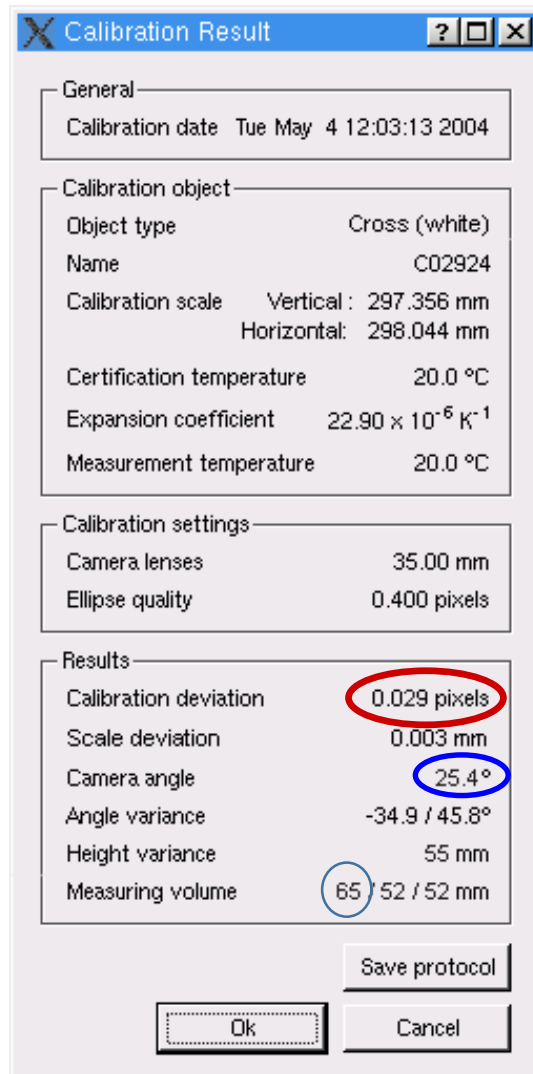
Figure 4.4. Final Result of Calibration

4.3.2 EPS Samples

EPS samples of 1pcf, 1.25pcf, 1.5pcf and 2pcf densities were tested. Three kinds of specimens were used; conventional 2in cubes, four 2in cube samples combined and 4in by 2in by 4in samples (as shown in Figure 4.5). Desired samples were trimmed using a hot wire cutter in the lab and the dimensions and the initial mass were recorded precisely before the tests.
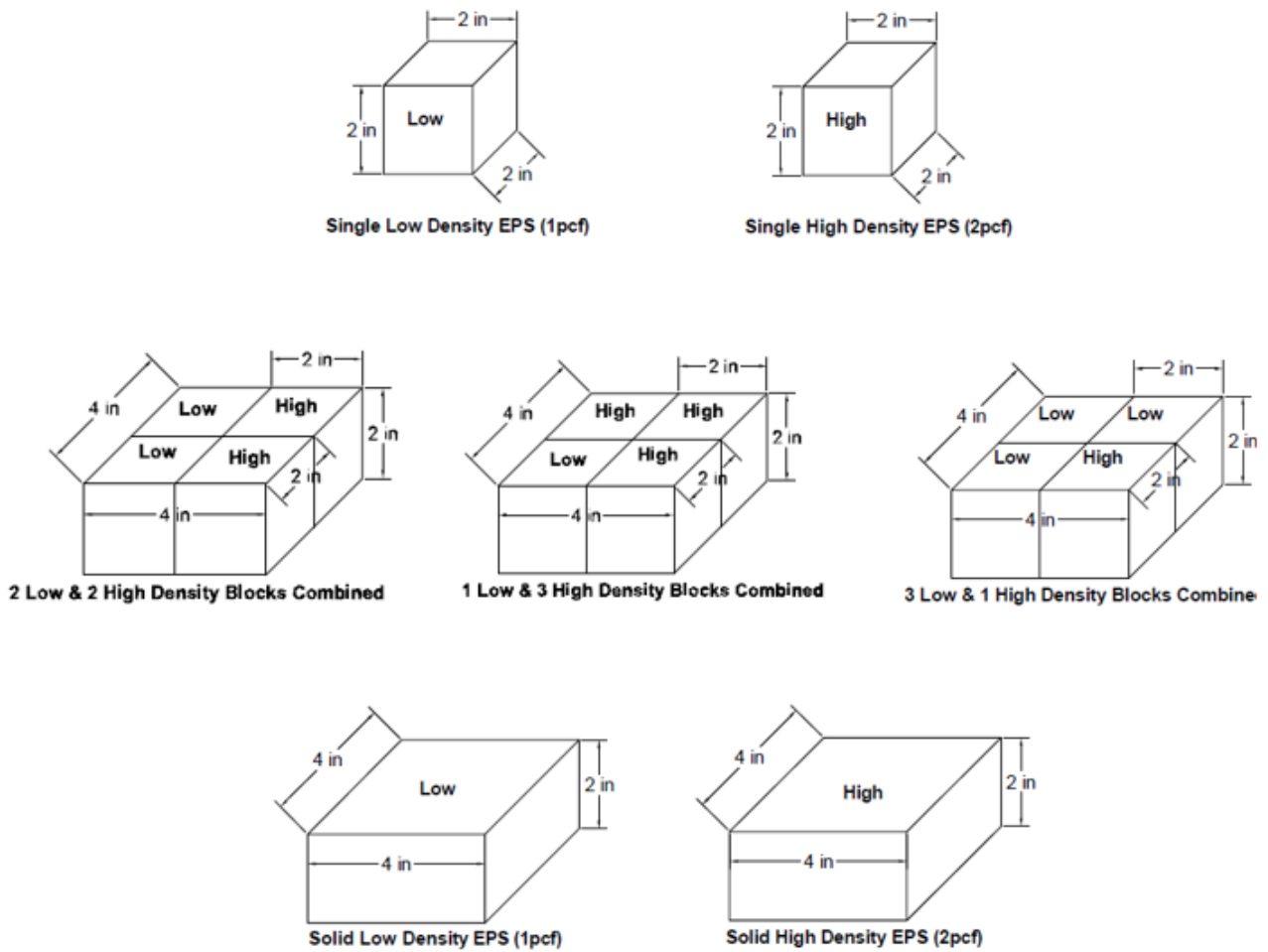
Figure 4.5. Tests Setup

For optical detection of deformation, the material surface structure should be relatively smooth. There should be a measureable surface pattern so as to clearly track the target image. Sample preparation consists of applying a regular or random high contrast dot pattern to the surface, typically with an airbrush. Thousands of unique correlation areas known as facets (typically up to about 15 pixels in size, for 5M camera is 19 pixels in size) are defined across the entire imaging area. A sharp contrast between patterns must exist for the system to work. First of all, the dimension of the surface traits should be small enough to produce a good raster.

63

Secondly, the pattern should be large enough to be distinctly identified. Therefore, in order to distribute the facets (Figure 4.6), the Rustoleum flat black spray paint was chosen to create a random pattern (Figure 4.7) over the EPS surface. The center of each facet is a measurement point that can be thought of as for an extensometer and strain rosette. These facet centers are tracked, in each successive pair of images, with accuracy up to 0.001 pixel.
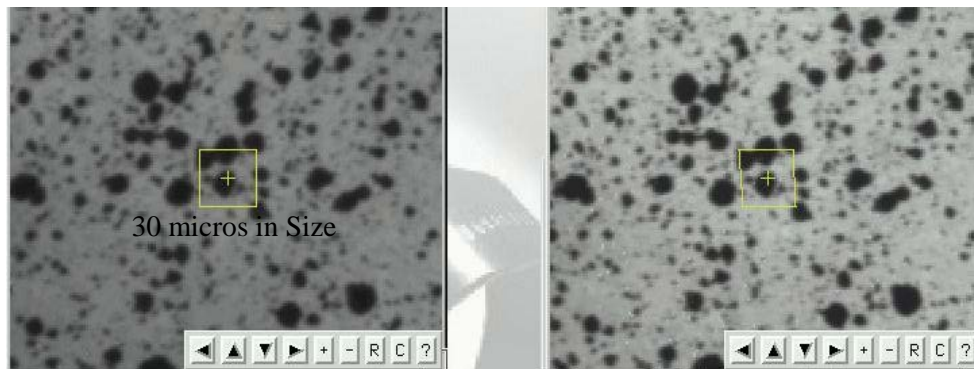
Figure 4.6. Tracking Facets of 19×19 Pixel Square with Sub-pixel Accuracy
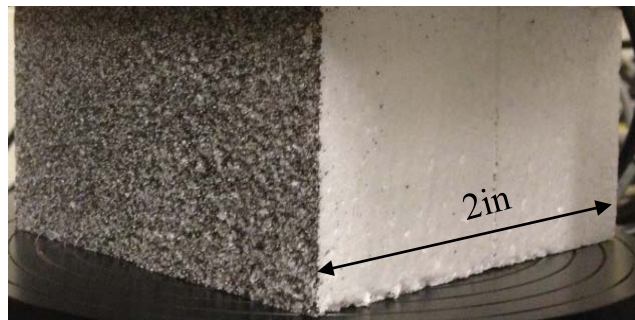
Figure 4.7. A Random or Regular Pattern with Good Contrast Applied to the Surface of the Test Object

4.3.3 Principles of Operation

The deformation of the EPS material under the applied load conditions was recorded by a pair of high resolution digital CCD cameras, which measured the

sample's 3D coordinates and the 3D deformations. The initial image processing defines unique correlation areas known as macro-image facets, typically 5-20 pixels square, across the entire imaging area. Each facet center was a measurement point.

The key to 3D Image Correlation is that it tracks changes in an applied micro-pattern (random pattern), rather than a projected pattern, using ordinary white light. The system tracks this random pattern applied to the measurement surface with sub-pixel accuracy. This means that as long as the object remains within the field of view of the cameras, all of the local deformations can be tracked. Then the strain can be derived once the deformations are tracked. Thus, large deformations can be analyzed in a single measurement.

As shown in the Figure 4.2, the camera pair was simply placed in front of the test sample at the calibrated working distance. The recorded results from ARAMIS system are the 3D shape of the component, the 3D displacements, and the derived strains. 3D coordinates of each facet determined for each picture set was recorded by the software. 3D coordinates can be synchronized to 2D by using photogrammetry technology.
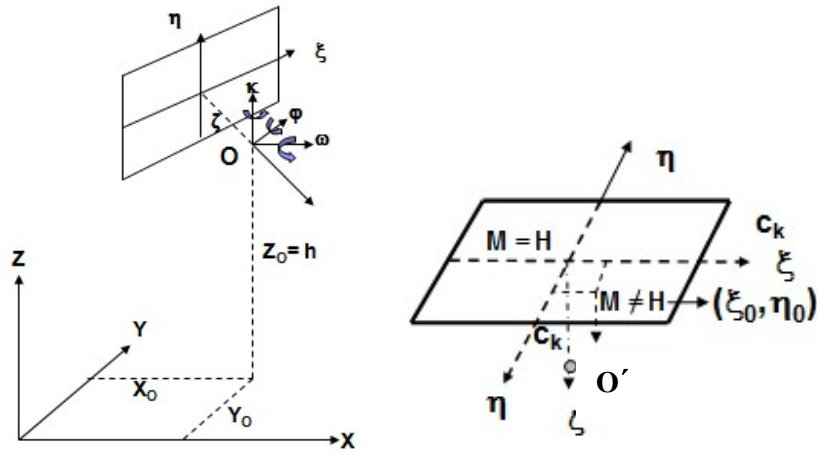
(a) Object 3D Coordinate System   (b) Image 2D Coordinate System
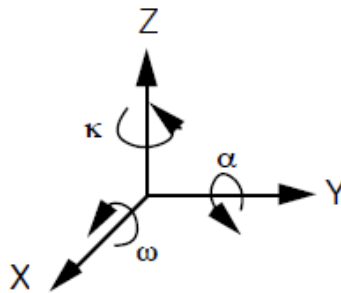
(c) Rotation Parameters

Figure 4.8. Coordinate Systems of Transferring 3D Coordinate to 2D

The mapping function for transferring 3D coordinates (Figure 4.8 (a)) to 2D (Figure 4.8 (b)) can be expressed as shown in Equation 4.1 and 4.2.

$$\xi = \xi_0 - c_k \frac{r_{11}(X-X_0)+r_{12}(Y-Y_0)+r_{13}(Z-Z_0)}{r_{31}(X-X_0)+r_{32}(Y-Y_0)+r_{33}(Z-Z_0)} \quad \text{............... Equation 4.1}$$

$$\eta = \eta_0 - c_k \frac{r_{21}(X-X_0)+r_{22}(Y-Y_0)+r_{32}(Z-Z_0)}{r_{31}(X-X_0)+r_{32}(Y-Y_0)+r_{33}(Z-Z_0)} \quad \text{............... Equation 4.2}$$

Where,

ξ, η = Measured Point coordinates of the 2D image;

ξ_0, η_0 = Principle Point coordinates of the 2D image;

66

X, Y, Z = Coordinates of the 3D object point;

X_0, Y_0, Z_0 = Position of the reference at the instant of imaging;

c_k = Focal length of the camera lens;

r_{ij} = Nine direction cosines expressing the angular orientation.

The meaning of the coordinates can be shown in Figure 4.8. The coefficients in Equation 4.1 and 4.2 can be explained in the rotation matrix R (Equation 4.3). To rotate **O** to a new point **O′**, it is set **O′ = RO**. The nine components in Equation 4.3 are functions of three rotation parameters ω, α and κ, where Omega (ω) will describe rotation about the X-axis, Alpha (α) will describe rotation about the Y-axis, and Kappa (κ) will describe rotation about the Z-axis (as shown in Figure 4.8 (c)). Rotation are not commutative, the rotations of the points are defined to occur in the following order: first rotate the point around the Z-axis, the around the Y-axis, and finally the X-axis (See details in Appendix). The coordinate system is defined to be right-handed. Then the rotation matrix R can be defined as (Equation 4.4):

$$R = \begin{bmatrix} r_{11} & r_{12} & r_{13} \\ r_{21} & r_{22} & r_{23} \\ r_{31} & r_{32} & r_{33} \end{bmatrix} \quad \ldots\ldots\ldots\ldots\ldots\ldots\ldots\ldots\text{Equation 4.3}$$

$$R = \underbrace{\begin{bmatrix} cos\kappa & sin\kappa & 0 \\ -sin\kappa & cos\kappa & 0 \\ 0 & 0 & 1 \end{bmatrix}}_{\text{Rotation around Z-axis}} \cdot \underbrace{\begin{bmatrix} cos\alpha & 0 & -sin\alpha \\ 0 & 1 & 0 \\ sin\alpha & 0 & cos\alpha \end{bmatrix}}_{\text{Rotation around Y-axis}} \cdot \underbrace{\begin{bmatrix} 1 & 0 & 0 \\ 0 & cos\omega & sin\omega \\ 0 & -sin\omega & cos\omega \end{bmatrix}}_{\text{Rotation around X-axis}} \ldots\ldots \text{ Equation 4.4}$$

Multiplying the three individual rotations yields the desired rotation matrix

(Equation 4.5):

$$R = \begin{bmatrix} cos\kappa \cdot cos\alpha & sin\kappa \cdot cos\omega + cos\kappa \cdot sin\alpha \cdot sin\omega & sin\kappa \cdot sin\omega - cos\omega \cdot sin\alpha \cdot cos\kappa \\ -sin\kappa \cdot cos\alpha & cos\kappa \cdot cos\omega - sin\kappa \cdot sin\alpha \cdot sin\omega & sin\omega \cdot cos\kappa + cos\omega \cdot sin\alpha \cdot sin\kappa \\ sin\alpha & -sin\omega \cdot cos\alpha & cos\omega \cdot cos\alpha \end{bmatrix}$$

…..………………………..……….…………..……….. Equation 4.5

Therefore, the terms are:

$r_{11} = cos\kappa \cdot cos\alpha$

$r_{12} = sin\kappa \cdot cos\omega + cos\kappa \cdot sin\alpha \cdot sin\omega$

$r_{13} = sin\kappa \cdot sin\omega - cos\omega \cdot sin\alpha \cdot cos\kappa$

$r_{21} = -sin\kappa \cdot cos\alpha$

$r_{22} = cos\kappa \cdot cos\omega - sin\kappa \cdot sin\alpha \cdot sin\omega$

$r_{23} = sin\omega \cdot cos\kappa + cos\omega \cdot sin\alpha \cdot sin\kappa$

$r_{31} = sin\alpha$

$r_{32} = -sin\omega \cdot cos\alpha$

$r_{33} = cos\omega \cdot cos\alpha$

After synchronizing the 3D coordinates into 2D, modified data can be

presented as ASCII (American Standard Code for Information Interchange) exports

to support further analysis and comparison. Color plots, movies and section line

diagrams can be reported as well. Although only two picture sets are required to

measure the change from zero to maximum load, multiple image sets provide a

progressive measurement of deformations and strains.

4.3.4 Test Results

ARAMIS documents the 3D deformations in the different load stages. In order to get the strain distribution among the EPS blocks, the locations of points (as shown in Figure 4.9) were captured with time.
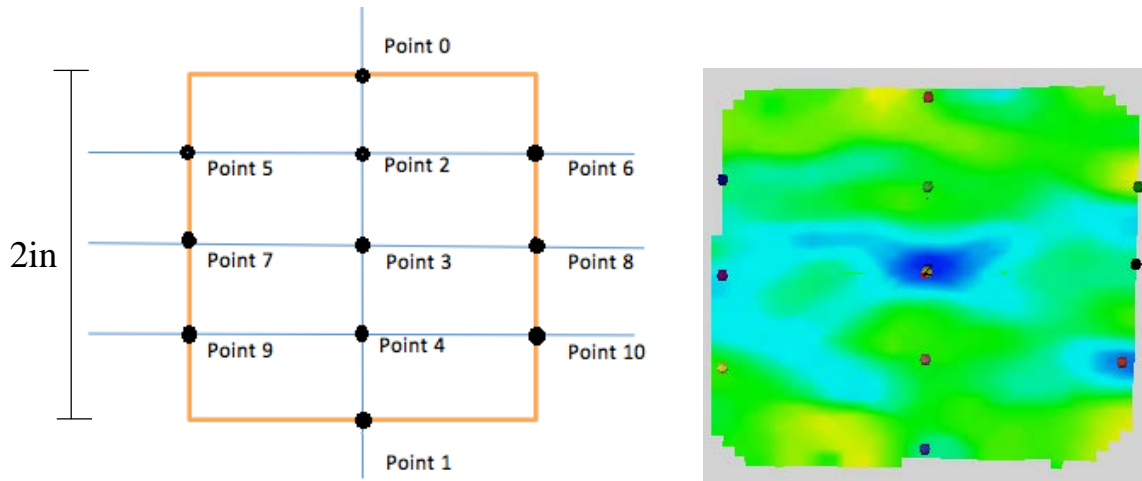
Figure 4.9. Points Captured with Time

4.3.4.1 Test Results for 2in Cube Samples
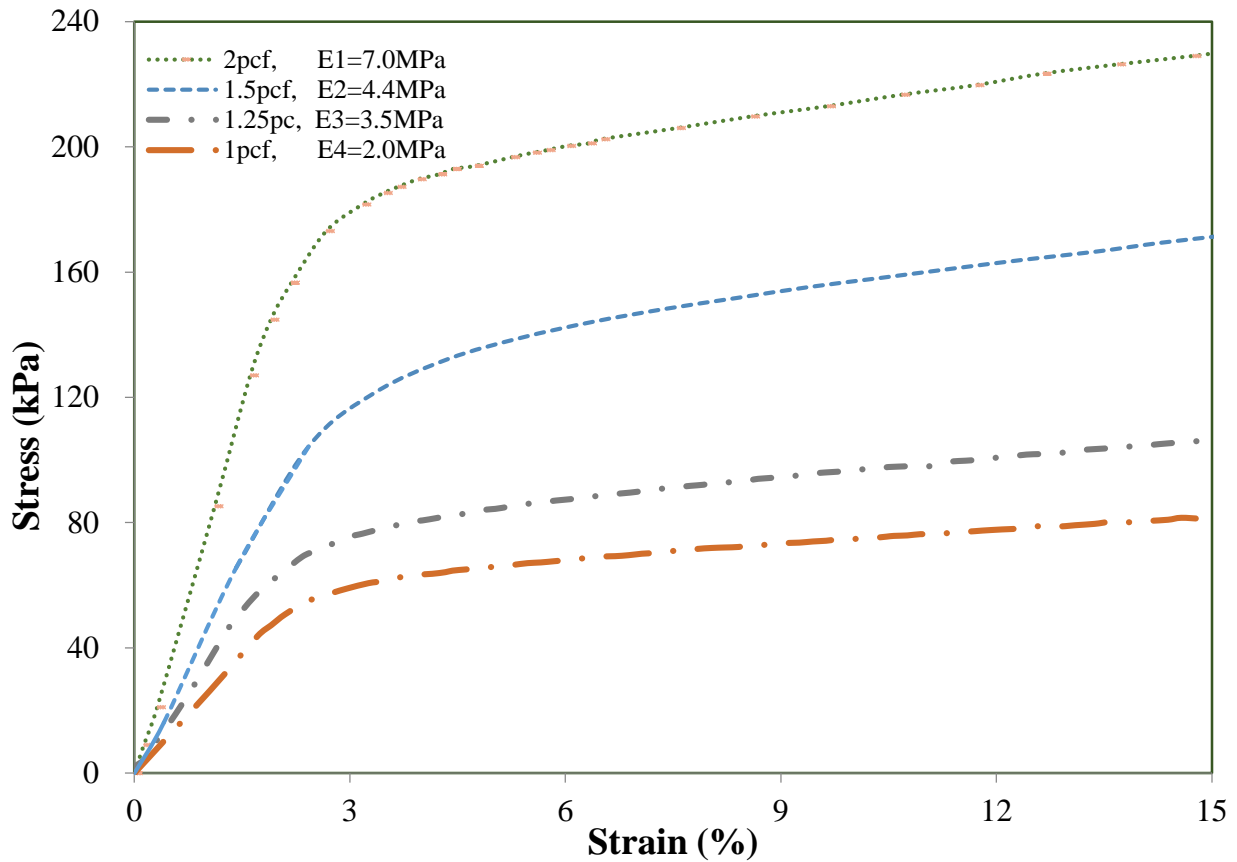
Figure 4.10. Stress-Strain Distribution Curves from Traditional Testing of 2in
Cube Samples

Figure 4.10 displays the stress-strain curves for 1, 1.25, 1.5 and 2pcf

densities obtained from traditional testing of 2in cube samples. The moduli of EPS

blocks increase with density. The results would be compared to results from

combining different densities of EPS. As for those curves, only global stress-strain

results were produced by using GeoJac machine. Strains developed at different

locations within EPS blocks cannot be followed. The ARAMIS results show the

details of strain distribution at different locations and loading stages.
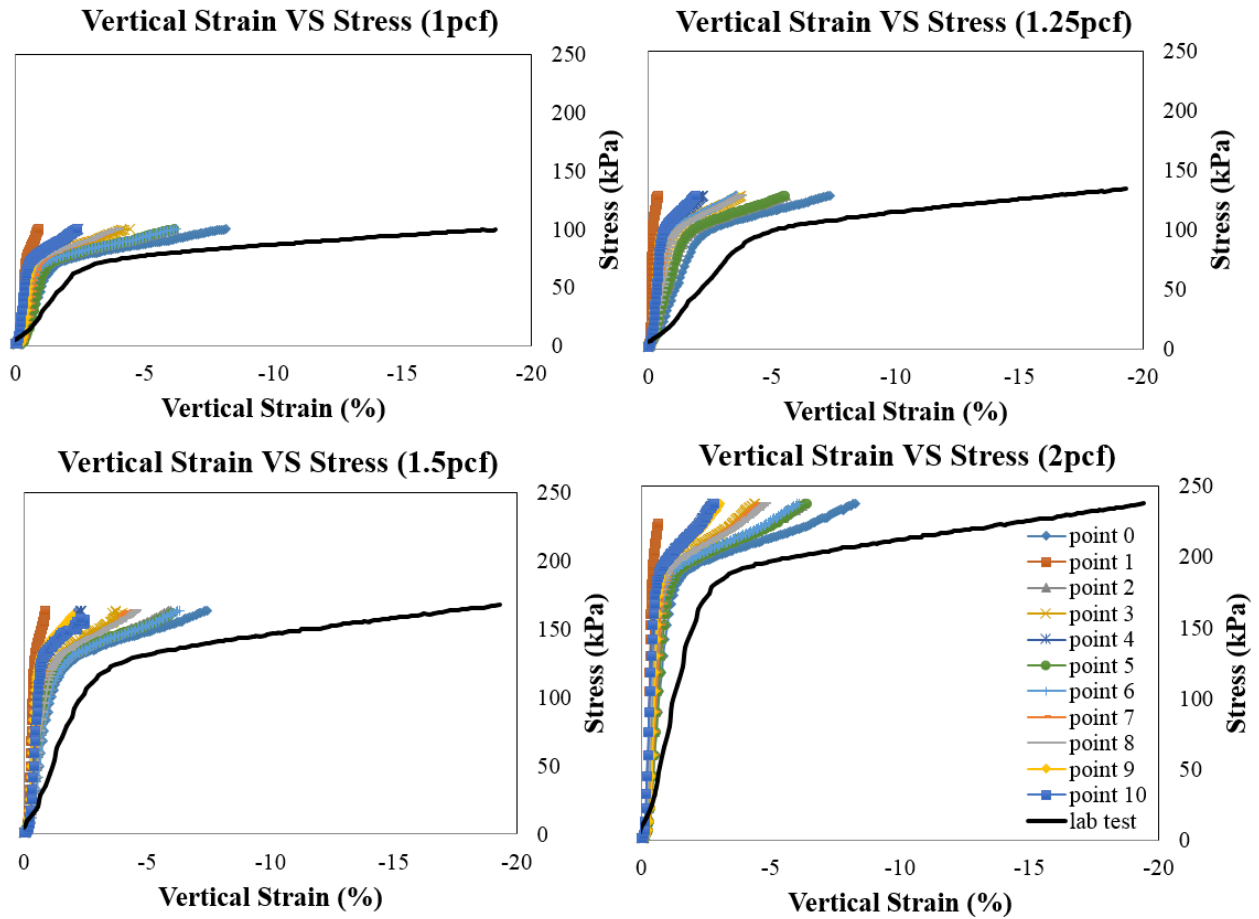
Figure 4.11 (a) Strain Derived from Displacement
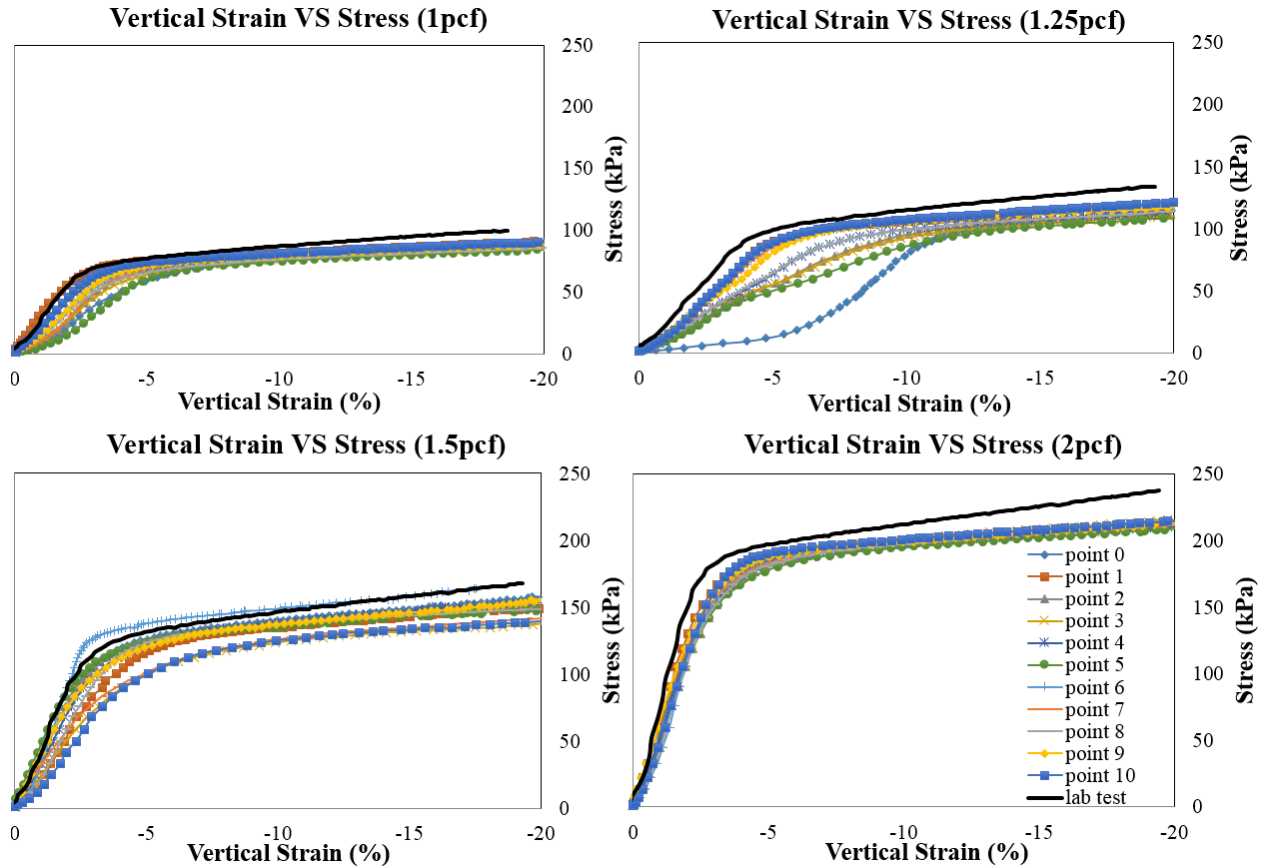
Figure 4.11 (b) Measured/Recorded Strain

Figure 4.11. Test Results from Detection of Displacements by both LVDT and ARAMIS during Axial Loading of 2in Cube Samples for 1, 1.25, 1.5 and 2pcf densities

Figure 4.11 shows the test results from both LVDT and ARAMIS. The black curves were drawn by using the data acquisition from the GeoJac system, which present the global stress-strain behavior of the whole block. The other curves were from ARAMIS system by locating different points. The strain values in Figure 4.11 (a) are derived from the recorded displacement values. According to Figure 4.11 (a), the minimum strain (displacement) developed at certain stress levels is located at Point 1, which is close to the lower boundary of EPS blocks. The

72

maximum strain (displacement) developed at certain stress levels is located at

Point 0, which is close to the upper boundary. The points at the same layer (Point 5,

2, 6 and Point 7, 3, 8 and Point 9, 4, 10) of the EPS blocks have similar strain

(displacement) developed at the same stress level. The average/global stress-strain

curves (black curves) show relative lower strength in modulus than all the other

curves from local points of the EPS blocks for all the density types. This

observation suggests the traditional way of determining modulus of EPS blocks is

conservative. The strain values in Figure 4.11 (b) are recorded values from

ARAMIS system directly. The internal strain values for different points/locations

at any stress level is different. The lab test global strain value is conservative

compare to local strain values. It is not easy to see the peak strain location from the

stress-strain curves for all the density types. The detailed strain variation could be

shown from the images captured from ARAMIS videos.
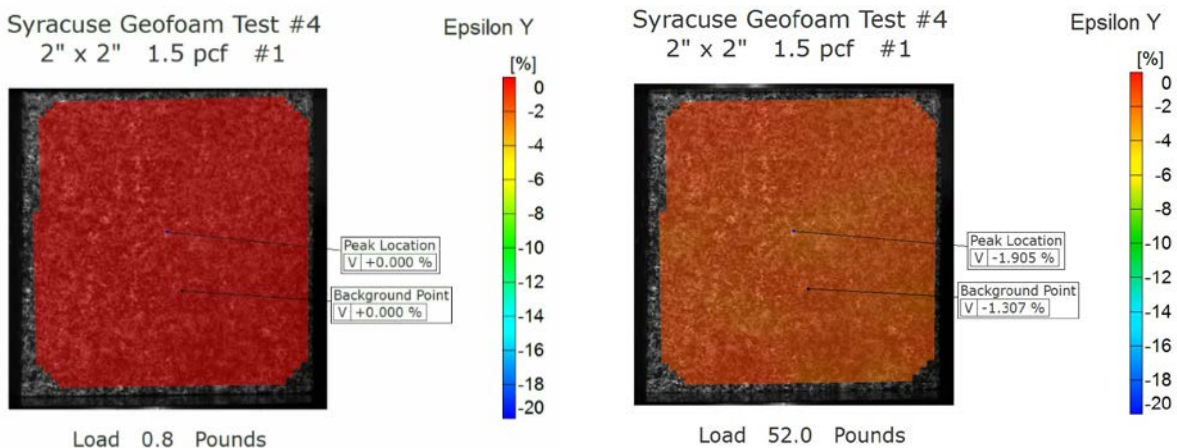
(a) Beginning (0% global strain)   (b) 2% global strain
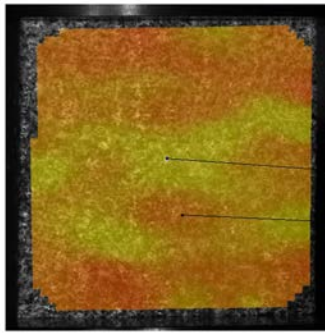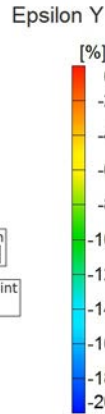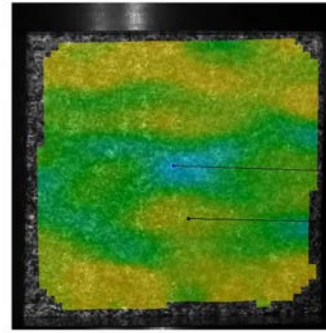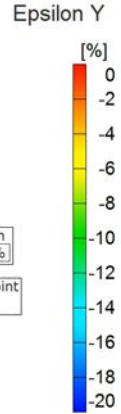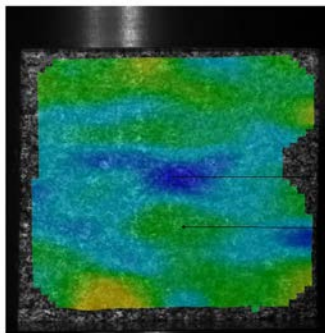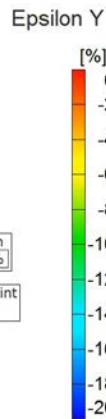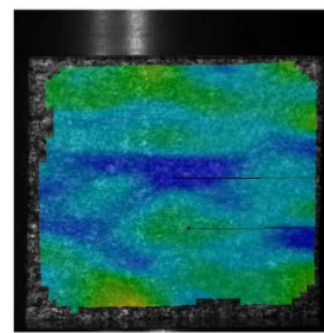
(c) 4.4% global strain

(d) 9.9% global strain

(e) 14.9% global strain

(f) End (18% global strain)
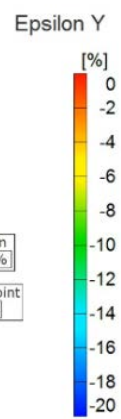
Figure 4.12. Images Captured During the Loading Process for the 2in Cube Samples of 1.5pcf Density

The videos of the loading process from each of the EPS blocks were recorded. Figure 4.12 shows the images captured at several strain levels for the 2in cube samples of 1.5pcf density. The strain developed in y direction changed with time. The strain distribution at the beginning of the loading process (Figure 4.12 (a)) is uniform. With the increase of loading on top of the EPS block, differential strains were produced. At the loading stage to 2% global strain (Figure 4.12 (b)),

74

the peak strain location is in the center of the EPS block with 1.9% strain, while

the minimum strain is 1.3%. There is only 0.6% strain difference at a lower global

strain level (2%). Loading to higher global strain level up to 4.4%, 9.9% and 14.9%

(Figure 4.12 (c), (d) and (e)), the local strain difference are 3.1%, 7.3% and 10%

respectively. At the end of the loading stage (18% global strain, Figure 4.12 (f)),

there is up to 11% differential strain within the EPS block. The differences of local

strain increase with the global strain level. For all the loading stages, the global

strain produced by using traditional LVDT lie between the peak and lowest strain.

Figure 4.12 also presents that strain development for the cellular structure of EPS

is in crushing normal to the direction of loading rather than inclined shear bands as

occur for soil and other rigid materials.
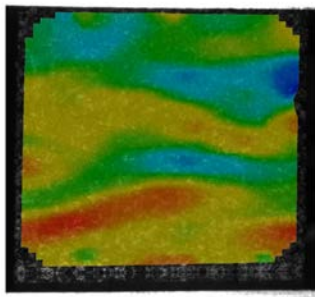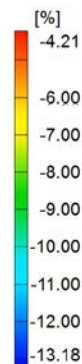
(a) 8.6% global strain   (b) 8.5% global strain
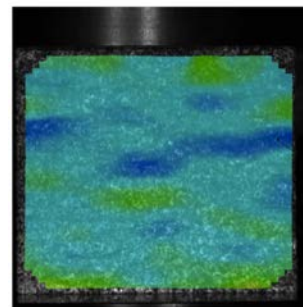
(c) 8.7% global strain   (d) 8.6% global strain
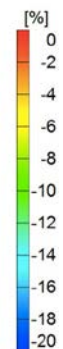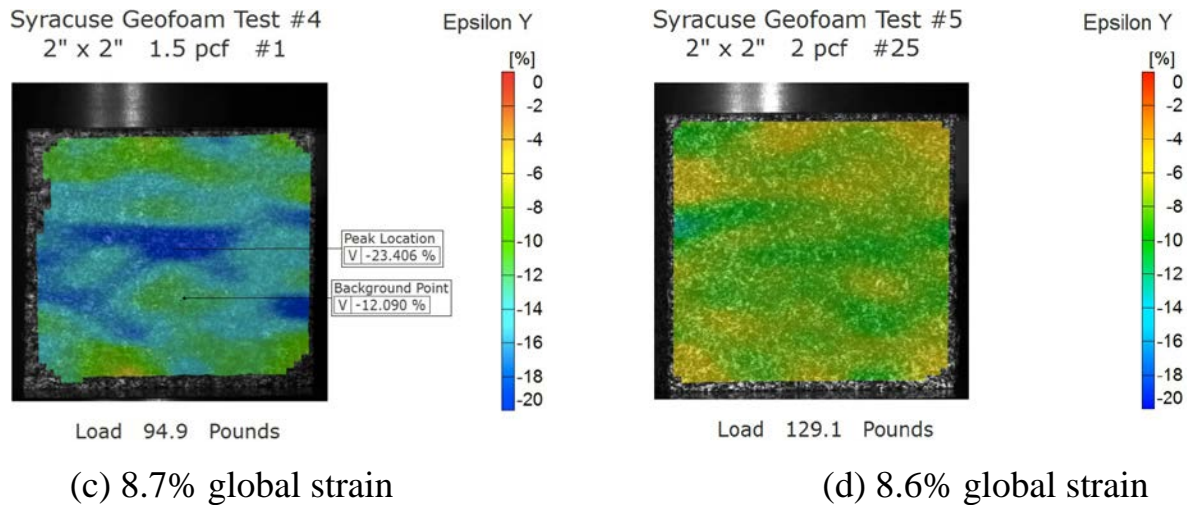
Figure 4.13. Images of the Strain Distribution at Certain Load Levels of the 2in Cube EPS Blocks for Different Densities

Images of strain distributions at different load levels for different EPS densities are shown in Figure 4.13. To reach a certain train level (8.7%), EPS with density of 1, 1.25, 1.5 and 2pcf can carry 52.7, 74.2, 94.9 and 129.1lbf load (91, 128, 164 and 223kPa stress) respectively. The higher density EPS blocks carry more load than lower density EPS. As for the strain distribution with loading, for 1.5pcf EPS (Figure 4.12), the strain in y direction changed with load level. The strain distribution at the beginning of the loading process was uniform and became highly non-uniform with increasing load and strain development. The difference of local strain increase with the global strain level. Regardless of the densities, strain development in EPS is predominately in crushing normal to the direction of loading rather than along shear bands for all densities.

4.3.4.2 Test Results for 4 by 2 by 4in Samples & 2in Cubes of Combined Densities

In order to test the performance of the ARAMIS system for different sample sizes, and the strain distribution for samples with combined densities, the 4 by 2 by 4in solid EPS samples and four 2in cube samples combined tests were conducted.
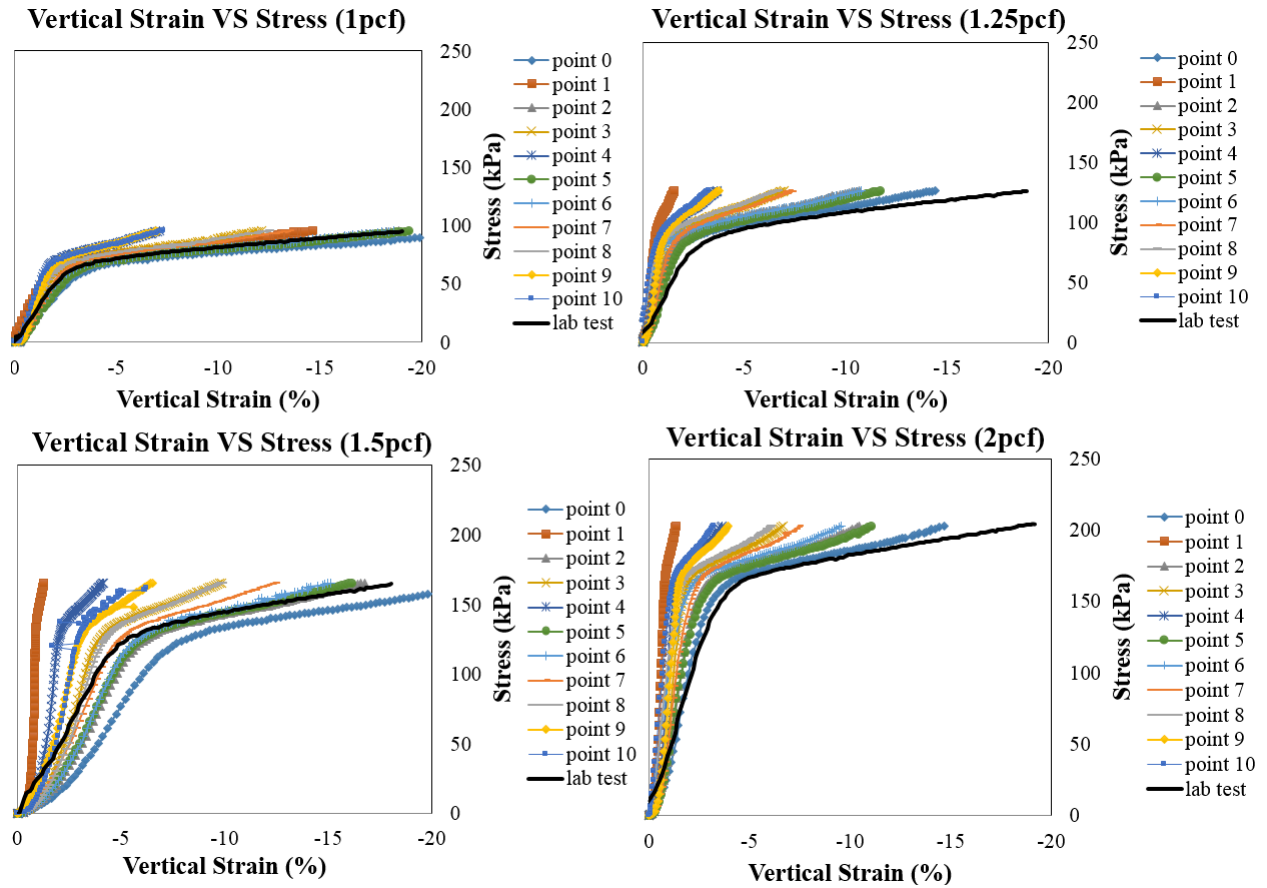
Figure 4.14 (a) Strain Derived from Displacement
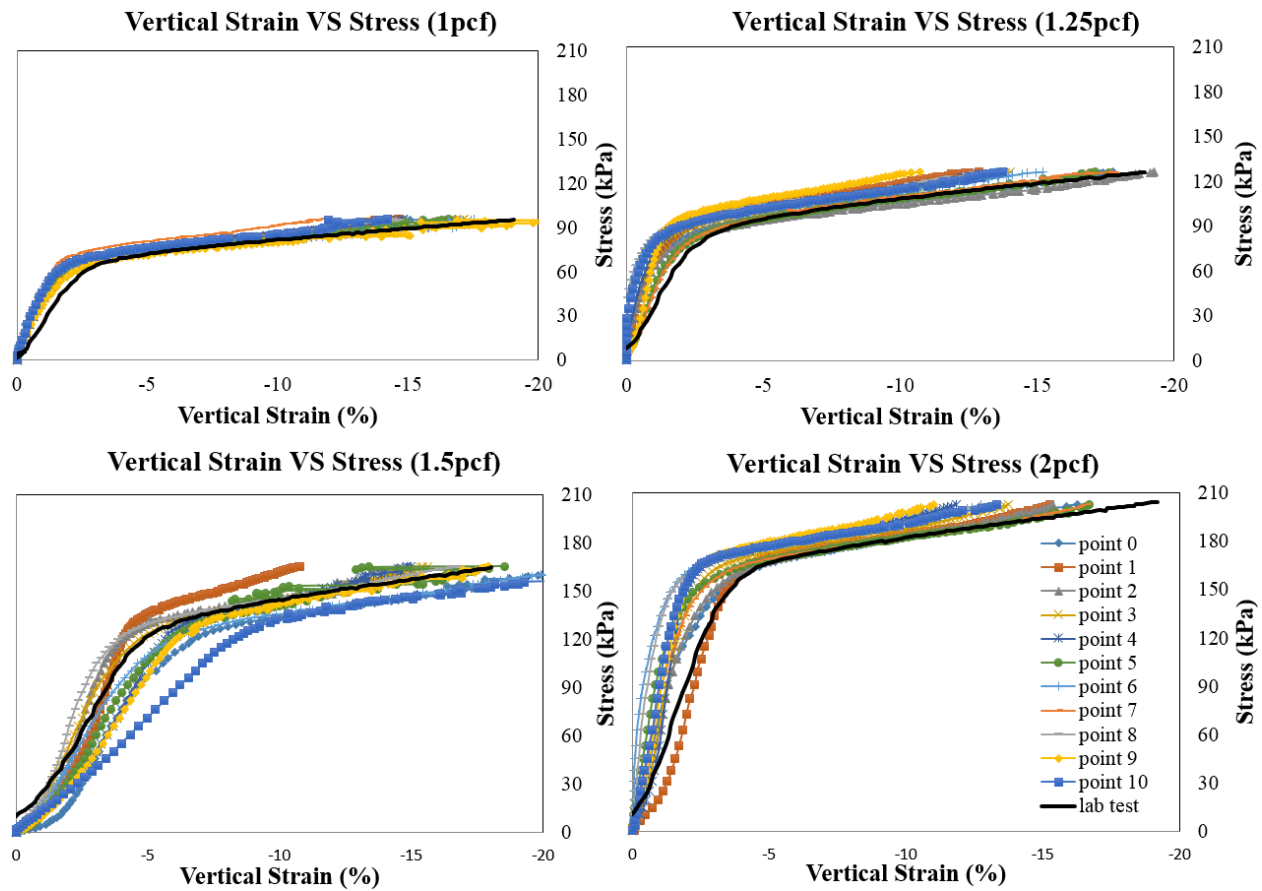
Figure 4.14 (b) Mesured/Recorded Strain

Figure 4.14. Test Results from Both Geojac and Aramis for the 4 by 2 by 4in Solid EPS Samples with Different Densities

Figure 4.14 shows the test results from both Geojac and ARAMIS for the 4 by 2 by 4in solid EPS samples. This presents similar patterns as the results of 2in cube samples (Figure 4.11). It can be concluded that the optical non-contact ARAMIS system can accommodate any sample size and full-scale models to directly detect displacements of selected points or image facets. As shown in Figure 4.14, the GeoJac lab test results (black curves) show comparatively lower strength in modulus than the other curves from local points of the EPS blocks.

78
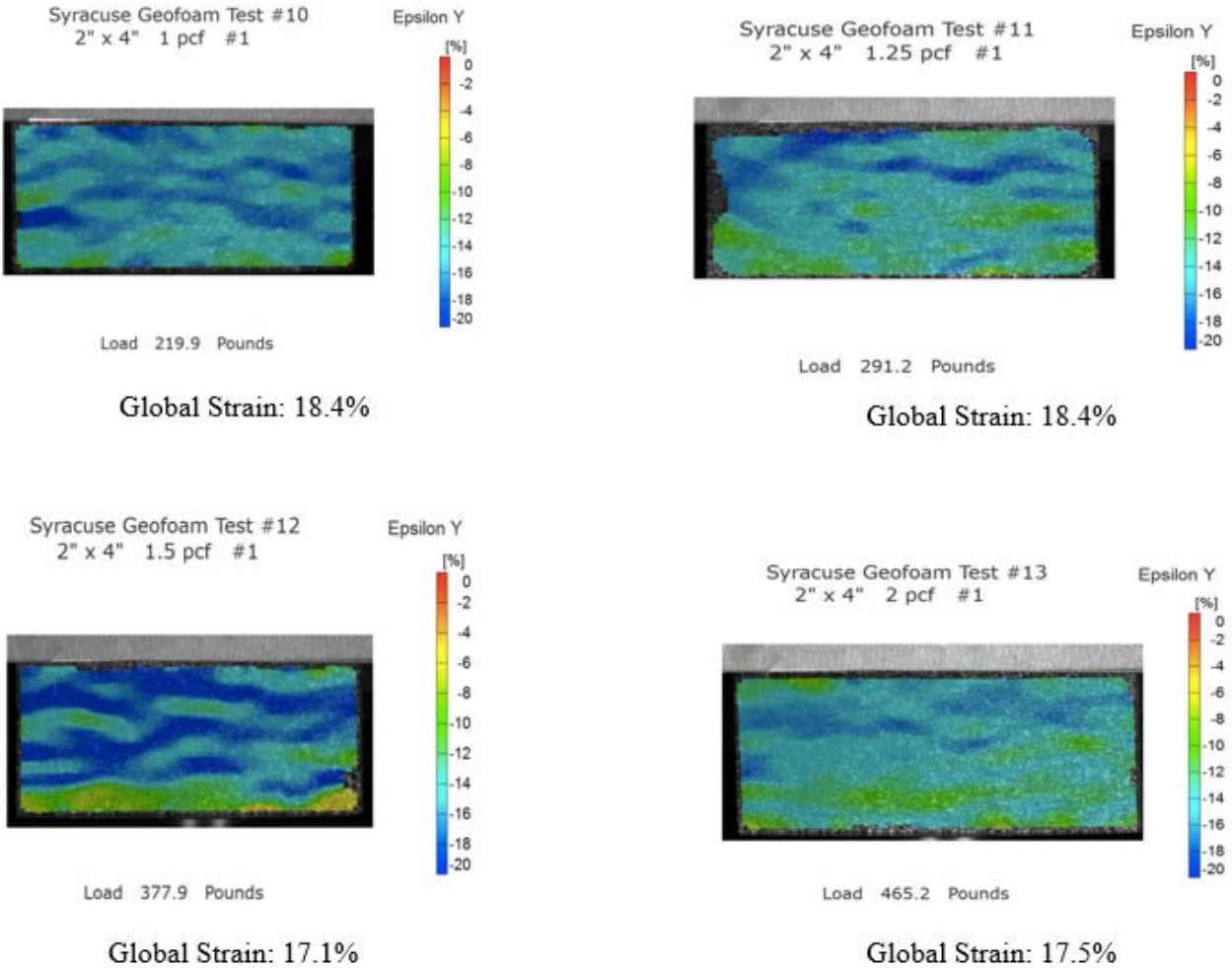
Figure 4.15. Images of the Strain Distribution at almost the Same Strain Level for 4 by 2 by 4in Solid EPS Samples of Different Densities

Figure 4.15 displays images of strain distributions at almost the same global strain level for 4 by 2 by 4in solid EPS samples of different densities. To reach a certain train level (18%), EPS with density of 1, 1.25, 1.5 and 2pcf can carry 220, 291, 378 and 465lbf load (95, 125, 163 and 201kPa), respectively. The higher density EPS blocks carry more load than lower density EPS. The images show that

the strain distribution are not uniform and the strain development for the EPS

structure are in crushing normal to the direction of loading.

(a) Beginning   (b) End
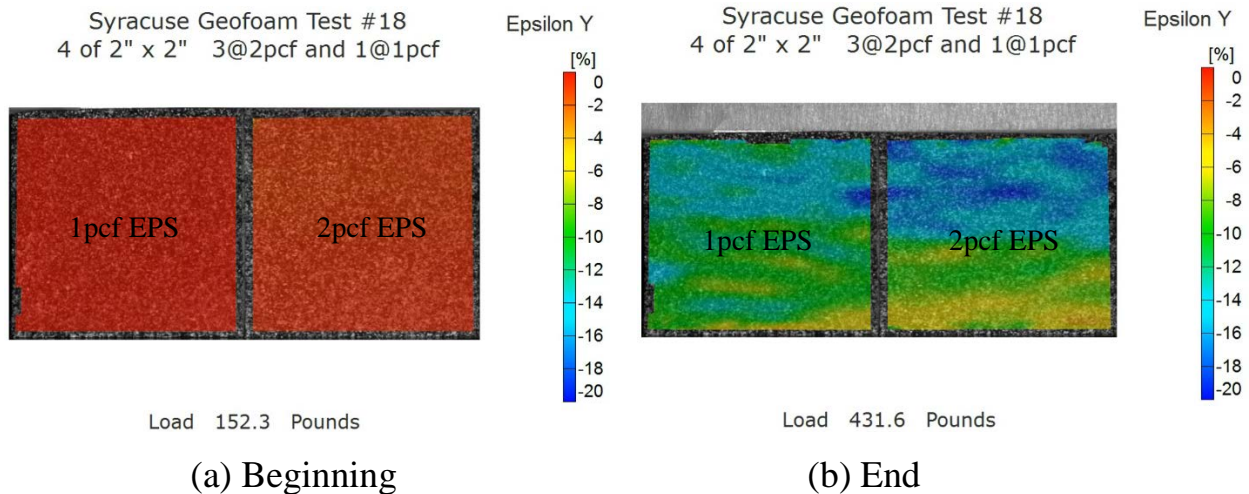
Figure 4.16. Images Captured at the Beginning and End of the Loading Process for
the 4in by 2in by 4in Samples with Combined 1 & 2pcf Densities

Images captured at the beginning and end of the loading process for the 4in

by 2in by 4in samples with combined 1 & 2pcf densities EPS are shown in Figure

4.16. For this test, the boundary displacement conditions were controlled because

of the rigid loading plate. It is difficult to show the strain distribution at the top and

lower boundary because of the rigid boundary. With mixed EPS densities at a load

level of 432lbf (Figure 4.16 (b), the left 2in cube block, which was with 1pcf

density, had around 12% differential strain. While the right 2 in cube block with

density of 2pcf had 20% differential strain. This indicates the dense (2pcf) had

more differential strain distribution compared to the weak (1pcf) EPS sample.

According to the stress-strain behavior of EPS geofoam, the EPS block with higher

density carried more load compared to the lower density EPS at the same strain level. In order to further study the load bearing behavior of mixed density combination, more tests with flexible boundary were performed as presented in next chapter.

4.4 Conclusions

1. The optical non-contact system can accommodate any sample size and full-scale models to directly detect displacements of selected points or image facets at high resolution and in 3D.

2. Synchronizing force sensing with displacement detection, directional moduli and Poisson's Ratios can be determined from one test sample.

3. It was verified that the traditional way of determining modulus of EPS blocks is conservative.

4. The strain distribution across the face of an EPS sample is initially uniform and becomes highly non-uniform with increasing load and strain development. The difference of local strain are small at lower global strain level and high at higher global strain level. For mixed density tests, the dense (2pcf) EPS blocks were carrying more loads. As a result, the strain level was in between the higher level for 1pcf and lower level for 2pcf.

5. Time lapse images and video recordings show progressive strain development for the cellular structure of EPS is in crushing normal to the direction

of loading rather than inclined shear bands as occur for soil and other rigid

materials.

CHAPTER 5

EFFECTS OF COMBINING DIFFERENT DENSITIES

AND LOCATION OF THE EPS BLOCKS

5.1 Background

The construction process of geofoam material can be varied. The performance of geofoam can be affected by factors such as the quality control and density of the EPS blocks. Sometimes, EPS blocks are placed with mixed densities due to the poor quality control. Experienced constructors place EPS blocks in layers of uniform density and with staggered vertical joints. But there was no previous research or lab tests to validate such guidance.

To investigate the importance of quality assurance and proper installation of EPS geofoam blocks, lab tests with and without different densities and also with and without vertical continuous joints were performed. Lab tests were also simulated in FLAC (Finite Difference Model).

5.2 Lab Test Setup

As shown in Figure 5.1, by using the GeoJac loading frame, the samples can be perpendicularly loaded without confining stress in accordance with ASTM D 1621. The load cell that is suspended from the crossbar of the loading frame detects the applied vertical force. The vertical displacement is registered by the displacement transducer (LVDT).
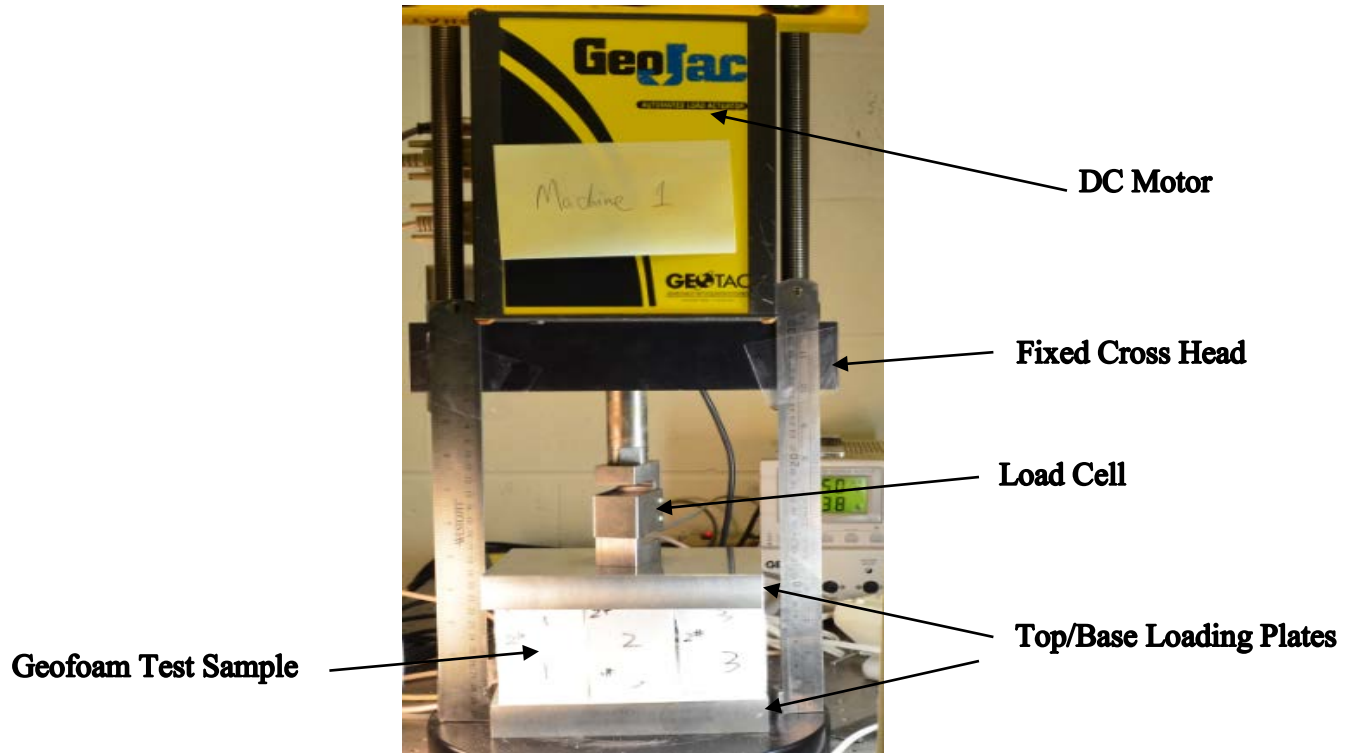
Figure 5.1. GeoJac System Setup

A camera on a tripod was set up in front of the test samples to continually record the loading process. After the test setup, the images were recorded for different loading stages. Then the deformation of EPS blocks and loading stages were observed and compared with the position of EPS blocks before loading.

5.3 Lab Test Process

Experiments were conducted on five or six EPS blocks in 2 layers with either uniform or mixed densities.

(1) In the first test series, six 2in cube samples were stacked in two layers of three blocks with continuous vertical joints. Three tests were done by using the six

EPS blocks with the same density of 1pcf (as shown in Figure 5.2), 1.25pcf and

2pcf respectively.
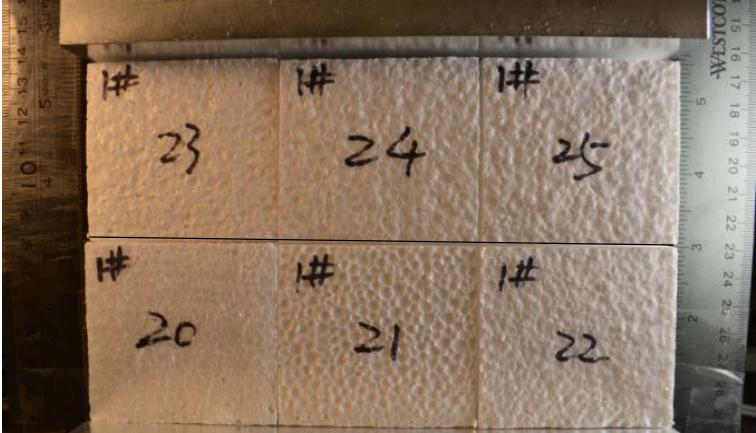
Figure 5.2. Six 2in Cube Samples with All 1pcf Density Stacked in 2 Layers with
Continuous Vertical Joints

(2) In the second test series, six 2in cube samples were stacked in 2 layers of

three blocks with continuous vertical joints, but with adjacent EPS pieces of 2

different densities, such as 1 & 1.25pcf EPS combined and 1 & 2pcf EPS

combined (as shown in Figure 5.3).
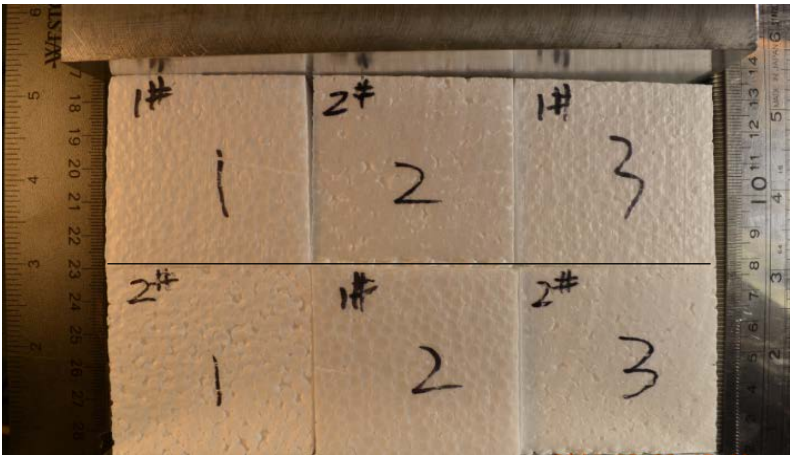
Figure 5.3. Six 2in Cube Samples with Mixed 1&2pcf EPS Stacked in 2 Layers
with Continuous Vertical Joints

(3) In the third test series, five samples were stacked in two layers, replacing the three 2in cube samples on the top layers with two 3in wide blocks. For these tests with two upper and three lower blocks, the vertical joints were staggered and no continuous vertical joints existed across the two layers. Three tests were done by using the five EPS blocks with the same density of 1pcf (as shown in Figure 5.4), 1.25pcf and 2pcf, respectively.
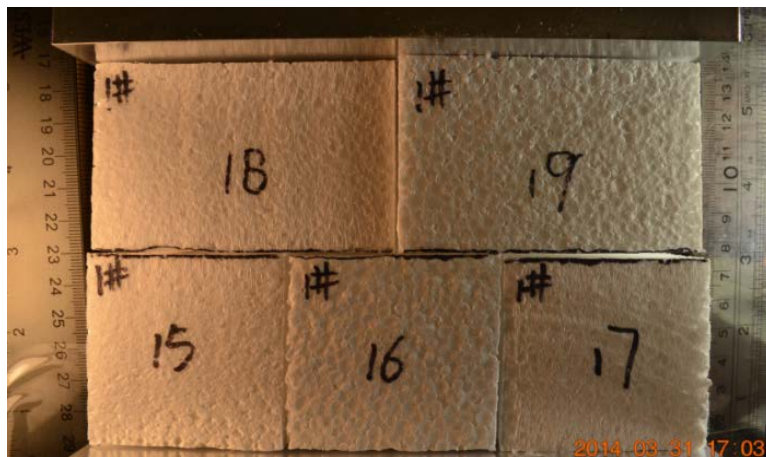
Figure 5.4. Five EPS Blocks with All 1pcf Density Stacked in 2 Layers without Continuous Vertical Joints

(4) The fourth test series was the same as the third but with mixed lower and higher density EPS pieces in the top and lower layers of 1 & 1.25pcf EPS, and 1 & 2pcf EPS combinations (as shown in Figure 5.5). One test was made with three higher density EPS and two lower density EPS (Figure 5.5), while another was with three lower density EPS and two higher density EPS.

Figure 5.5. Five EPS Blocks with Mixed 1&2pcf EPS Stacked in 2 Layers without Continuous Vertical Joints

5.4 Test Results

According to the images captured before and after tests (Figure 5.6), samples deformed equally when the densities were the same. The interface between the upper and lower blocks remained horizontal, for both cases with and without continuous vertical joints (6 and 5 EPS samples).

Before Loading   After Loading

Figure 5.6 (a). Six 2in Cube Samples with Uniform Density Stacked in 2 Layers with Continuous Vertical Joints

Before Loading	After Loading

Figure 5.6 (b). Five 2in Cube Samples with Uniform Density Stacked in 2 Layers without Continuous Vertical Joints

Figure 5.6. EPS Blocks with All 1pcf Density

In the mixed density tests, the lower density blocks deformed more than the higher density blocks. The initially horizontal interface between the layers became uneven (Figure 5.7) for both cases with and without continuous vertical joints. The unevenness of the interface between the upper and lower blocks was less for the tests containing five blocks without continuous joints (Figure 5.7 (b) and (c)) compared to the tests using six EPS blocks with continuous vertical joints (Figure 5.7 (a)).
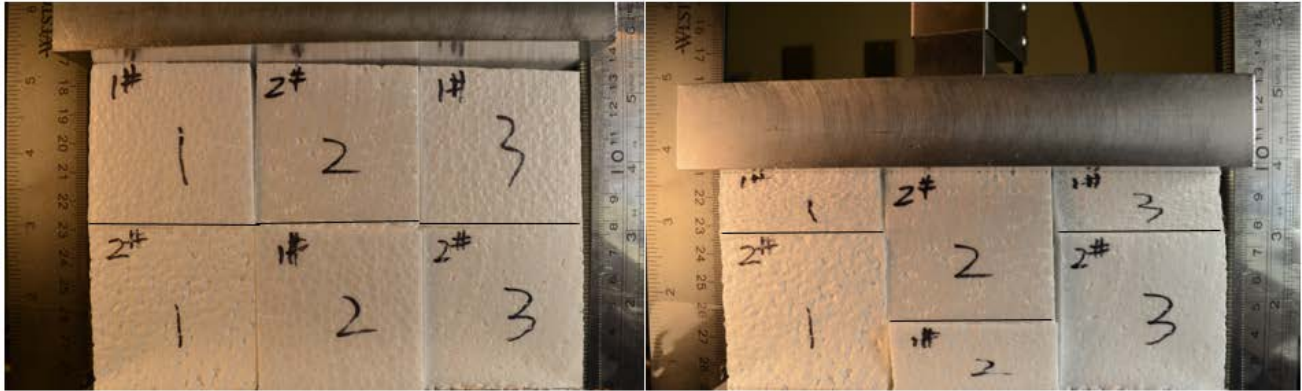
| Before Loading | After Loading |

Figure 5.7 (a). Six 2in Cube Samples with Mixed Densities Stacked in 2 Layers with Continuous Vertical Joints

| Before Loading | After Loading |

Figure 5.7 (b). Five 2in Cube Samples with Mixed Densities Stacked in 2 Layers without Continuous Vertical Joints
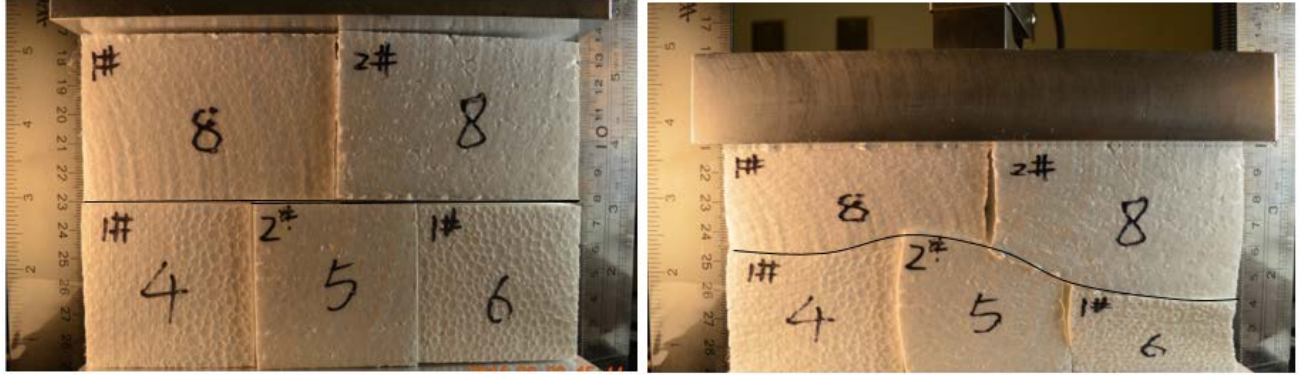
Before Loading   After Loading

Figure 5.7 (c). Five 2in Cube Samples with Mixed Densities Stacked in 2 Layers
without Continuous Vertical Joints

Figure 5.7. EPS Blocks with Combined 1pcf&2pcf Density
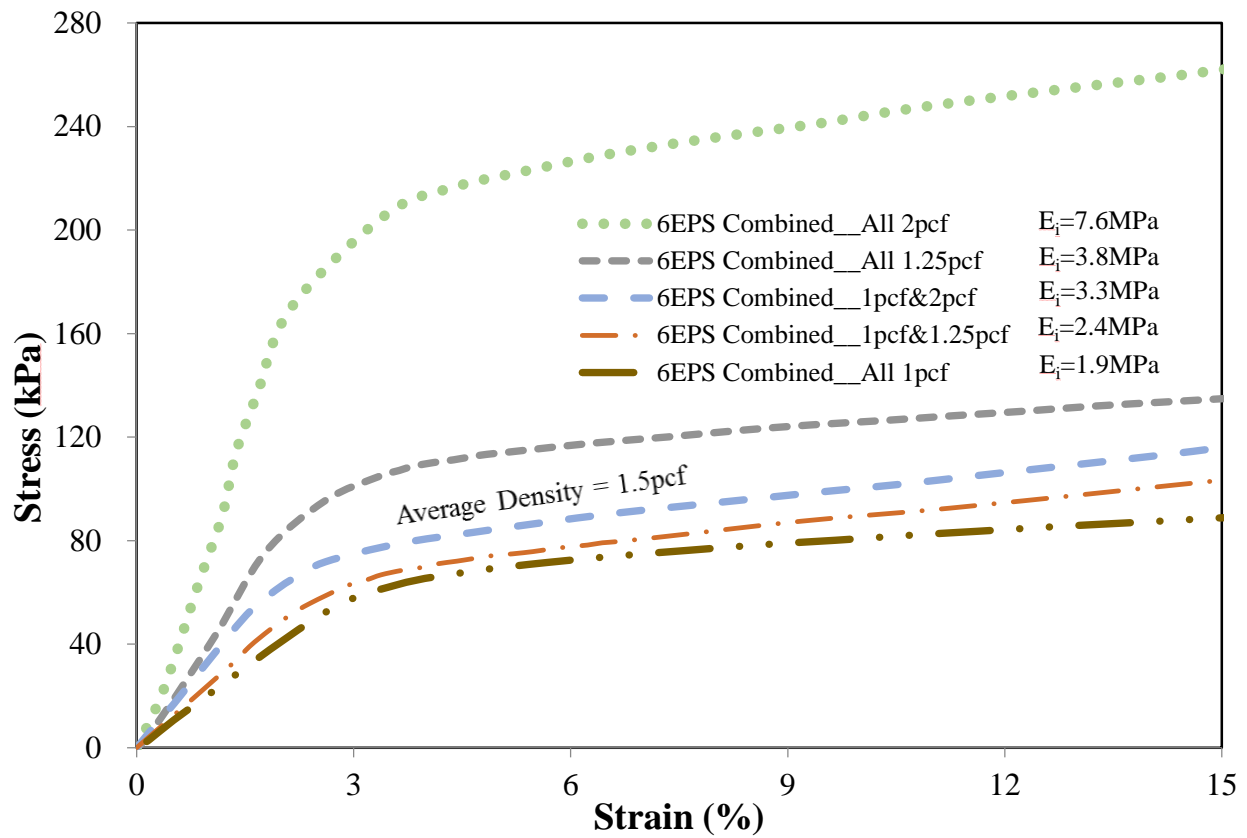
Figure 5.8. Stress-Strain Curves for All the Six EPS Blocks Combined Tests

90

Figure 5.8 shows the stress-strain curves for six EPS blocks of the same and combined densities. The results indicate EPS blocks with mixed densities had initial modulus in between the modulus values for the same lower and upper densities. The strengths at 1, 5 and 10 percent strain for the uniform upper density set were higher than the corresponding strengths for the mixed density set. The mixed lower density EPS samples reduced the strength of the higher density EPS samples. The modulus of the combined density blocks were higher than the modulus of the lower density EPS. However, a uniform 1.25pcf density set had higher modulus and strength than a combination of 1 and 2pcf densities; even though the average densities is 1.5pcf and greater than the uniform set of 1.25pcf in Figure 5.8.
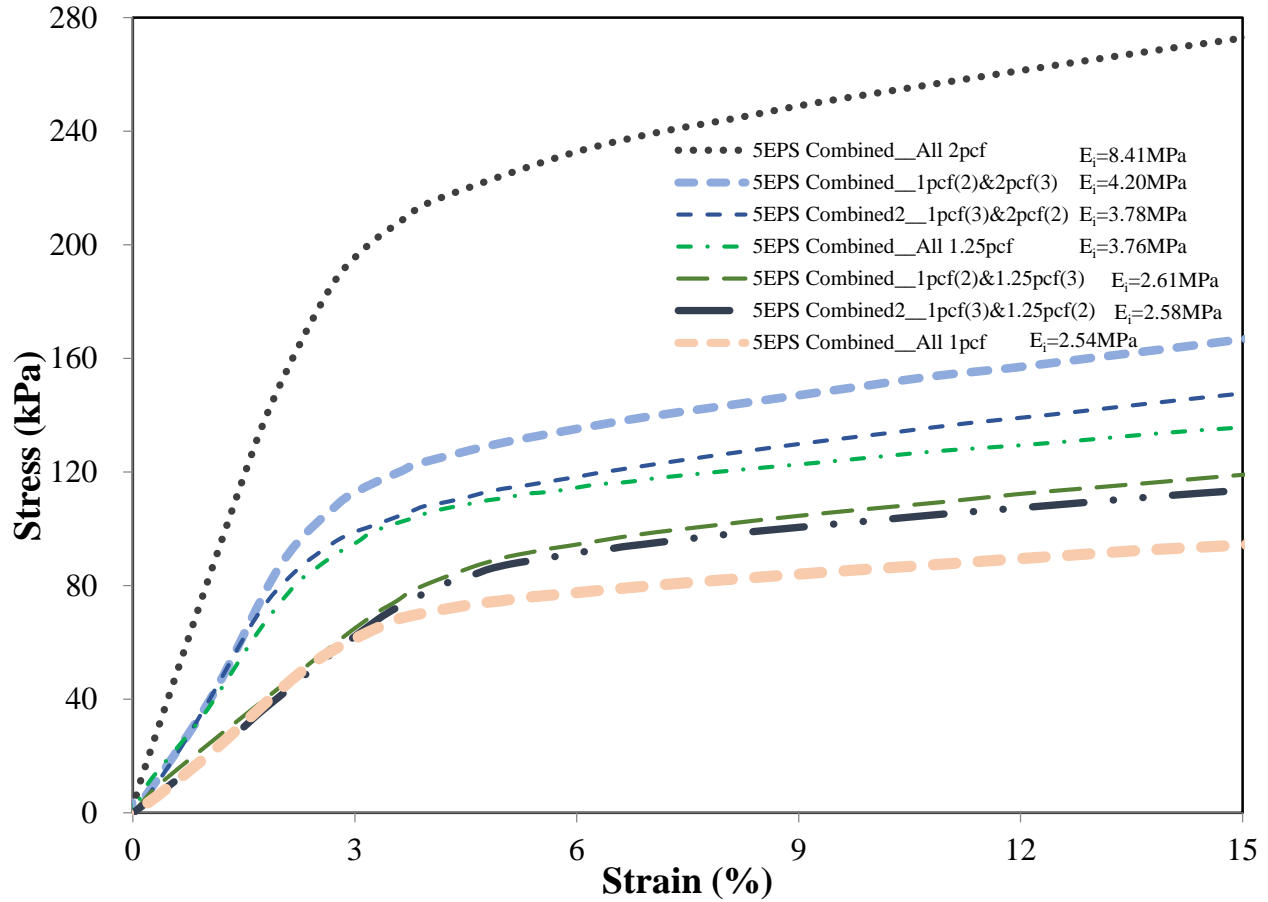
Figure 5.9. Stress-Strain Curves for All the Five EPS Blocks Combined Tests

Figure 5.9 displays the stress-strain curves for five EPS blocks. The general

tendency showed a similar pattern as the six EPS blocks combined tests. The

results demonstrate the initial modulus of EPS blocks with mixed densities are

intermediate between the initial modulus of lower and upper densities. The mixed

lower density EPS samples reduced the strength of the higher density EPS. The

strengths at 1, 5 and 10 percent strain for the uniform upper density set were higher

than the corresponding strengths for the mixed density set. The modulus of the

combined density blocks were higher than the modulus of the lower density EPS.

92

The EPS blocks with more lower-density EPS tended to have much closer strength as the blocks with all lower density.
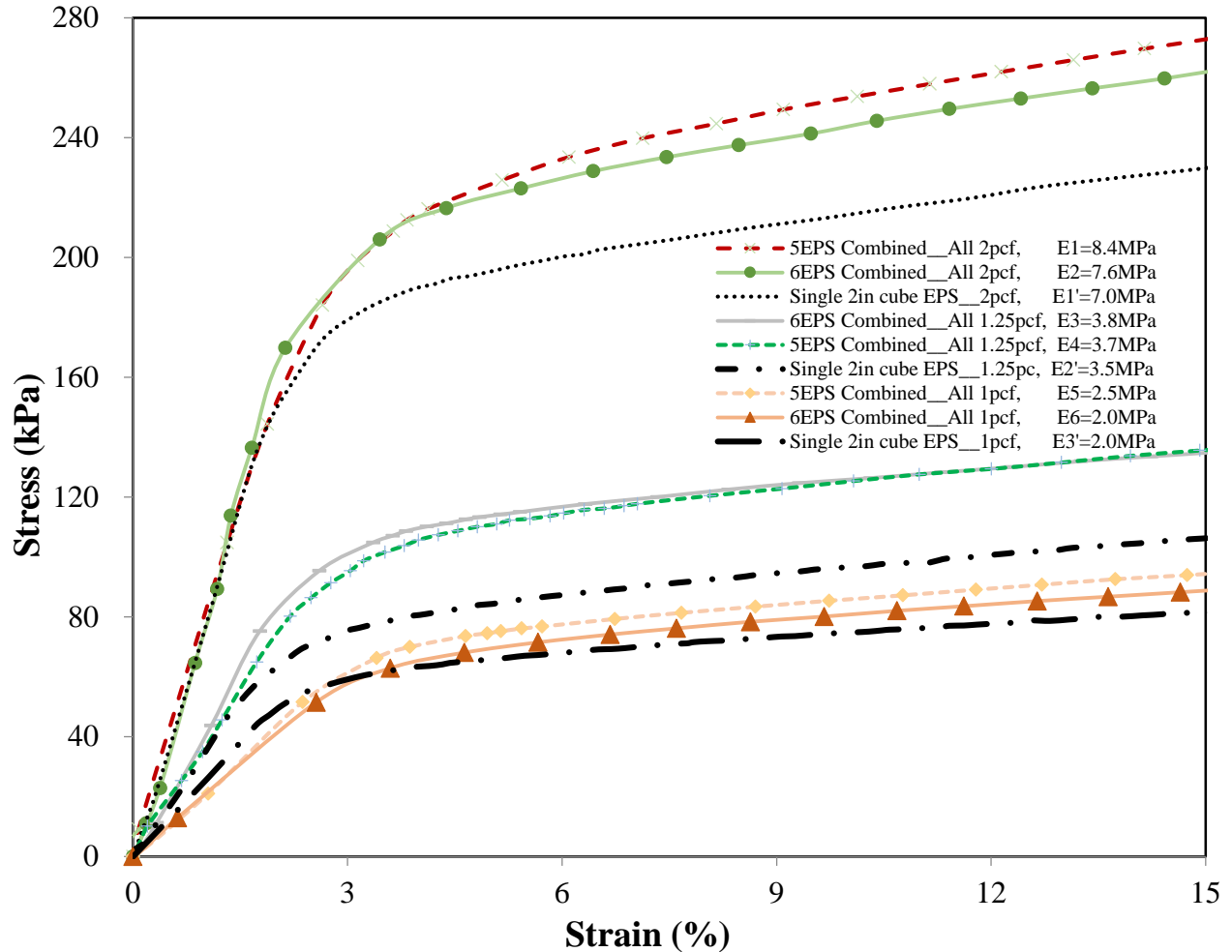
Figure 5.10. Combination of All the Test Results with Uniform Densities EPS

Figure 5.10 characterizes all the test results with single standard size EPS, and uniform density EPS, including the tests with and without continuous vertical joints. The strengths at 1, 5 and 10 percent strain, and initial modulus for the uniform 1.25pcf density EPS sets are almost the same for both cases of with and without continuous joints. The strengths for the case of without continuous joints at

5 and 10 percent strain are slightly higher than for the continuous joints and much higher than for the single sample of 2pcf densities. The existence of continuous joints did not significantly affect the initial modulus of the EPS blocks.
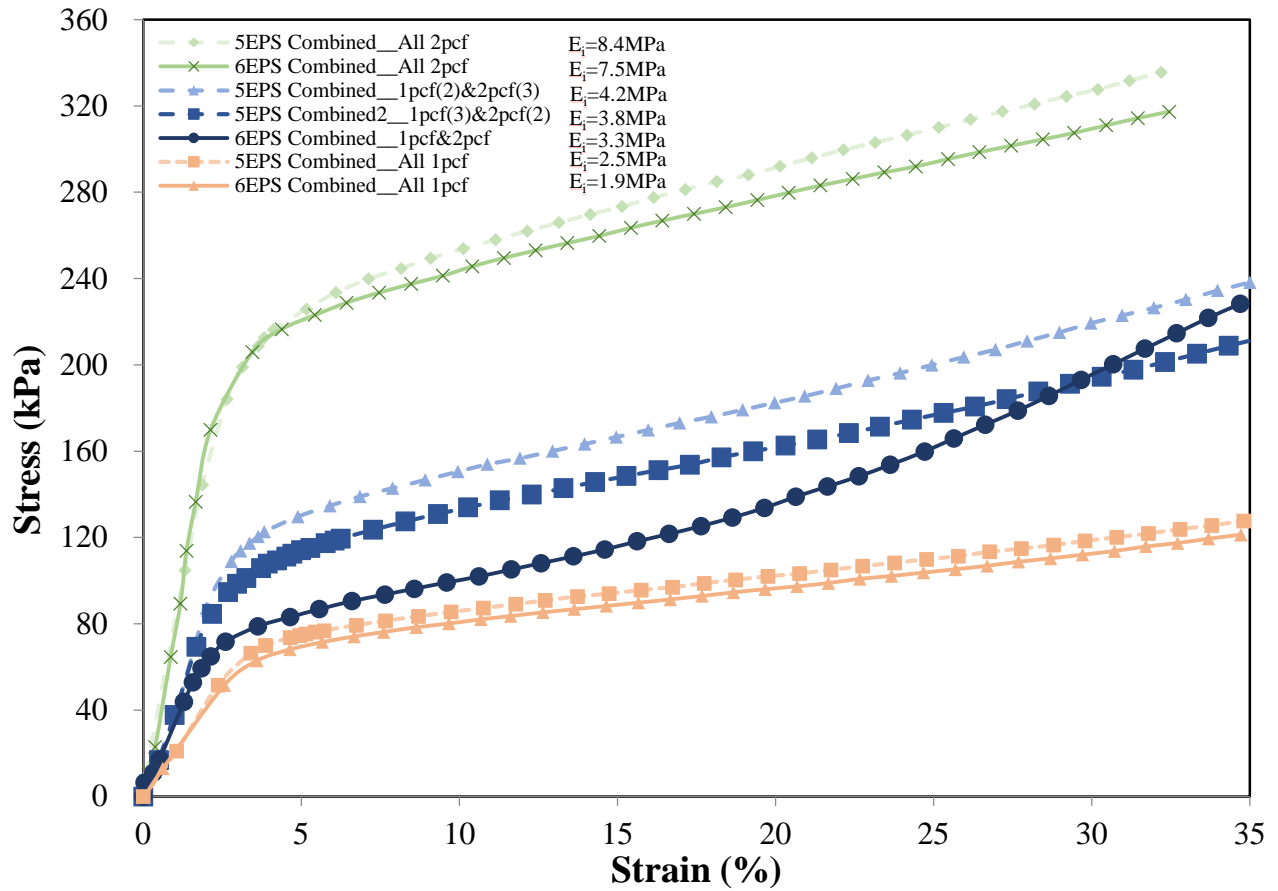
Figure 5.11. Combination of All the Test Results with Uniform and Mixed Densities EPS

The combination of all the test results with uniform and mixed density EPS is shown in Figure 5.11. There is only a slight reduction of EPS stiffness for uniform density EPS because of the continuous joints (Figure 5.10). The effect of the continuous joints is significant when the EPS blocks were of mixed densities.

94

Block alignments and transition zones are essential in geofoam installation. Continuous vertical and horizontal joints between EPS blocks should be avoided by staggering the blocks so as to increase the integrity of the fill. It is also shown in Figure 5.11 that the strength change is proportional to the volume of higher and lower density EPS. The strength of blocks with more higher-density EPS is higher than the strength of blocks with more lower-density EPS. All the moduli of the combined density blocks were higher than the moduli of the lower-density EPS. Even though the mixed density cases produced unevenness along the layer interface between the upper and lower blocks, the strengths increased comparing to the lower-density EPS. In general, in mixed density cases, the specified density is likely the higher density. Therefore, the overall performance would be less than for the specified blocks.

5.5 FLAC 7.0 Modeling Results

Table 5.1. Parameters Used in FLAC Modeling

EPS Type	Density (kg/m³)	Elastic Modulus, E (MPa)	Bulk Modulus, B (MPa)	Shear Modulus, G (MPa)
Weak EPS	20	E, 2.0	0.8	G, 0.9
Strong EPS	30	E_r, 8.0	3.3	G_r, 3.6

The lab tests were modeled in FLAC (Itasca, 2014) to examine internal stress and deformation distributions. The EPS properties were obtained from

previous lab test results and are shown in Table 5.1. With these parameters, FLAC was used to model the unconfined compression test response to single and mixed EPS geofoam density combinations.

(1) Rigid Boundary Condition

The tests conducted in the lab were unconfined compression loading by rigid end plates that imposed uniform displacement along the plate interfaces. Therefore, to simulate the rigid end boundary, a constant velocity of -0.000169m/s (10%/min strain rate) was applied at the top of the sample keeping the bottom fixed. Even though the real boundary condition applied at the top of EPS blocks was free, the top boundary was shown fixed only due to the application of constant velocity to displace the sample downward.

As for the mixed density modeling, interface condition were considered. FLAC provides interfaces that are characterized by Coulomb sliding and/or tensile separation. Interfaces have the properties of friction, cohesion, dilation, normal and shear stiffness, and tensile strength. The normal (K_N) and shear stiffness (K_S) of EPS blocks were separately determined as $1.05 \times 10^4 MPa/m$ and $4.7 \times 10^3 MPa/m$ using Equation 5.1 and 5.2. Joint pacing S of 0.01in was used.

$$\text{Normal Stiffness:} \quad K_N = \frac{E \cdot E_r}{S(E_r - E)} \qquad \text{Equation 5.1}$$

$$\text{Shear Stiffness:} \quad K_S = \frac{G \cdot G_r}{S(G_r - G)} \qquad \text{Equation 5.2}$$

Figure 5.12 and Figure 5.13 present the boundary and interface conditions of

FLAC model for the cases of mixed density EPS blocks with and without

continuous joints. For field conditions, vertical gaps may be closed in the presence

of confining pressures. The joint spacing S could be very small and even negligible.

The normal and shear stiffness would be very high. Therefore, the interface

element condition may not be important for FLAC Modeling of buried geofoam

with confining pressure.
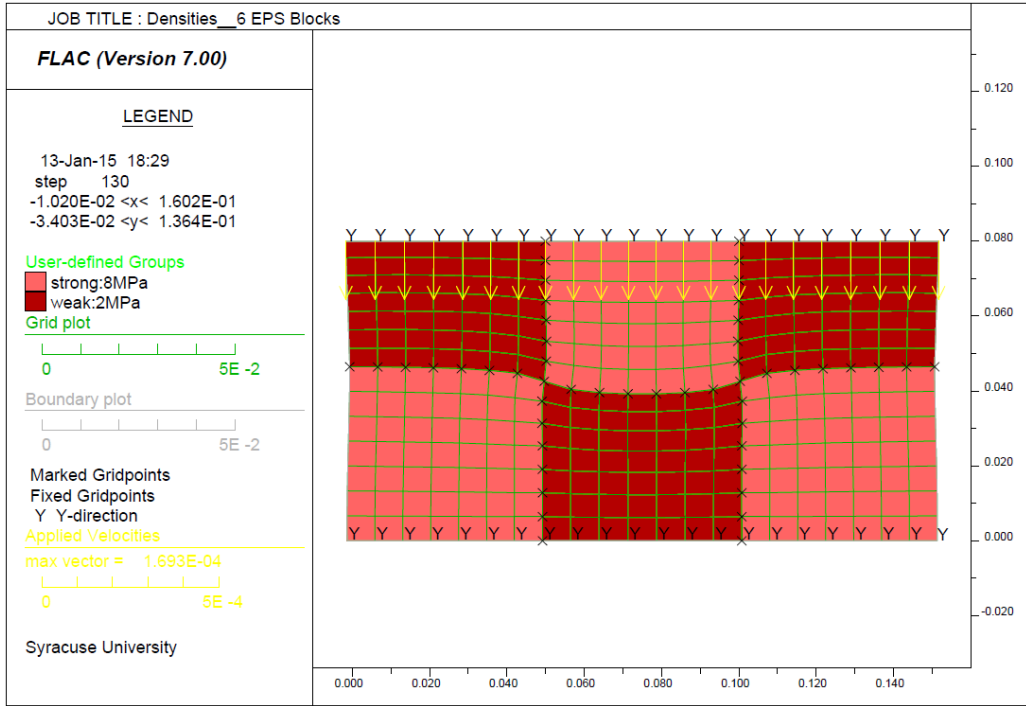
Figure 5.12 (a). Without Interface Element
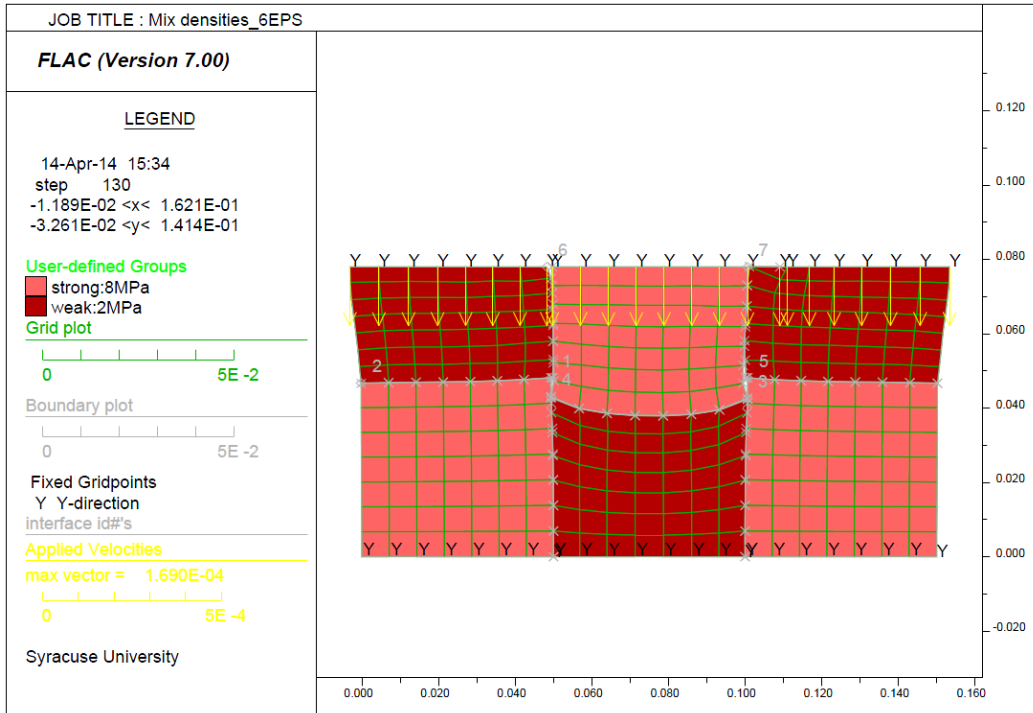
Figure 5.12 (b). With Interface Element

Figure 5.12. Boundary and Interface Conditions of FLAC Model for Cases of

Mixed Density EPS Blocks with Continuous Joints

98
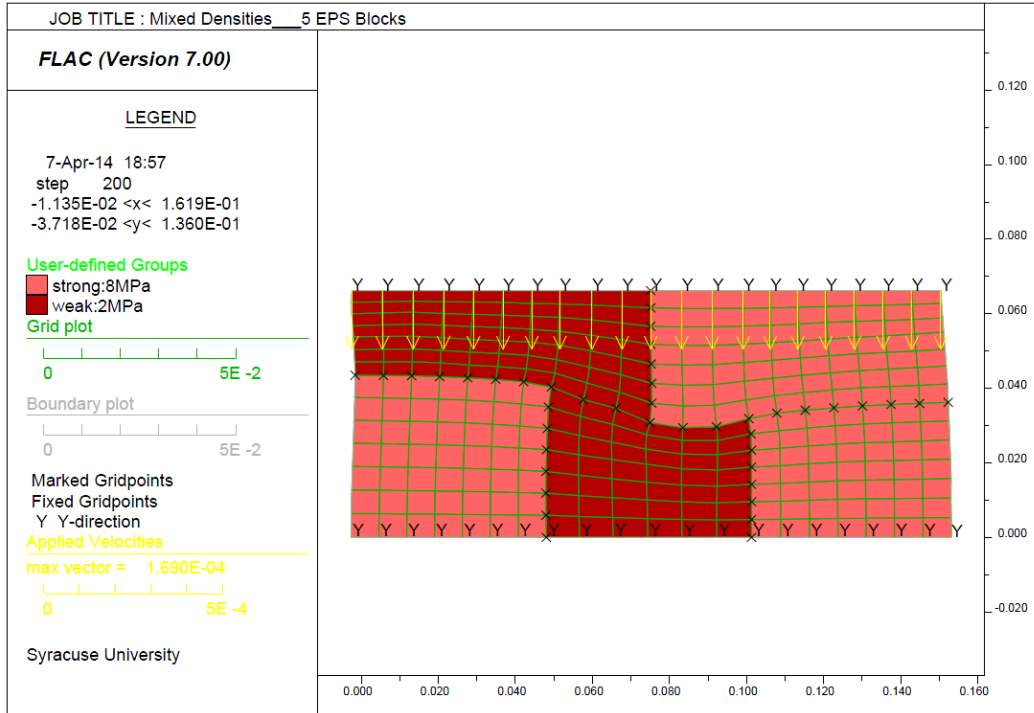
Figure 5.13 (a). Without Interface Element
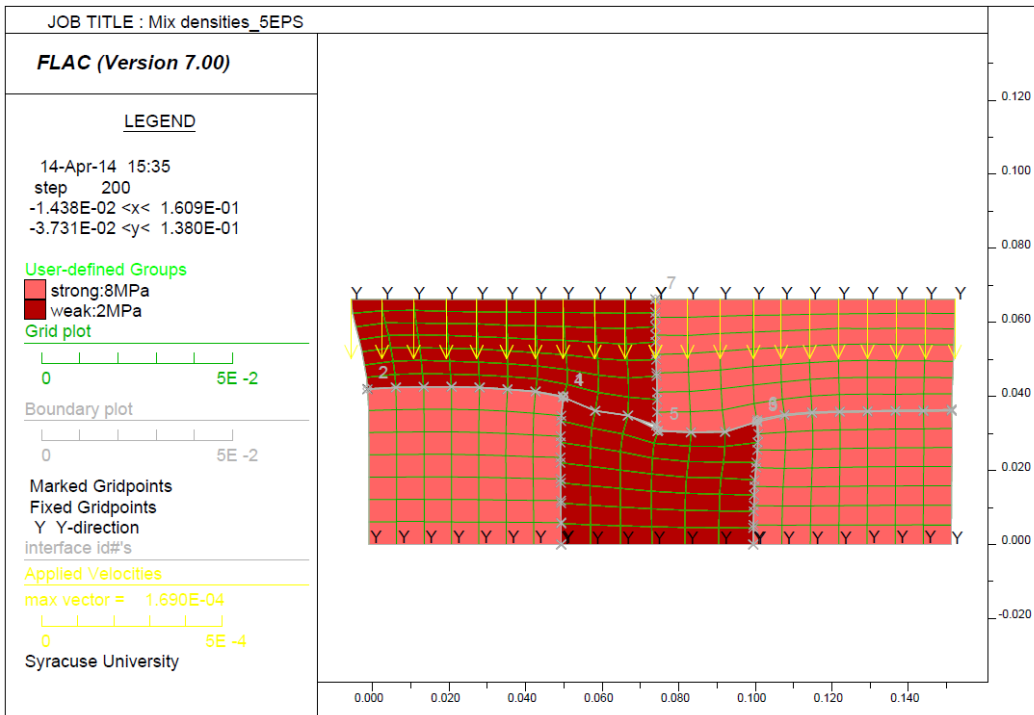
Figure 5.13 (b) With Interface Element

Figure 5.13. Boundary and Interface Conditions of FLAC Model for Cases of

Mixed Density EPS Blocks without Continuous Joints

99

The stress-stain relationships obtained from FLAC analysis are presented in Figure 5.14 to Figure 5.18 with the accompanying lab testing results and recorded photos. Within working strain level, the results from the FLAC output agreed reasonably well with the test data. The y displacement plots support that the single density blocks deformed uniformly with regular stress patterns. The mixed density blocks displayed differential deformation and stress distribution. The y-stress plots and y displacement plots show that the dense blocks carried more load and blocks of lower density deformed more. High differential pressures that exceeded the pressure applied at the top boundary developed in the portions of dense blocks adjacent to low density blocks. The non-uniformity in density contributed to the development of internal pressures that exceeded allowable levels for the specified geofoam grade. Depending on the densities of surrounding blocks, the edges of a block deformed unevenly.
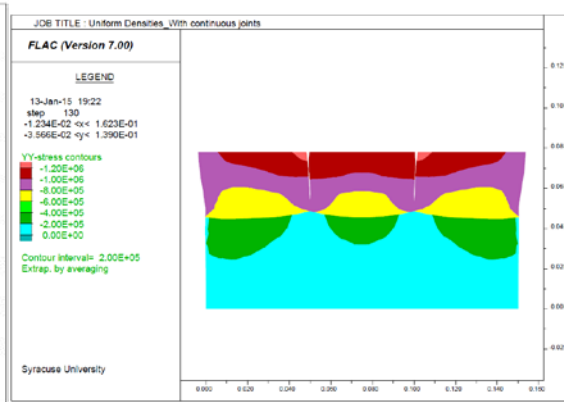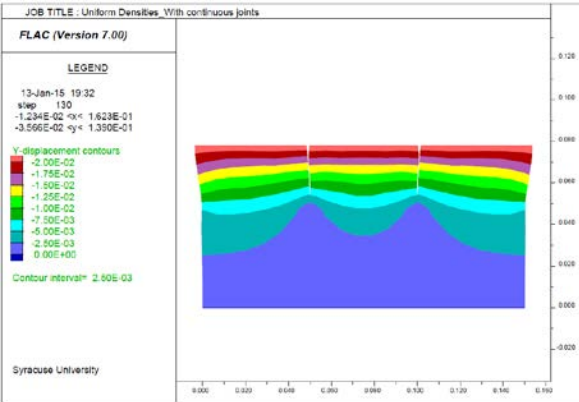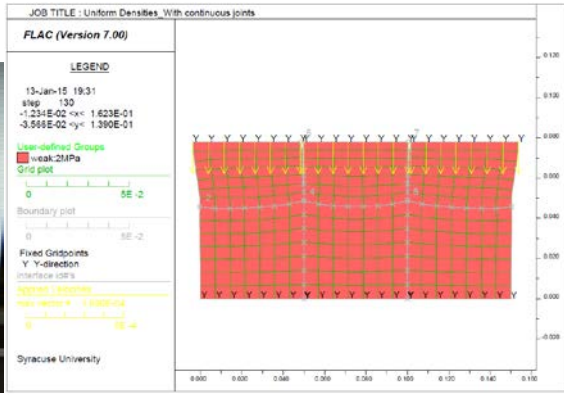
Figure 5.14. 6 blocks of 1pcf EPS: With Continuous Joints_Uniform Density
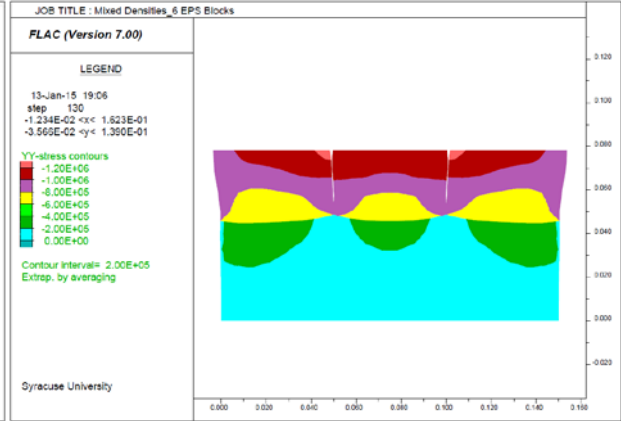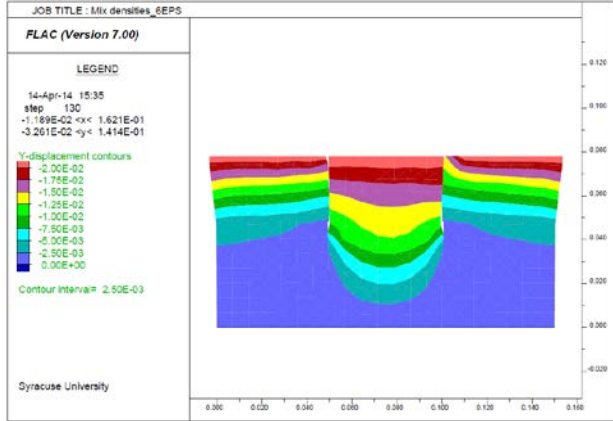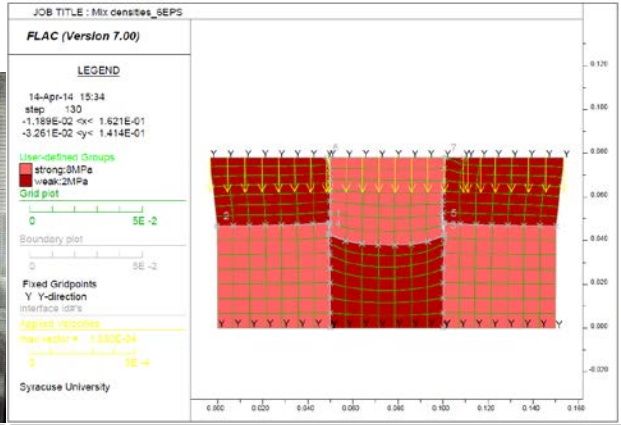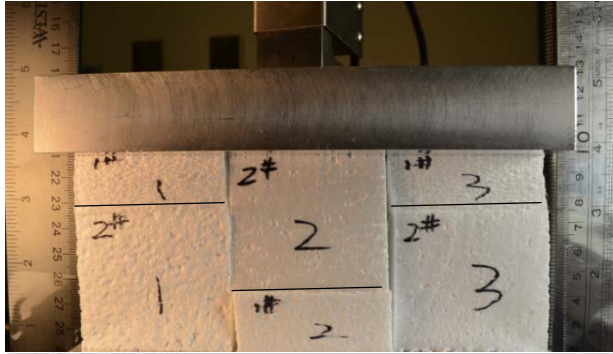
Figure 5.15. 6 blocks of 1 & 2pcf: 15mm global displacement @ 130sec
With Continuous Joints_Mixed Density
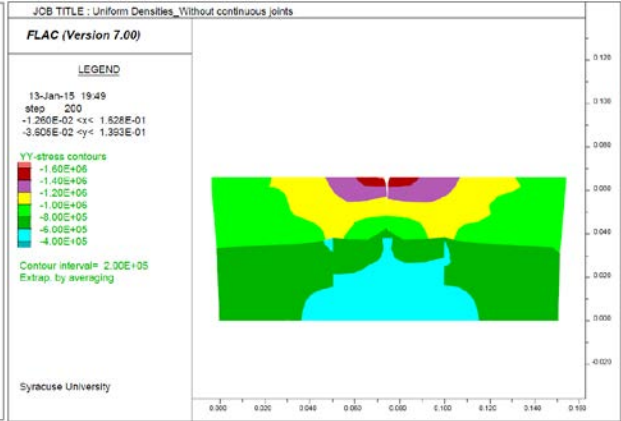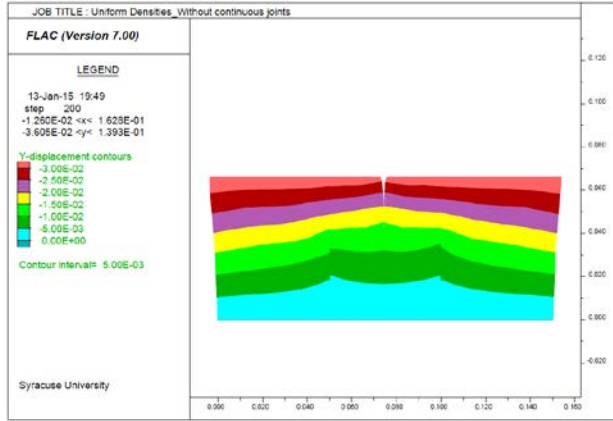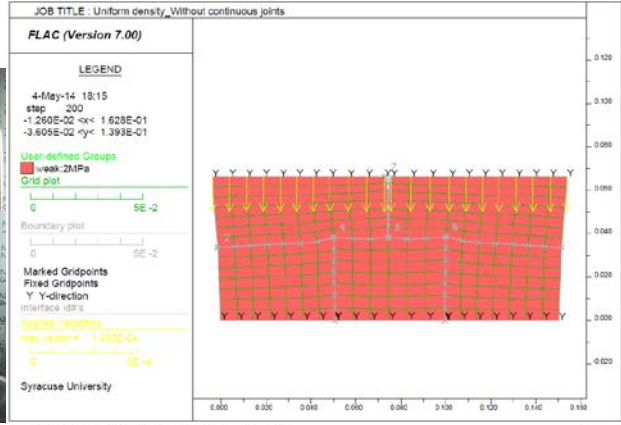
Figure 5.16. 5 blocks of 1pcf EPS: Without Continuous Joints_Uniform Density
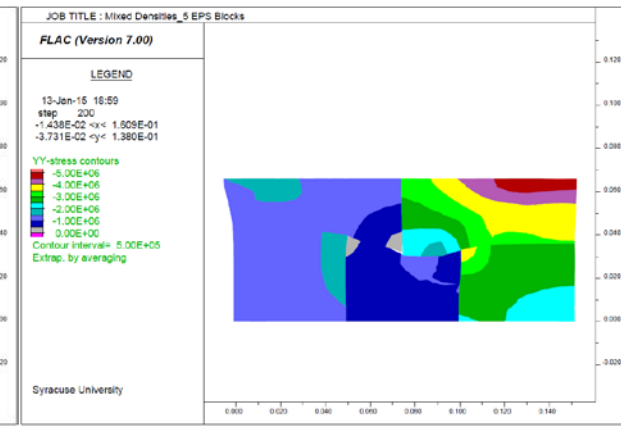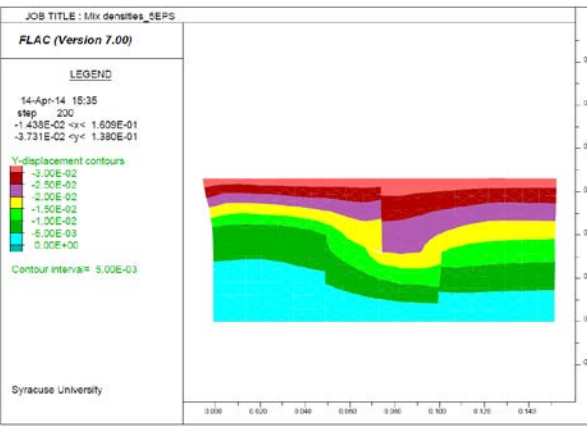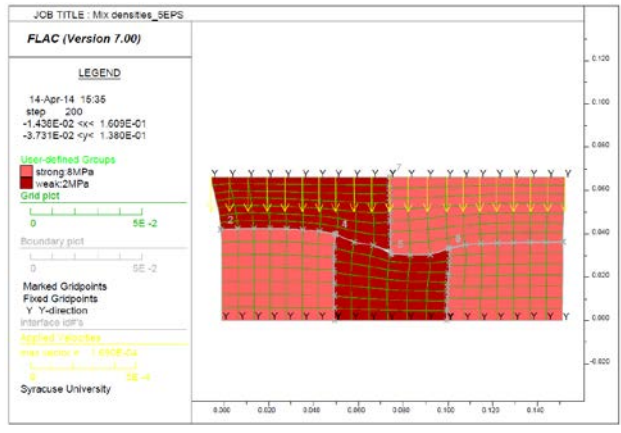
Figure 5.17. 5 blocks of 1 & 2pcf: 27mm global displacement @ 200sec
Without Continuous Joints_Mixed Density
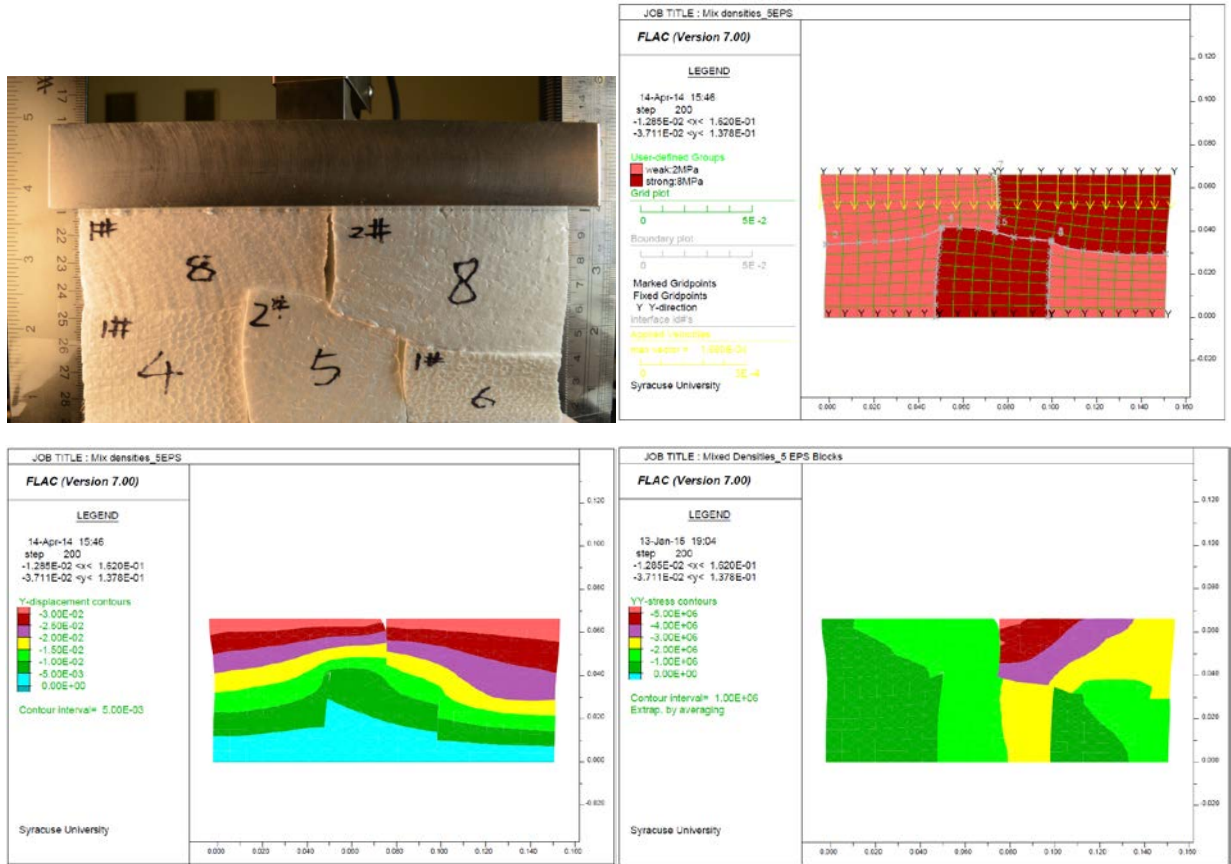
Figure 5.18. 5 blocks of 1 & 2pcf: 30mm global displacement @ 200sec
Without Continuous Joints_Mixed Density

(2) Flexible Boundary Condition

The model of rigid boundary and constant displacement rate conditions indicated non-uniform boundary pressures (Figure 5.14 to Figure 5.18). In the field, the top surface of geofoam is more likely subjected to approximate flexible boundary loading conditions. The geofoam base boundary conditions in the field is the same as the condition in the lab. The alternative boundary conditions were simulated in FLAC models of the lab tests. A uniform pressure of 75kPa was applied on the top boundary to simulate soil cover or pavement structure. The

modeling results are shown in Figure 5.19 and Figure 5.20. The modeling results with a flexible boundary also show the low density blocks deformed more and the high density blocks carried more load. Installing EPS blocks with mixed densities and continuous vertical joints (Figure 5.19) result in non-uniform stress and strain distribution and differential deformation.
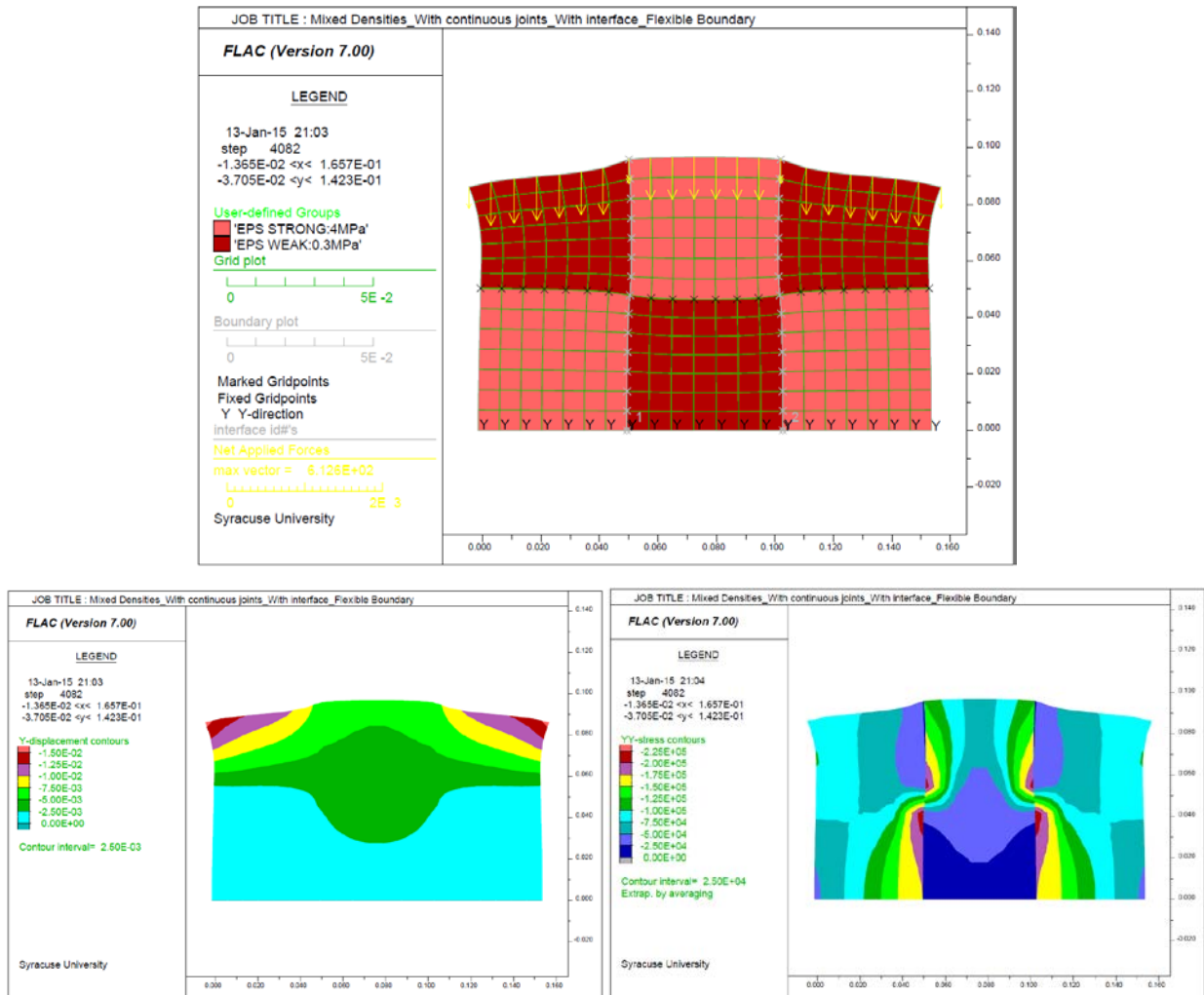
Figure 5.19. FLAC Modeling Results of Mixed Densities and with Continuous Vertical Joints Condition with Flexible Top Loading Boundary
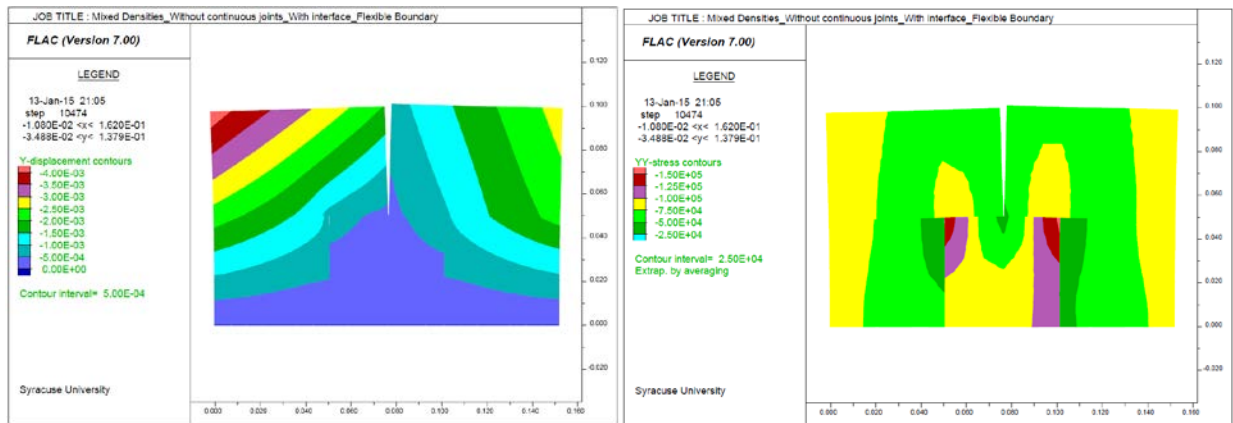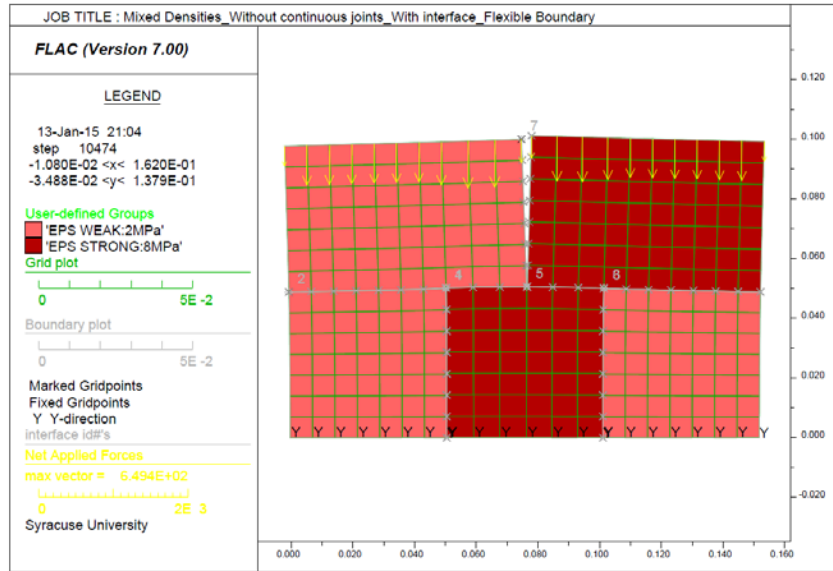
Figure 5.20. FLAC Modeling Results of Mixed Densities and without Continuous
Vertical Joints Condition with Flexible Top Loading Boundary

5.6 Conclusions

Based on the lab test and FLAC modeling results, the following conclusions
can be made:

1. Stress-strain curves for combined low and high density EPS blocks lie
between stress-strain curves for all high density and all low density blocks.

107

2. EPS blocks with staggered vertical joints had higher strengths and lower deformations than EPS blocks separated by continuous vertical joints.

3. The combined density tests show higher density EPS blocks deform much less than adjacent low density blocks at the same load stage.

4. The lab results suggest it is important not to mix high and low density EPS blocks in the same layer.

5. EPS blocks should be installed with staggered vertical joints to minimize differential movements.

6. Even though the mixed density case will cause the unevenness of the interface between the upper and lower blocks according to the images captured during loading process, the strength increases. However, in actual cases, the high density blocks tend to be the specified blocks. Thus the performance of the mixed blocks would be inferior to the uniform high density specified blocks.

CHAPTER 6

CONCLUSIONS AND RECOMMENDATIONS

Engineering performances of EPS geofoam has been presented in this investigation. The effect of induced anisotropy on the stress-strain behavior of EPS geofoam, the effect of combining different EPS densities and also the different stress-strain reactions for the condition of with or without continuous joints are analyzed by using traditional stress-strain measurement and newly developed ARAMIS image analysis. The following conclusions and recommendations are made:

1. Loading and unloading cycles to max of 40% working stress did not produce significant modulus degradation. Loading to post-yield stage and full unloading and reloading cycles produced significant modulus degradation of up to 56~68% of initial modulus. Loading to post-yield stage and partial unloading and reloading cycles produced much less modulus degradation than full unloading and reloading cycles. On unloading and reloading, the proportional limit increases with accumulated strain. The results suggested controlled pre-stressing of geofoam fill can be beneficial in reducing initial deformations while improving the allowable working stress range. EPS geofoam tends to develop softer reloading modulus but continue to strain harden, and stiffen beyond the max load history level. If pre-straining results in suppressing creep deformation, the increase in proportional

109

limit and moderate degradation in response to partial unloading and reloading cycles may be a favorable development.

2. The optical non-contact system can accommodate any sample size and full-scale models to directly detect displacements of selected points or image facets at high resolution and in 3D. Synchronizing force sensing with displacement detection, directional moduli and Poisson's ratios can be determined from one test sample. It was verified that the traditional way of determining modulus of EPS blocks is conservative. The strain distribution across the face of an EPS sample is initially uniform and becomes highly non-uniform with increasing load and strain development. The difference of local strain are small at lower global strain level and high at higher global strain level. For mixed density tests, the dense (2pcf) EPS blocks were carrying more loads. As a result, the strain level was in between the higher level for 1pcf and lower level for 2pcf. Time lapse images and video recordings show progressive strain development for the cellular structure of EPS is in crushing normal to the direction of loading rather than inclined shear bands as occur for soil and other rigid materials.

3. Stress-strain curves for combined low and high density EPS blocks lie between stress-strain curves for all high density and all low density blocks. EPS blocks with staggered vertical joints had higher strengths and lower deformations than EPS blocks separated by continuous vertical joints. The combined density

tests show higher density EPS blocks deform much less than adjacent low density blocks at the same load stage. The lab results suggest it is important not to mix high and low density EPS blocks in the same layer. EPS blocks should be installed with staggered vertical joints to minimize differential movements. Even though the mixed density case will cause the unevenness of the interface between the upper and lower blocks according to the images captured during loading process, the strength increases. However, in actual cases, the high density blocks tend to be the specified blocks. Thus the performance of the mixed blocks would be inferior to than the uniform high density specified blocks.

Appendix: Rotation Matrices

1. Derivation of 2D Rotation Matrix
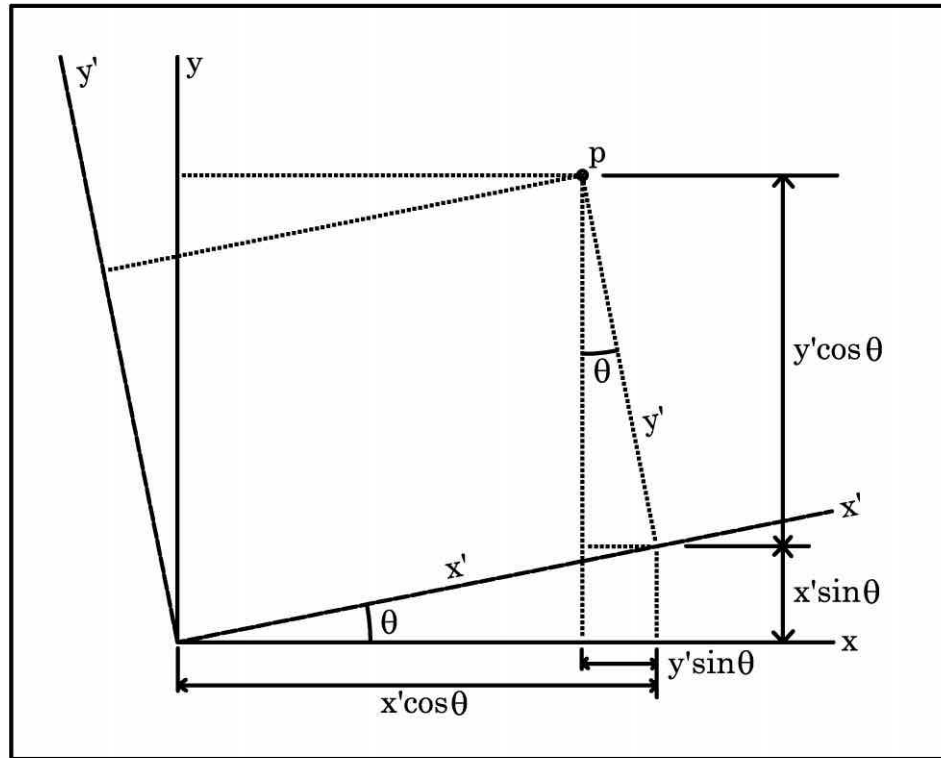
Figure 1. Coordinates of Point p in Two D Systems

Write the (x, y) coordinates in terms of the (x', y') coordinates by inspection,

$$x = x'cos\theta - y'sin\theta$$

$$y = x'sin\theta + y'cos\theta$$

In matrix form,

$$\begin{bmatrix} x \\ y \end{bmatrix} = \begin{bmatrix} cos\theta & -sin\theta \\ sin\theta & cos\theta \end{bmatrix} \begin{bmatrix} x' \\ y' \end{bmatrix}$$

Multiplying on the left by the transpose of the matrix (it is orthogonal so transpose equals inverse),

$$\begin{bmatrix} x' \\ y' \end{bmatrix} = \begin{bmatrix} cos\theta & sin\theta \\ -sin\theta & cos\theta \end{bmatrix} \begin{bmatrix} x \\ y \end{bmatrix}$$

This represents the basic equation describing 2D rotations. Note that the sense of the angle θ is defined by the right hand rule. A positive rotation means that if the thumb of the right hand is pointed along the positive direction of the rotation axis (z), then the fingers curl in the positive direction, i.e. counterclockwise. We will adopt the convention that rotation means a rotation of the *coordinate axes*, not the *point*. If the axes are rotated counterclockwise, then the point itself appears to rotate clockwise, with respect to fixed axes. See Figure 2 below.

(a) Counterclockwise Rotation of Axes   (b) Clockwise Rotation of Point
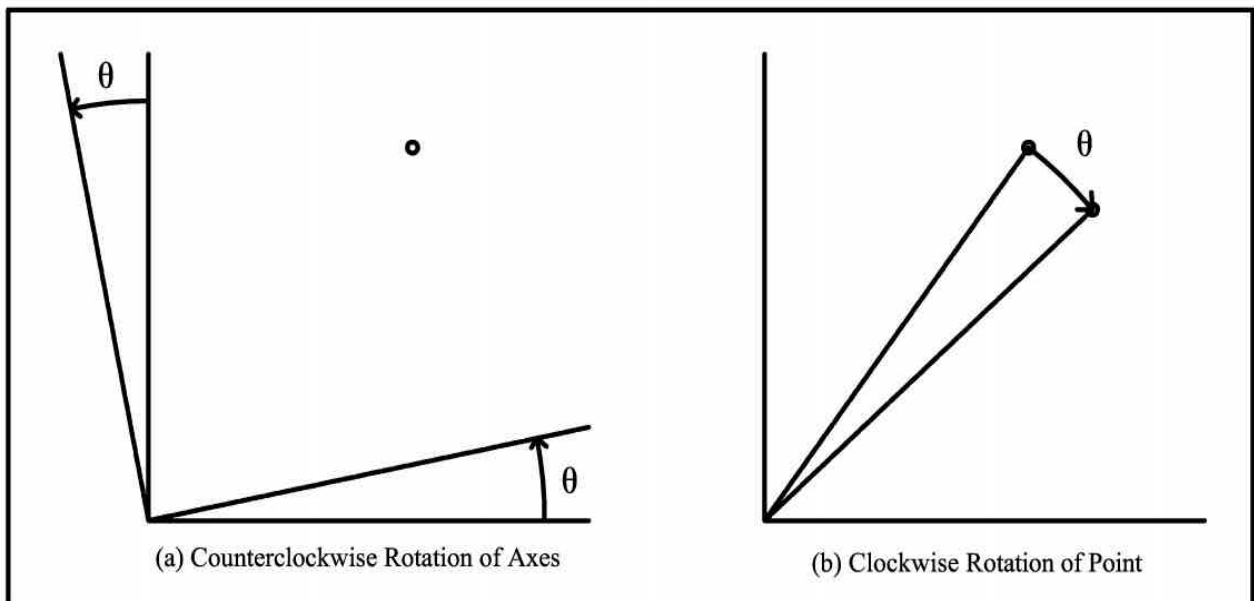
Figure 2. Equivalence of Rotating Axes in one Direction, and a Point in the Opposite Direction

113

2. Derivation of 3D Elementary Rotation Matrices

We can extend the prior development into 3D rotations by constructing elementary 3D rotation matrices. The elementary 3D rotation matrices are constructed to perform rotations individually about the three coordinate axes. We begin with the rotation about the z-axis (k, or kappa), since it is virtually identical to what was just developed. We keep the same xy transformation but add an identity transformation for the z-coordinate, since it will not change during a rotation about the z-axis. See Figure 3.

$$\begin{bmatrix} x' \\ y' \\ z' \end{bmatrix} = \begin{bmatrix} \cos\kappa & \sin\kappa & 0 \\ -\sin\kappa & \cos\kappa & 0 \\ 0 & 0 & 1 \end{bmatrix} \begin{bmatrix} x \\ y \\ z \end{bmatrix} = R_k \begin{bmatrix} x \\ y \\ z \end{bmatrix}$$
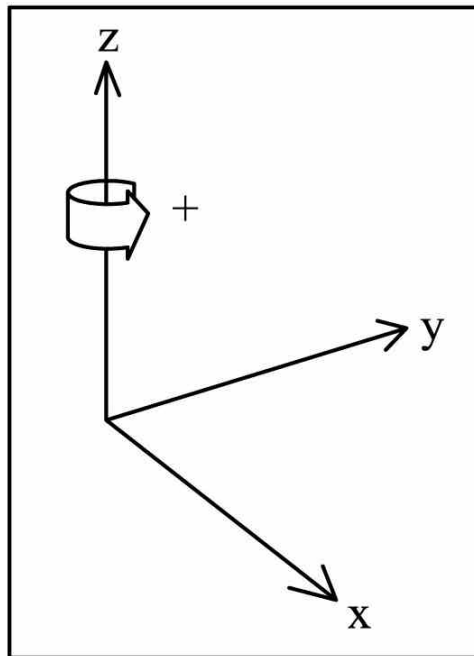
Figure 3. Rotation about the z-axis

Next let us consider a rotation about the x-axis. Photogrammetrists call this rotation ω, or omega. See the drawing in Figure 4. We can relate this back to our prior derivation by letting the y-axis *play the role of x,* and letting the z-axis *play the role of y*. If we do that then we can write the 3D elementary rotation matrix directly by inspection, albeit with a coordinate component order that is not conventional. Then we can rearrange the order and thereby obtain the conventional elementary matrices.

The equation, written by inspection,

$$\begin{bmatrix} y' \\ z' \\ x' \end{bmatrix} = \begin{bmatrix} cos\omega & sin\omega & 0 \\ -sin\omega & cos\omega & 0 \\ 0 & 0 & 1 \end{bmatrix} \begin{bmatrix} y \\ z \\ x \end{bmatrix}$$

For the vector on the right we want to move the first two elements down, and the third element we want to move to the first position. That corresponds to moving the first two columns of the matrix to the right, and moving the third column to the first column position.

$$\begin{bmatrix} y' \\ z' \\ x' \end{bmatrix} = \begin{bmatrix} 0 & cos\omega & sin\omega \\ 0 & -sin\omega & cos\omega \\ 1 & 0 & 0 \end{bmatrix} \begin{bmatrix} x \\ y \\ z \end{bmatrix}$$

115
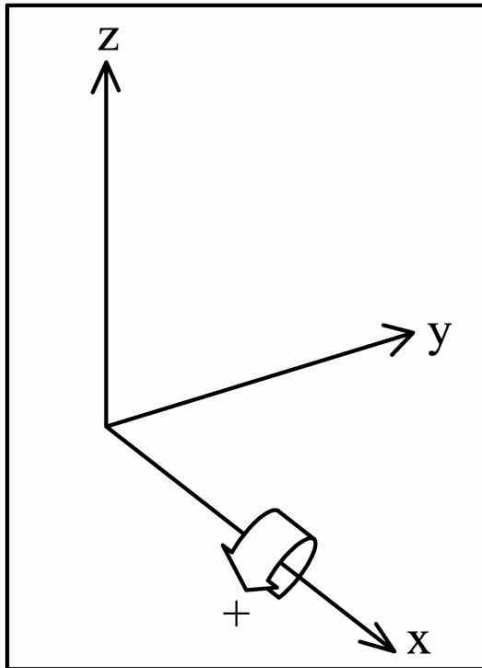
Figure 4. Rotation about the *x*-axis

For the vector on the left we want to move the two top elements down, and we want to move the third element up to the top. This corresponds to moving the corresponding matrix rows in the same way. This completes the elementary rotation about *x*.

$$
\begin{bmatrix} x' \\ y' \\ z' \end{bmatrix} = \begin{bmatrix} 1 & 0 & 0 \\ 0 & cos\omega & sin\omega \\ 0 & -sin\omega & cos\omega \end{bmatrix} \begin{bmatrix} x \\ y \\ z \end{bmatrix} = R_\omega \begin{bmatrix} x \\ y \\ z \end{bmatrix}
$$

Figure 5 shows a rotation about the *y*-axis. In order to be able to write the rotation matrix directly, imagine that the *z*-axis is *playing the role of* the *x*-axis, and the *x*-axis is *playing the role of* the *y*-axis. With that coordinate order, we write the matrix directly, in terms of the angle, α (Alpha).

$$\begin{bmatrix} z' \\ x' \\ y' \end{bmatrix} = \begin{bmatrix} cos\alpha & sin\alpha & 0 \\ -sin\alpha & cos\alpha & 0 \\ 0 & 0 & 1 \end{bmatrix} \begin{bmatrix} z \\ x \\ y \end{bmatrix}$$

In order to rearrange the order of the vector on the right, we must slide the last two matrix columns left, and move the leftmost column over to the right.

$$\begin{bmatrix} z' \\ x' \\ y' \end{bmatrix} = \begin{bmatrix} sin\alpha & 0 & cos\alpha \\ cos\alpha & 0 & -sin\alpha \\ 0 & 1 & 0 \end{bmatrix} \begin{bmatrix} x \\ y \\ z \end{bmatrix}$$
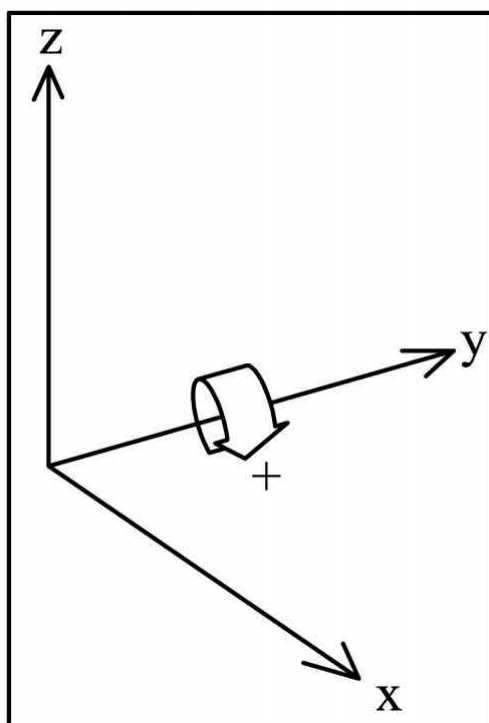
Figure 5. Rotation about the *y*-axis

In order to put the elements of the vector on the left into the conventional *x y z* order, we must slide the bottom two matrix rows up, and move the top row down to the bottom.

117

$$\begin{bmatrix} x' \\ y' \\ z' \end{bmatrix} = \begin{bmatrix} cos\alpha & 0 & -sin\alpha \\ 0 & 1 & 0 \\ sin\alpha & 0 & cos\alpha \end{bmatrix} \begin{bmatrix} x \\ y \\ z \end{bmatrix} = R_\alpha \begin{bmatrix} x \\ y \\ z \end{bmatrix}$$

This completes the elementary rotation about *y*. These elementary matrices can be combined to create any 3D rotation. In photogrammetry the usual order of the rotations is lastly kappa (*z*) first, then alpha (*y*), and omega (*x*). A matrix applied first is on the right, therefore the general composite rotation is,

$$R = R_k R_\alpha R_\omega$$

Writing out all of the elements of the composite rotation we get,

$$R = \begin{bmatrix} cos\kappa \cdot cos\alpha & sin\kappa \cdot cos\omega + cos\kappa \cdot sin\alpha \cdot sin\omega & sin\kappa \cdot sin\omega - cos\omega \cdot sin\alpha \cdot cos\kappa \\ -sin\kappa \cdot cos\alpha & cos\kappa \cdot cos\omega - sin\kappa \cdot sin\alpha \cdot sin\omega & sin\omega \cdot cos\kappa + cos\omega \cdot sin\alpha \cdot sin\kappa \\ sin\alpha & -sin\omega \cdot cos\alpha & cos\omega \cdot cos\alpha \end{bmatrix}$$

References

ASTM D 6817, ASTM D 1621, C 165, EN 826 or ISO 844.

Taylor, D. W. (1948), "Fundamental of Soil Mechanics", John Wiley and Sons, Inc., New York, NY.

Coleman, T.A., (1974), "Polystyrene Foam Is Competitive Lightweight Fill", Civil Engineering, Vol. 44, No.2, pp. 68-69.

Aabøe, R., (1981), "Plastic Foam in Road Embankments, Norwegian Road Research Laboratory, Oslo, Norway.

Aabøe, R., (1985), "Plastic Foam in Road Embankments: Experience with Expanded Polystyrene as a Lightweight Fill Material in Road Embankments", Norwegian Road Research Laboratory, Oslo, Norway.

Aabøe, R., (1987), "13 Years of Experience with Expanded Polystyrene as a lightweight Fill Material in Road Embankments", Norwegian Road Research Laboratory, Publication No. 61, Oslo, Norway, pp. 21-27.

van Dorp, T., (1988), "Expanded Polystyrene Foam as Light Fill and Foundation Material in Road Structures", International Congress on Expanded Polystyrene, Pre-print, Milan, Italy, 19p.

Yeh, S., T., and Gilmore, J., B., (1989), "Application of EPS for Slide Correction, Stability and Performance of Slopes and Embankments II, ASCE Geotechnical Special Publication, NY, USA, No. 31, pp. 1444-1456.

Eriksson, L., and Trank, R., (1991), "Properties of Expanded Polystyrene, Laboratory Experiments", Swedish Geotechnical Institute, Linköping, Sweden.

BASF Corp., (1993), "Styropor Foam as a Lightweight Construction Material for Base-Course", Styropor Technical Information, BASF Corp., Ludwigshafen, Germany.

Mimura, C., S., and Kimura, S., A., (1995), "A Lightweight Solution", Geosynthetics 95 Conference Proceedings, Vol. 1, Nashville Tennessee, USA, pp. 39-51.

Thompsett, D., Walker, A., Radley, R., and Grieveson, B., (1995), "Design and Construction of Expanded Polystyrene Embankments", Construction and Building Materials, U.K., Vol. 9, No. 6, pp. 403-411.

Frydenlund, T., E., and Aabøe, R., (1996), "Expanded Polystyrene-The Light solution", Proceedings of the International Symposium on EPS Construction Method, Tokyo, Japan, pp 31-46.

van Dorp, T., (1996), "Building on EPS Geofoam in the "Low-Lands" Experiences in the Netherlands", Proceedings of the International Symposium on EPS Construction Method, Tokyo, Japan, pp. 59-69.

Sun, M.C., (1997), "Engineering Behavior of Geofoam (Expanded Polystyrene) and Lateral Pressure Reduction in Substructures", Master's Thesis, Syracuse University, New York.

Duškov, M., (1997), "EPS as a Light Weight Sub-Base Material in Pavement Structures", Ph.D. Thesis, Delft University of Technology, Delft, the Netherlands.

Negussey, D., (1997), "Properties & Applications of Geofoam", Society of the Plastic Industry, Inc., Washington, D.C., USA.

BASF Corp., (1997), "Styropor Technical Information", Technical Information, BASF Corp., Germany.

Horvath, J., (1998), "Mathematical Modeling of the Stress-Strain-Time Behavior of Geosynthetics Using the Findley Equation: General Theory and Application to EPS-Block Geofoam", Manhattan College Research Report No. CE/GE-98-3, Bronx, N.Y.

Negussey, D., (1998), "Putting Polystyrene to Work", Civil Engineering, American Society of Civil Engineering, NY, USA, Vol. 68, No. 3, pp. 65-67.

GeoTech, (1998), "Geofoam Compressible Inclusions: A Conceptual Guide to Analysis and Design", GeoTech System Corporation, VA, USA.

BASF Corporation (1998), "Styropor Foam as a Lightweight Construction Material for Road Base-Courses," Styropor Technical Information, Ludwigshafen, Germany.

Jutkofsky, W., S., Teh, S., J., and Negussey, D., (2000), "Stabilization of an Embankment Slope with Geofoam", Transportation Research Board, 79th Annual Meeting, Paper No. 00-1315, Washington, D.C., USA.

Cole, B., (2000), "How EPS Foam Saved the City of Issaquah 1.2 Million Dollars and One Year of Construction Time", Preprint Paper, Syracuse Geofoam Seminar, Salt Lake City, Utah, USA.

Elragi, A., (2000), "Selected Engineering Properties and Applications of EPS Geofoam", Ph.D. Thesis, State University of New York, Syracuse, N.Y.

Sheeley, M., (2000), "Slope Stabilization Utilizing Geofoam", Master's Thesis, Syracuse University, New York.

Elragi, A., Negussey, D., and Kyanka, G., (2000), "Sample Size Effects on the Behavior of EPS Geofoam", Proceedings of the Soft Ground Technology Conference, ASCE Geotechnical Special Publication 112, Noordwijkerhout, the Netherlands.

Dimitrios K. Atmatzidis, Emmanuel G. Missirlis and Dimitrios A. Chrysikos, (2001), "An Investigation of EPS Geofoam Behavior in Compression", EPS geofoam 2001 3rd International Conference.

Srirajan, S., (2001), "Recycled Content and Creep Performance of EPS Geofoam in Slope Stabilization", Master's Thesis, Syracuse University, New York.

Anasthas, N., (2001), "Young's Modulus by Bending Tests and Other Engineering Properties of EPS Geofoam", Master's Thesis, Syracuse University, Syracuse, NY.

Negussey, D. (2007), "Design Parameters for EPS Geofoam", Soils and Foundations, Japanese Geotechnical Society, Vol. 47, No. 1, pp. 161 - 170.

Lingwall, B. N. (2011), "Development of an Expanded Polystyrene Geofoam Cover System for Pipelines at Fault Crossings, Dissertation", University of Utah, Department of Civil and Environmental Engineering, Salt Lake City, Utah.

T Ahmed Awol, (2012), "A Parametric Study of Creep on EPS Embankments", Master's Thesis, Norwegian University of Science and Technology.

GeoJac user manual

ARAMIS user manual

FLAC 7.0 user manual